
Electronic Thesis and Dissertation Repository

10-7-2021 1:00 PM

Free fatty acid treatment alters autophagy during mouse preimplantation embryo development

Zuleika C. L. Leung, *The University of Western Ontario*

Supervisor: Watson, Andrew J., *The University of Western Ontario*

Co-Supervisor: Betts, Dean H., *The University of Western Ontario*

A thesis submitted in partial fulfillment of the requirements for the Master of Science degree in Physiology and Pharmacology

© Zuleika C. L. Leung 2021

Follow this and additional works at: <https://ir.lib.uwo.ca/etd>



Part of the [Developmental Biology Commons](#), and the [Reproductive and Urinary Physiology Commons](#)

Recommended Citation

Leung, Zuleika C. L., "Free fatty acid treatment alters autophagy during mouse preimplantation embryo development" (2021). *Electronic Thesis and Dissertation Repository*. 8160.
<https://ir.lib.uwo.ca/etd/8160>

This Dissertation/Thesis is brought to you for free and open access by Scholarship@Western. It has been accepted for inclusion in Electronic Thesis and Dissertation Repository by an authorized administrator of Scholarship@Western. For more information, please contact wlsadmin@uwo.ca.

Abstract

Obesity-induced hyperlipidemia is one of the main factors for female infertility. Hyperlipidemia, specifically with high levels of palmitic acid (PA) and oleic acid (OA), interferes with preimplantation development. Autophagy is essential in early embryo development but, it is unknown whether hyperlipidemia affects autophagic mechanisms in preimplantation embryos. It was hypothesized that PA will alter autophagy in preimplantation mouse embryos and that the subsequent effects will be reversed by OA. PA impaired blastocyst development by arresting embryos at the 8-cell stage. PA also elevated early embryo autophagy by increasing autophagosome formation, decreasing maturation, and disrupting degradation. Co-treatment with OA showed developmental delay at the early preimplantation stages but restored blastocyst formation. OA treatment also counteracted PA-induced effects on autophagy. Overall, PA altered autophagy at various levels, was reversed by the addition of OA. Ultimately, we aim to assist obese patients by offsetting the negative effects of hyperlipidemia on preimplantation embryo development.

Keywords

Autophagy, Embryo, Lysosomal activity, Non-esterified fatty acids, Preimplantation development, Obesity

Summary for Lay Audience

Obesity is a one of the main factors for infertility in Canadian females. Levels of fatty acids like palmitic acid (PA) and oleic acid (OA) are elevated in obese individuals. Previously, we reported that PA disrupts mouse embryonic development and addition of OA reversed those effects. Autophagy is another important mechanism in early embryo development in which useless contents are packaged into autophagosomes for degradation to be reused in other cellular functions. Despite the importance of autophagy in embryonic development, it is undefined whether autophagy is affected by elevated levels of fatty acids in preimplantation embryos. To determine the effects of PA and OA, mouse embryos were treated with PA and OA, alone and in combination for up to 48 hours. PA prevented embryonic development by arresting development at the 8-cell stage. PA also resulted in elevated levels of autophagy by disrupting autophagosome formation and lowering autophagosome maturation and degradation. OA addition to PA treatment resulted in developmental delay at the early embryonic stages but restored normal levels of development at the later stages. Additionally, PA and OA co-treatment reversed PA-effects on autophagic mechanisms of preimplantation mouse embryos. Overall, PA impaired development and elevated autophagy and the addition of OA counteracted those effects. With these findings, we expect to help obese individuals with their fertility problems by offsetting the negative effects of obesity on preimplantation embryo development.

Co-Authorship Statement

All experiments and designed, performed, and analyzed by Zuleika Leung in consultation with Dr. Andrew Watson and Dr. Dean Betts.

Acknowledgment

They say it takes a village to raise a child. I'm so grateful to have many people who encouraged and supported me, the child (at heart), through this endeavor.

First and foremost, a huge thank you to my parents and my brother. Thank you for all that you have done and sacrificed to support me through this journey. Thank you for encouraging me to achieve something I've never dreamed of achieving. Thank you for being there whenever I feel lost. Thank you for supporting me unconditionally through this career path that I don't even know where I would end up in; thank you for believing in me when I am not so sure myself. A big shout out to my brother, for really stepping up these few years when I'm out and about trying to figure things out for myself. Your encouragement was one of the reasons I decided to go into graduate school, and I wouldn't have done it without your support throughout these years. To my aunts and uncles, thank you all for supporting me through this journey and for being interested in my work even though it doesn't make sense to you.

To Dr. Watson and Dr. Betts, I am so grateful to have you both as my supervisors. Your interest and excitement in my work really encouraged me to do better and achieve more. Thank you for believing in me and giving me the freedom to try new things for my project. Your guidance throughout these few years really shaped this project and I couldn't have completed my thesis without your constant support.

To Michele, thank you for your behind-the-scenes assistance for these past two years. From training me in flushing to helping me calculate dilution factors, thank you for making this journey a worry-free one for me. It was an invaluable learning experience because of you. To Hailey, thank you for encouraging me to learn as much as I can during my program. Thank you for taking time out of your busy schedule to train me in cell work and western blot with the limited time that I have. I really appreciate you for helping me with my experiment and being excited for me when my experiments worked.

To the members of the Betts/Watson lab, working in the lab was fun because of you all. Thank you all for being open to a chat or rant or even going for a walk or coffee run. You all

made this journey so much more bearable, especially during COVID days. To Grace, I love that we started the program together and finished it together. From messing up our RNA extraction to weekend confocal sessions, we had our good days and bad days in the lab, but it was such a great time when we went through it together. It was nice to have someone to share this wild experience with. Cheers to the fun time we had!

To the members of the DDTA lab, thanks for all the fun at the office. I very much enjoyed spending time with you all chatting away and our pre-COVID socials.

To my close friends, thanks for being there for me when I need and always be so supportive of my life choices. Thank you all for taking care of me, especially on my low days, and making sure that I take a break so that I won't feel burnt out.

Last, but not least, a big thank you to the funding sources that supported my MSc journey: the Children's Health Research Institute and the WSRG.

List of Abbreviations

α -ATZ	α -antitrypsin Z
ADB	Antibody dilution buffer
AMBRA	activating molecule in Beclin-1-regulated autophagy 1
ANOVA	Analysis of variance
ART	Assisted reproductive technology
AMP	Adenosine monophosphate
AMPK	AMP-activated protein kinase
ATG	Autophagy related gene
ATP	Adenosine triphosphate
BafA1	Bafilomycin A1
BAX	Bcl-2-associated X
BCA	Bicinchoninic acid
Bcln1	Beclin-1
Bcl-2	B-cell lymphoma 2
BMI	Body mass index
BSA	Bovine serum albumin
CQ	Chloroquine
COC	Cumulus-oocyte complex
COX-2	Cyclooxygenase-2
Ct	Cycle threshold
DAG	Diacylglycerol
DGAT	Diacylglycerol acyltransferase
ECL	Enhanced chemiluminescence
ER	Endoplasmic reticulum
FADH ₂	Flavin adenine dinucleotide (reduced form)
FFA	Free fatty acid
GnRH	Gonadotrophin-releasing hormone
GPT2	Glutamic-pyruvate transaminase 2
GDP	Guanosine diphosphate

GTP	Guanosine triphosphate
hCG	Human chorionic gonadotropin
HER2	Human epidermal growth factor receptor 2
HOPS	Homotypic fusion and vacuolar protein sorting
HPG	Hypothalamic-pituitary-gonadal
hpi	Hours post-hCG injection
H2A	Histone H2A
ICM	Inner cell mass
ICSI	Intracytoplasmic sperm injection
IGF-1R	Insulin-like growth factor type-1 receptor
IL-6	Interleukin-6
IL-8	Interleukin-8
IP	Intraperitoneal
IRE1	Inositol-requiring enzyme 1
IUI	Intrauterine insemination
IVF	<i>In vitro</i> fertilization
IVM	<i>In vitro</i> maturation
JNK	Jun N-terminal kinase
KSOMaa	Potassium simplex optimization media with amino acids
LC3	Light Chain 3
LD	Lipid droplet
LH	Luteinizing hormone
LUC	Luciferase
LYAAT-1	Lysosomal amino acid transporter 1
mESC	Mouse embryonic stem cells
MCP-1	Monocyte chemotactic protein-1
MM	Master mix
mTOR	Mammalian target of rapamycin
NADH	Nicotinamide adenine dinucleotide
NAFLD	Non-alcoholic fatty liver disease
NBR1	Neighbour of BRCA1 gene 1
NEFA	Non-esterified fatty acid

OA	Oleic acid
PA	Palmitic acid
PAGE	Polyacrylamide gel electrophoresis
PBS	Phosphate buffered saline
PCR	Polymerase Chain Reaction
PERK	Protein kinase R-like endoplasmic reticulum kinase
PI3K	Phosphatidylinositol 3-kinase
PI3P	Phosphatidylinositol-3 phosphate
PMSG	Pregnant mare's serum gonadotropin
P62	Ubiquitin-binding protein p62
qPCR	Quantitative polymerase chain reaction
ROS	Reactive oxygen species
RT	Reverse Transcription
SA	Stearic acid
SCD1	Stearoyl-CoA desaturase-1
SEM	Standard error of mean
SNARE	Soluble N-ethylmaleimide-sensitive factor-attachment protein receptor
TAG	Triacylglycerol
TE	Trophectoderm
UCP-2	Uncoupling protein 2
ULK1	UNC-51-like kinase 1
UPR	Unfolded protein response
WHO	World Health Organization
XBP1	X-box binding protein 1
ZGA	Zygotic genome activation
3-MA	3-methyladenine

Table of Contents

Abstract	ii
Summary for Lay Audience	iii
Co-Authorship Statement.....	iv
Acknowledgment	v
List of Abbreviations	vii
Table of Contents	x
List of Figures	xiv
List of Appendices	xvi
Chapter 1	1
1 Introduction	1
1.1 Preimplantation Embryo Development	1
1.1.1 Cleavage Division.....	1
1.1.2 Blastocyst Formation	2
1.2 Female Infertility	4
1.3 Assisted Reproductive Technologies (ART).....	4
1.4 Obesity.....	5
1.5 Obesity on Female Reproductive Health.....	6
1.6 Lipid Metabolism.....	8
1.7 Lipid Metabolism in Female Reproduction.....	9
1.8 Non-esterified Fatty Acids (NEFA).....	10
1.9 Palmitic Acid (PA)	11
1.9.1 Structure and Source of PA.....	11
1.9.2 The Effect of PA on Embryo Development.....	12
1.9.3 The Effects of PA on Other Cell Types	13

1.10Oleic Acid (OA)	14
1.10.1 Structure and Source of OA.....	14
1.10.2 The Effects of OA on Embryo Development	14
1.10.3 The Effects of OA on Other Cell Types	15
1.11Palmitic Acid (PA) and Oleic Acid (OA) Co-treatment.....	16
1.11.1 PA and OA Co-treatment on Embryo Development	16
1.11.2 PA and OA Co-treatment on Other Cell Types	17
1.12Cell Stress in Preimplantation Embryos	18
1.13Autophagy.....	20
1.13.1 Initiation of Autophagy: Autophagosome Formation.....	20
1.13.2 Autophagosome Maturation: Autolysosome	27
1.13.3 Autophagosome Degradation with Lysosomes	30
1.14Autophagy in Preimplantation Embryos	32
1.15Autophagy in other cell types	33
1.16Lipotoxicity and Autophagy	33
1.17Rationale	34
1.17.1 Objectives and Hypotheses.....	35
1.17.2 Specific Aims.....	35
1.17.3 Hypothesis.....	36
Chapter 2.....	37
2 Materials and Methods.....	37
2.1 Animals and Ethics Approval.....	37
2.2 Mouse Embryonic Stem Cell (mESC).....	37
2.3 NEFA Preparation	37
2.4 Embryo Culture	37
2.5 mESC Culture.....	38

2.6 Mouse Superovulation and Mating.....	39
2.7 Embryo Collection.....	39
2.8 Developmental Stage Analysis	40
2.9 mESC Cell Morphology	42
2.10 RNA Extraction and Reverse Transcription (RT)	42
2.11 Polymerase Chain Reaction (PCR).....	42
2.12 Quantitative Polymerase Chain Reaction (qPCR).....	43
2.13 Transcript Analysis.....	43
2.14 Immunofluorescence Staining	44
2.15 Confocal Microscopy and Image Acquisition	44
2.16 Image Analysis	45
2.17 Protein Extraction and Quantification	45
2.17.1 Protein Extraction and Quantification of Mouse Embryos.....	45
2.17.2 Protein Extraction and Quantification of mESC.....	45
2.18 Western Blot	46
2.18.1 Sample Preparation of Mouse Embryos	46
2.18.2 Sample Preparation of mESC	46
2.18.3 Polyacrylamide Gel Electrophoresis (PAGE) and Protein Transfer.....	46
2.18.4 Ponceau S Staining and Antibody Incubation	47
2.19 Protein Detection and ECL Imaging.....	47
2.20 Volumetric Analysis	47
2.21 Statistical Analysis.....	48
Chapter 3.....	49
3 Results	49
3.1 Effects of PA and OA on Preimplantation Development.....	49
3.2 Autophagic profile throughout preimplantation development	53

3.3	Effects of PA and OA on overall autophagy	56
3.4	Effects of PA and OA on autophagosome formation	64
3.5	Effects of PA and OA on autophagosome maturation and degradation	67
	Chapter 4.....	71
4	Discussion	71
4.1	NEFA effects on mouse preimplantation development.....	72
4.2	Autophagy throughout preimplantation development.....	74
4.3	NEFA effects on preimplantation embryo autophagy	78
4.4	NEFA effects on autophagosome formation	82
4.5	NEFA effects on autophagosome maturation and degradation	84
4.6	Conclusion and Significance	88
	References.....	91
	Appendices.....	103
	Appendix A: Western blot assay for preimplantation embryos.....	104
	Appendix B: Chloroquine assay to measure autophagic flux.....	106
	Appendix C: Chloroquine effects on preimplantation development	111
	Appendix D: Effects of PA and OA on mESC autophagy	114
	Appendix E: Ethics Approval	116
	Curriculum Vitae	117

List of Figures

Figure 1. Summary of mammalian preimplantation embryo development and developmental events.	3
Figure 2. Summary of inactivated autophagy under nutrient-rich conditions.	22
Figure 3. Summary of autophagosome formation.	25
Figure 4. Summary of autophagosome maturation.	29
Figure 5. Summary of autophagosome degradation.	31
Figure 6. Representative images of mouse preimplantation embryo at each preimplantation stage.	41
Figure 7. Representative images of embryos cultured in NEFA treatments.....	51
Figure 8. Developmental stage progression of embryos after NEFA treatments	52
Figure 9. Autophagic marker transcript abundance in preimplantation development.....	54
Figure 10. Autophagy marker LC3-II in preimplantation embryo development.....	55
Figure 11. Autophagic marker transcript abundance in NEFA-treated embryos	58
Figure 12. Autophagy marker LC3-II in NEFA-treated embryos after 18 hrs. of NEFA treatment	59
Figure 13. Autophagy marker LC3-II in NEFA-treated embryos after 24 hrs. of NEFA treatment	60
Figure 14. Autophagy marker LC3-II in NEFA-treated embryos after 30 hrs. of NEFA treatment	61
Figure 15. Autophagy marker LC3-II in NEFA-treated embryos after 40 hrs. of NEFA treatment	62

Figure 16. Autophagy marker LC3-II in NEFA-treated embryos after 48 hrs. of NEFA treatment	63
Figure 17. Autophagic flux of embryos after NEFA+/- CQ treatment for 40 hours.	65
Figure 18. Representative images of LC3-II puncta in embryos after NEFA+/- CQ treatment for 40 hours.	66
Figure 19. Autophagosome-lysosome co-localization in embryos after 40 hrs. of NEFA treatments	68
Figure 20. Autolysosome in embryos after 40 hrs. of NEFA treatments	69
Figure 21. LysoTracker signal in embryos after NEFA treatments for 40 hrs.	70
Figure 22. Summary Figure: Effects of PA and OA on autophagy in mouse preimplantation embryos.....	90

List of Appendices

Appendix A: Western blot assay for preimplantation embryos.....	104
Appendix B: Chloroquine assay to measure autophagic flux.....	106
Appendix C: Chloroquine effects on preimplantation development	111
Appendix D: Effects of PA and OA on mESC autophagy	114
Appendix E: Ethics Approval	116

Chapter 1

1 Introduction

1.1 Preimplantation Embryo Development

Preimplantation embryo development occurs within the reproductive tract of the mother. Preimplantation embryo development defines the period from the fertilization of an oocyte with a sperm to the attachment of an embryo to the uterine wall (Shi and Wu 2009). Fertilization occurs when a sperm enters the oocyte and a zygote is formed, initiating preimplantation development (Li and Winuthayanon 2017). Preimplantation embryo development can be separated into two parts – cleavage division(s) and blastocyst formation (cavitation) (Shi and Wu 2009).

1.1.1 Cleavage Division

Cleavage division (cell division) begins approximately 24 to 36 hours after fertilization (O'Farrell et al. 2004). The one-cell zygote subdivides into two-, four-, eight-, then 16-cells and on at approximately 12-hour intervals from the two-cell stage to the early blastocyst stage (O'Farrell et al. 2004). At the two-cell stage, mouse embryos undergo zygotic genome activation (ZGA). ZGA enables the activation of embryonic genome (mRNA transcription and protein translation) while degrading maternal oogenic products (Lee et al. 2014). ZGA plays an important role in activating the genomic cascade or program that supports early preimplantation development and implantation of an embryo (Jukam et al. 2017). At the eight-cell stage, compaction of the embryo is triggered (Kojima et al. 2014). Compaction creates morula staged embryos, which are defined by a morphogenetic event that results in the individual outlines of all embryonic blastomeres (cells) disappearing, due to the formation of functioning cell to cell adherens junctions (Kojima et al. 2014). In addition, the blastomeres begin to lose their totipotency, which is the ability to differentiate into all developmental cell types (Chazaud and Yamanaka 2016). Compaction thus initiates the process of developmental cell fate determination and cell differentiation (Chazaud and Yamanaka 2016). It is a

necessary prelude to blastocyst formation and ultimately embryo implantation. Summary of cleavage division during preimplantation development is displayed in **figure 1**.

1.1.2 Blastocyst Formation

Following compaction and morula formation, blastocyst formation or cavitation is initiated (Kojima et al. 2014). The blastocyst consists of a fluid-filled cavity, an outer cell layer known as the trophectoderm (TE), and an inner cell core known as the inner cell mass (ICM) (Frankenberg et al. 2016). Cavitation begins as a morula cavitates with fluid transport into the embryo via ion channels, resulting in the formation of a nascent fluid-filled blastocyst cavity (Kojima et al. 2014). The volume of the fluid within the cavity is controlled by the trophectoderm undergoing regulatory changes to retain or release fluid, thereby expanding or contracting the blastocyst (Wiley 1984). The blastomeres polarized during compaction express lineage-specific genes for TE or ICM development (Chazaud and Yamanaka 2016). The trophectoderm mediates embryo implantation by interacting with the uterine wall and eventually contributes directly to the placenta at implantation and as placentation events are initiated (Frankenberg et al. 2016). The inner cell mass consists of pluripotent cell types that represent the origin of the three primary germ layers (Chazaud and Yamanaka 2016). The timing from cavitation to implantation takes approximately 24 hours in the mouse (O'Farrell et al. 2004). Summary of blastocyst formation during preimplantation development is displayed in **figure 1**.

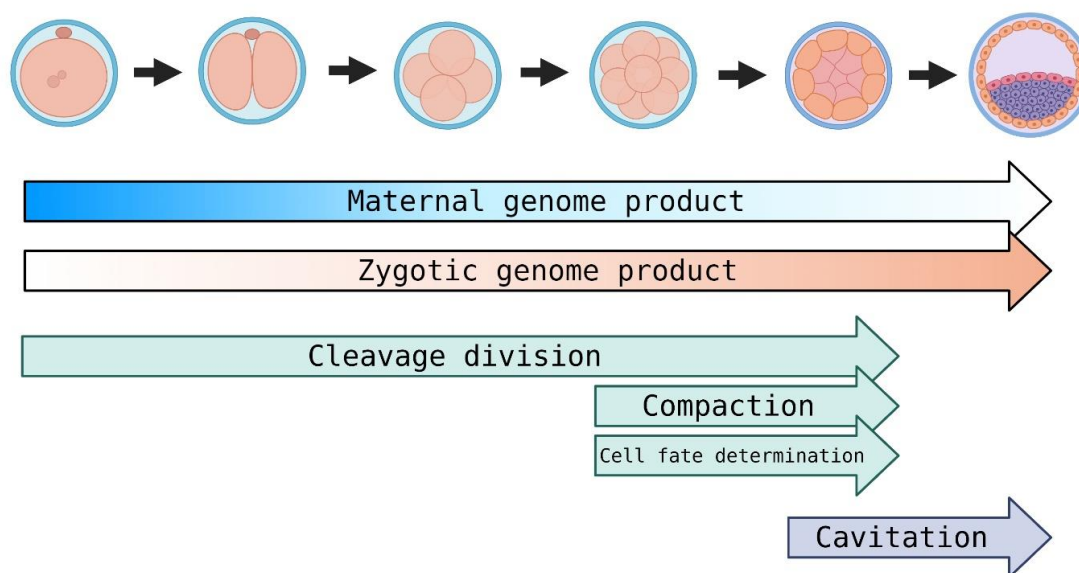


Figure 1. Summary of mammalian preimplantation embryo development and developmental events.

Mammalian preimplantation embryo development starts after fertilization of an oocyte by a sperm to form a zygote. The zygote undergoes cleavage divisions and compaction to eventually form a blastocyst. Main developmental events are displayed. Time of developmental events differ between each mammalian species. Maternal genome product diminishes over time as preimplantation embryos progress through each cell stages; zygotic genome product is gradually produced over time as the embryo progresses through preimplantation stages. Cleavage division occurs throughout development, from the 1-cell stage to the morula stage and beyond. At the 8-cell stage, compaction and cell fate determination occurs to prepare for blastocyst formation. Cavitation occurs at the morula stage as fluid-filled cavity is formed to create a blastocyst with trophectoderm and pluripotent inner cell mass. Created with BioRender.com.

1.2 Female Infertility

Infertility defines the inability of otherwise healthy human couples to achieve pregnancy within a year of unprotected intercourse. The World Health Organization (WHO) estimates that infertility affects 186 million individuals worldwide (World Health Organization). The global burden of disease study in 2017 identified that infertility prevalence rate significantly increased by 15 % from 1990 to 2017 (Sun et al. 2019). This study discovered that countries with high socioeconomic development, for example, Canada, had the highest increase in infertility rate in females. Roughly 16 % of Canadian couples experience infertility and at least 40 % of the time it is due to difficulties experienced by females (Public Health Agency of Canada). Female infertility is influenced by many factors including age, genetics, as well as lifestyle-related factors. Presently, the mean maternal age of first childbirth is 30 in European countries (Vander Borgh and Wyns 2018). Fertility declination correlates to maternal age and was reported to begin as early as 25 years of age (Eijkemans et al. 2014). Eijkemans *et al.* (2014) analyzed that age-related infertility exponentially increases from 4.5 % at age 25 to about 50 % at age 40, likely due to the loss of oocyte number and quality. Genetics could also predispose women of conditions and diseases that affect fertility, for example, polycystic ovary syndrome, that result in irregular ovulation pattern (Franks 2008). Lifestyle choices like smoking, alcohol, and drug consumptions are evidently factors for infertility that impairs reproductive functions (Vander Borgh and Wyns 2018).

1.3 Assisted Reproductive Technologies (ART)

As the infertility rate increases, many people turn to assisted reproductive technologies (ART) for their fertility needs. In 2010, the International Federation of Fertility Societies reported that there are at least 4400 ART clinics worldwide (Jones Jr. et al. 2011), with 37 ART clinics across Canada in 2019 (Canadian Fertility & Andrology Society). According to the Canadian Assisted Reproductive Technologies Register, more than 35,000 ART treatment cycles were initiated in 2019 and resulted in about 17,000 clinical pregnancies (Canadian Assisted Reproductive Technologies Registry (CARTR) Plus). Some of the ART interventions performed in 2019 were *in vitro* fertilization (IVF),

intracytoplasmic sperm injection (ICSI), intrauterine insemination (IUI), *in vitro* oocyte maturation (IVM), and frozen embryo transfer, to name a few.

1.4 Obesity

As classified by the World Health Organization (WHO), individuals with a body mass index (BMI) of 25 or more are considered overweight; and individuals with a BMI of 30 or more are considered obese. The WHO estimated that in 2016, more than half of the adults worldwide were overweight or obese (World Health Organization). Statistics Canada (2019) also reported that 63 % of Canadian adults were overweight or obese in 2018; 57 % of them are females within that population. Obesity is defined as a chronic disease by the Obesity Society (Jastreboff et al. 2019) resulting from an excess accumulation of lipid that leads to inflammation, perhaps metabolic disorder, and certainly stress in many parts of the body. It impairs vital bodily functions by placing stress on the cardiac system, weakening immunity, and disrupting endocrine functions (Conway and Rene 2004). High BMI levels are associated with a higher risk of cardiovascular disorder, according to the Framingham Heart study (Wilson et al. 2002). Analysis of the study identified a strong connection between increased risk for heart failure correlating with increasing BMI level, in which the risk of heart failure increases by 5 and 7 % for each increment of BMI levels in males and females, respectively (Kenchiah et al. 2002). Obesity also suppresses immunity. The analysis of the National Health and Nutrition Examination Survey III by the US Centers for Disease Control revealed associations between BMI levels and pulmonary infection rate (Ubags et al. 2016). Specifically, high levels of serum leptin, released by the accumulation of adipose tissue, increases risk for pulmonary infections by impairing neutrophil function (Ubags et al. 2016). Hyperleptinemia is also associated with an increased risk of death from pneumonia, as evident from the analysis of Influenza A pandemic in 2009 (Louie et al. 2011). These studies support the recent discovery that obesity predisposes COVID-19 patients to more severe symptoms (Sattar et al. 2020). Additionally, obesity disrupts endocrine functioning, namely insulin resistance. Elevated levels of glucose and free fatty acids in the circulation stimulates additional release of insulin by the pancreas to initiate glucose uptake (Lauterbach and Wunderlich 2017). Excessive release of insulin decreases

insulin sensitivity of the liver and peripheral muscles, eventually contributing to insulin resistance and metabolic diseases as a result (Lauterbach and Wunderlich 2017).

1.5 Obesity on Female Reproductive Health

Studies have clearly determined that obesity negatively affects reproductive health in both sexes, but in women, these effects include menstrual abnormalities (Seif et al. 2015), ovarian dysfunction (Nteeba et al. 2014), diminished oocyte quality (Hou et al. 2016), reduced endometrial sensitivity for implantation (Rhee et al. 2016), and overall significant reduction in pregnancy rate (Broughton and Moley 2017). Overweight and obese women have twice the likelihood of experiencing irregular menstrual cycles than healthy individuals (Wei et al. 2009). These women experience heavier menstrual bleeding, compared to normal and underweight women. (Mena et al. 2021). Additionally, obesity and high body fat percentage is significantly associated with mean menstrual cycle length of longer than 32 days compared to an average of 28 days in healthy individuals (Lay et al. 2021). Luteinizing hormone (LH), a gonadotrophin hormone that regulates the menstrual cycle and initiates ovulation of an oocyte, is implicated in these obesity related effects in women. A study of obese teenagers with abnormal menstrual cycles found a significantly higher LH pulse frequency than that of healthy-weight girls (Yoo et al. 2006). Another study of obese adult women identified a lower amplitude of LH secretion than normal-weighted women, although no difference in LH pulse frequency was observed in this study (Jain et al. 2007). Along with many others, these studies support that normal secretory pattern of gonadotrophin hormones like LH are implicated in women with high BMI levels. Normally, leptin production from adipose tissue stimulates the hypothalamic-pituitary-gonadal (HPG) axis that induces gonadotrophin-releasing hormone (GnRH) expression in the brain to produce LH at the gonads (Tsatsanis et al. 2015). Under obese conditions, high leptin levels from excess adipose tissue continuously stimulate the HPG axis and eventually lead to leptin resistance which disrupts regulation of GnRH and LH levels (Tsatsanis et al. 2015). Changes in gonadotrophin hormones from elevated body fat disrupt normal menstrual cycle, which contributes to reduced reproductive competency of obese women.

A meta-analysis identified that overweight and obese women (BMI > 25 kg/m²) experience significantly higher odds for miscarriage than women with normal BMI, regardless of the method of conception (Metwally et al. 2008). Elevated body fat levels disrupt ovarian functions by inducing inflammation and macrophage infiltration. Mice placed under a prolonged high fat diet displayed increased ovarian tissue inflammation and lowered pregnancy rate (Skaznik-Wikiel et al. 2016). In women undergoing IVF treatments, monocyte chemoattractant protein-1 (MCP-1) levels were positively correlated with rising BMI in serum and follicular fluid (Buyuk et al. 2017). MCP-1 is an important factor for the recruitment and infiltration of immune cells. Although MCP-1 is normally elevated during the menstrual cycle to support ovulation (Bornstein et al. 2004), obesity appears to increase MCP-1 expression at the ovaries aberrantly. It results in the infiltration of additional monocytes and contributes to inflammation of the ovaries, thus impacting normal ovarian functions (Buyuk et al. 2017). Studies have suggested that elevated leptin levels in obese women may lower endometrial receptivity for embryo implantation due to the regulatory role of leptin in endometrial cells (Gonzalez and Leavis 2001; Broughton and Moley 2017). However, the role of elevated leptin in pregnancy is controversial as studies are inconsistent with regards to reporting obesity-induced hyperleptinemia as a factor for miscarriage (Brewer and Balen 2010). The decline in oocyte developmental competency is the key way in which hyperlipidemia reduces chances of a successful embryo implantation.

Obesity also disrupts endocrine functioning of reproductive hormones that are vital for a successful pregnancy. Hyperandrogenism, defined as the elevated levels of ovarian androgens, such as testosterone, is common in obese women (Poddar et al. 2017). Corbould (2007) identified that the chronic exposure to testosterone impairs glucose metabolism in subcutaneous adipose tissue. The phosphorylation of protein kinase C zeta, downstream of the insulin receptor in adipose tissue, was inhibited, thus resulting in insulin resistance and alters glucose uptake in adipose tissue (Corbould 2007). Hyperandrogenism contributes to insulin resistance and adipose accumulation at the ovaries, which exacerbates the effects of obesity on women's reproductive health (Zeng et al. 2019). In addition to the change in testosterone level, estrogen levels are also affected by BMI. The previously mentioned study by Shah *et al.* (2011) observed a

significantly lower estradiol level in women with a high BMI than women with a normal BMI. The lowered estradiol level supports the occurrence of reduced oocyte fertilization in the high BMI group (Shah et al. 2011), as proper estrogen levels are essential to support healthy oocyte maturation.

Lastly, it is evident that women with higher BMI levels have higher levels of triglycerides, insulin, and lactate present in the follicular fluid (Robker et al. 2009). Investigations of women undergoing IVF treatments, with different follicular free fatty acid levels have discovered an important correlation between higher follicular free fatty acid levels and increased poor-quality oocytes (Jungheim et al. 2011). Women displaying higher follicular free fatty acids also have fewer normally fertilized oocytes compared to women with a normal BMI and they experience a 50 % lower chance of achieving a clinical pregnancy after IVF treatments (Shah et al. 2011).

Overall, obesity is detrimental to not only maternal reproductive health, but more specifically to oocyte and early embryonic developmental competency. Most obese women of reproductive age experience difficulties with conception (Vahratian 2008), even with the help of ART. Women with high BMI levels have much lower ART success which in parts results from reduced oocyte developmental competence, *in vitro* fertilization success, and overall lower live birth rates (Shah et al. 2011). However, the underlying mechanisms that lead to these effects of obesity on fertility largely remain to be discovered.

1.6 Lipid Metabolism

Lipid metabolism covers the biochemistry of lipid biosynthesis and degradation. Nutrients like carbohydrates and lipids from dietary sources are processed by gut microbiota to be taken up by intestinal cells (Schoeler and Caesar 2019). These nutrients are then transported from the intestine to the liver and other peripheral organs like adipose and muscle tissues for metabolism. Under nutrient-rich environments, carbohydrates are processed through glycolysis into acetyl-CoA. Then, after a series of reactions through the lipogenic pathway, fatty acids are generated (Ameer et al. 2014). In the liver, these fatty acids act as an energy source and provide structural components for

cellular membrane; while in the adipose tissues, fatty acids are synthesized through lipogenesis and stored as lipid droplets for long-term energy storage (Nguyen et al. 2008). Lipids from dietary sources are taken up by intestinal cells and converted to triacylglycerol (TAG) to be transported in the circulation inside a chylomicron (Mansbach and Siddiqi 2010). The transport of TAG in a chylomicron to the liver and peripheral lipid metabolic sites enables lipoprotein lipase in capillaries to hydrolyze TAG for subsequent oxidation or storage of the energy source (Karpe et al. 2011). Under starvation, the breakdown of TAG and lipoprotein storage in the liver occurs to provide energy for organ system functioning. Fatty acid oxidation, the process in which acetyl-CoA is produced from fatty acids through the β -oxidation, occurs in support of energy expenditure (Nguyen et al. 2008). Ketogenesis also occurs to oxidize fatty acids in the conversion of acetyl-CoA into ketone bodies as a quick strategy against energy starvation (Nguyen et al. 2008). Lastly, hepatic lipoproteins are transported to the hepatocyte membranes to release TAG into the circulation. The circulatory transport of TAG to other organs like muscle tissues results in the breakdown of TAG through lipolysis to provide energy for muscle activity (Nguyen et al. 2008).

1.7 Lipid Metabolism in Female Reproduction

As described, lipid metabolism is an important source of energy for cell physiology. It provides energy for many organ systems including the reproductive system. The developmental competency of oocytes is highly dependent on cumulus cells and their ability to utilize glucose or fatty acids through glycolysis and β -oxidation, respectively, as an energy source (Warzych and Lipinska 2020, Richani et al. 2021). Cumulus cells contribute largely, via gap junctions, to oocyte development by supplying most of the ATP and substrates like pyruvate that are required for energy expenditure (Richani et al. 2021). Oocytes can also generate ATP although mitochondria are pre-mature. Richani *et al.* (2019) showed that the production of ATP in denuded mouse oocytes occur via the adenosine salvage pathway, though the ATP production was at a much lower level. The utilization of fatty acids in oocytes and cumulus cells is also an important source of energy as the inhibition of β -oxidation of mouse cumulus-oocyte complex inhibits oocyte maturation and reduces blastocyst development (Dunning et al. 2010). Fatty acids are

stored as TAG in lipid droplets in the oocytes until oxidation for energy consumption (Bradley and Swann 2019). The amount and composition of lipid droplets in the oocyte changes throughout follicular development and differs between species (Bradley and Swann 2019). Clearly, fatty acid metabolism is required to provide sufficient energy substrates like NADH, FADH₂, GTP, and ATP to support oocyte maturation. The energy produced from lipid metabolism also supports development of an early embryo, especially during the earliest cleavage events. For example, oxidation of stored TAG liberates fatty acids and phospholipids that support the increase of cell membrane surface area throughout preimplantation development (Bradley and Swann 2019).

1.8 Non-esterified Fatty Acids (NEFA)

Obesity results from the accumulation of adipose tissue, which is reflected by the level of non-esterified fatty acids (NEFA) in the serum (Boden 2011). NEFAs are fatty acids released into the circulation from adipose tissues, as a result of lipolysis of TAG in the adipocytes (Karpe et al. 2011). The release of NEFA allows transport of fatty acids to other organs to produce energy. Another major source of NEFA in the circulation is dietary lipid intake. These lipid droplets are transported to the liver as TAG in chylomicrons and must be hydrolyzed into NEFA by lipoprotein lipase before taken up for long-term storage (Karpe et al. 2011). Although early literature suggested that an increase in adipose tissue mass leads to elevated levels of NEFA in the circulation (Opie and Walfish 1963), many studies have shown the opposite. For example, McQuaid *et al.* (2011) reported that obese individuals have a systemic NEFA concentration no different from lean individuals. The rate of lipoprotein lipase activity in obese individuals was in fact lowered, which actually reduces the levels of NEFA released from the adipose tissue (McQuaid et al. 2011). Karpe *et al.* (2011) also completed a systematic review of the literature prior to 2009 and found that plasma NEFA concentration is unrelated to body fat mass. However, while the reliability of serum NEFA levels as an estimation for obesity or body fat accumulation is questioned, the composition and relative ratios of varying NEFAs in the circulation of obese individuals likely reflect the degree of negative effects related to the obese environment.

The follicular NEFA composition and ratios varies across individuals. Fatty acids in the circulation are transported to the ovaries and follicular fluid. Then the fatty acids are taken up by cumulus cells and transported into oocytes through fatty acid binding proteins in the cumulus cell-oocyte gap junctions (Aardema et al. 2019). Multiple studies reporting analyses of oocyte follicular fluids have found varying composition of fatty acids based on different diet composition and variation in tissue metabolic rate differences (Bradley and Swann 2019). However, analysis of human follicular fluids identified that approximately 45 % of total NEFAs are palmitic acid (PA) and oleic acid (OA) (Valckx et al. 2014). These free fatty acids are at an even higher circulatory concentrations in people who are overweight and obese compared to normal BMI individuals (Valckx et al. 2014).

NEFAs can be categorized into two main categories – saturated fatty acids and unsaturated fatty acids. Saturated fatty acids are fatty acids with no double-bonds between their carbon chain, whereas unsaturated fatty acids are fatty acids with at least one double-bond between their carbon chain. PA and OA are the most abundant saturated and non-saturated NEFAs, respectively, in the circulation, estimating at 23 % and 31 % of total NEFA, respectively of normal-weight subjects (Valckx et al. 2014).

1.9 Palmitic Acid (PA)

1.9.1 Structure and Source of PA

Palmitic acid (16:0; PA) is a 16-carbon saturated fatty acid. It can be synthesized in the body *de novo* through lipogenesis from other macromolecules and it is also be ingested in the diet (Carta et al. 2017). PA is abundant in palm oil, meat, and dairy products. Under nutrient-rich conditions, PA concentration is tightly controlled by desaturation to other unsaturated fatty acids like palmitoleate (16:1) for long-term lipid storage (Strable and Ntambi 2010). However, with an imbalance of PA homeostasis, implications in metabolism occurs leading to metabolic syndromes like insulin resistance and even cancer (Carta et al. 2017).

1.9.2 The Effect of PA on Embryo Development

The effects of PA on bovine and mouse preimplantation embryo development are previously described in the literature. PA is one of the major fatty acids making up approximately 25 % of total NEFA present in bovine follicular fluid (Leroy et al. 2005). A study by Aardema *et al.* (2019) reported a lowered uptake of PA compared to control in bovine oocytes. Lipid droplet sizes and numbers were also significantly smaller in PA-treated oocytes (Aardema et al. 2019). Additionally, oocyte maturation after fertilization was greatly reduced in a dose-dependent manner after PA-exposure (Aardema et al. 2011). Leroy *et al.* (2005) reported that *in vitro* maturation bovine oocytes in medium containing PA results in a significantly lower fertilization rate compared to control. Oocyte maturation was also disrupted by the presence of PA in the culture media, as a significantly higher percentage of oocytes experienced delayed progression through meiosis (Leroy et al. 2005). Furthermore, the effects of PA on bovine embryos investigated by Van Hoeck *et al.* (2011) found that high PA culture medium significantly lowered blastocyst development as well as increased apoptotic cell ratio. We have reported similar effects in mouse preimplantation development recently. After *in vitro* incubation of mouse embryos at the 2-cell stage in PA supplemented culture medium, Yousif *et al.* (2020) demonstrated impairments of mouse blastocyst development in a dose-dependent manner. Furthermore, it was identified that PA upregulated ER stress markers at the transcript level, providing evidence that exposure to elevated PA may induce cell stress that impairs mouse preimplantation development (Yousif et al. 2020). A similar study by Jungheim et al. (2011) reported a reduced cell count in mouse blastocysts after *in vitro* incubation with PA for 30 hrs. The researchers also identified a significantly upregulated Insulin-like growth factor type-1 receptor (IGF-1R) and glutamic-pyruvate transaminase 2 (GPT2) protein expression, which may contribute to abnormal insulin signaling in these embryos. When the PA-treated blastocysts were transferred into pseudo-pregnant female mice and grown to birth, those embryos developed into significantly smaller fetuses than the fetuses from control embryos (Jungheim et al. 2011). Although fetuses from PA-treated embryos were possibly growth-restricted, a catch-up growth pattern was observed, and those fetuses eventually grew heavier than control fetuses on day 50 (Jungheim et al. 2011). These findings imply that

PA exposure alone can lead to metabolic changes in the offspring, which shows relevancy to insulin resistance in obese individuals.

1.9.3 The Effects of PA on Other Cell Types

The effects of PA treatment on somatic cell types are extensively investigated. A study by Staiger *et al.* (2004) demonstrated the effects of PA treatment on cardiac cells by the expression of the inflammatory marker, interleukin-6 (IL-6). The researchers identified that PA induced significant increases in IL-6 mRNA and protein expression in coronary artery endothelial cells and coronary artery smooth muscle cells *in vitro* (Staiger *et al.* 2004). Additionally, a significant positive correlation between PA and IL-6 concentration in the circulation of non-diabetic individuals was observed (Staiger *et al.* 2004). These findings revealed that a high level of PA in the circulation contributes to cardiovascular inflammatory responses and potentially heightens the risk of cardiovascular diseases, as seen in diets with high saturated fats (Sacks *et al.* 2017). A PA-rich diet negatively affects pulmonary cell types as well. Chu *et al.* (2019) identified that a high PA diet increases the risk of lung fibrosis and mortality in mice. It was revealed that in mouse lung epithelial cells, PA treatment induces protein expression of ER stress pathway constituents and leads to apoptosis, which may explain the fibrotic phenotype observed *in vivo* (Chu *et al.* 2019). As lipid metabolism takes place in the liver, there is no doubt that PA levels can impose a negative effect on hepatic cells. Joshi-Barve *et al.* (2007) exposed HepG2 cells to excess PA to induce PA accumulation in the hepatocytes. The accumulation of PA in the hepatocytes induced significant increases in mRNA and protein expression of the inflammatory marker interleukin-8 (IL-8) (Joshi-Barve *et al.* 2007). It was suggested that enhanced IL-8 expression in the hepatocyte contributes to inflammation, which potentially plays a role in liver steatosis and liver diseases in obese individuals. Once again, it was demonstrated that PA induces inflammatory responses that contribute to severe pathophysiological conditions in multiple systems of the body.

1.10 Oleic Acid (OA)

1.10.1 Structure and Source of OA

Oleic acid (18:1; OA) is an 18-carbon monounsaturated fatty acid. It is a major component of olive oil, make up to 83 % of olive oil's total composition (Marcelino et al. 2019). Like PA, OA can be synthesized *de novo* through lipogenesis and thus dietary intake is not deemed a necessity. However, the recent increase in popularity of the Mediterranean diet places an emphasis on the beneficial effects of ingesting unsaturated fatty acids like OA. Recent research efforts have identified the Mediterranean diet, which consists of mostly fruits and vegetables, as well as the consumption of extra virgin olive oil as a main source of fats, reduces the risk of chronic diseases and mortality (Tosti et al. 2018). With promising results from multiple randomized clinical trials, the American Heart Association recommends lower intake of saturated fats and replacing fat intake with unsaturated fats to lower the risk of cardiovascular events (Sacks et al. 2017).

1.10.2 The Effects of OA on Embryo Development

Among the many NEFAs, OA is another major type of fatty acids found in the reproductive system, including the follicular fluid. It is estimated to make up approximately 30 % of total NEFA in bovine follicular fluid (Leroy et al. 2005). A study by Aardema *et al.* (2011) investigated the effects of OA treatment on bovine oocyte developmental competency and lipid metabolism. OA had no negative effect on oocyte maturation and *in vitro* exposure to OA simply increased lipid droplet sizes and numbers in the oocytes (Aardema et al. 2011). It was also indicated that OA was primarily metabolized into its subsequent products from β -oxidation or processed as TAG for long-term storage (Aardema et al. 2011). Similarly, Leroy *et al.* (2005) reported that *in vitro* incubation of bovine oocytes with OA had no significant effects on oocyte maturation as well as blastocyst development after fertilization. Another study of bovine embryos with exogenous medium supplementation with OA indicated a significant increase in cleavage rate at the 2-cell stage as well as a significant increase in blastocyst development (Karaşahin and Arıkan 2015). Generally, it is concluded that OA has no discernable negative impact on oocyte and early mammalian embryo developmental competency.

Recently, Yousif *et al.* (2020), from our laboratory, investigated the dose-dependent effects of OA up to 500 μ M on developing mouse preimplantation embryos and observed no significant impairments in blastocyst development at any tested dose. Cell morphology at all preimplantation cell stages was unaffected as well (Yousif *et al.* 2020). No differences were observed in ER stress mRNA transcript levels in OA-treated embryos; but it was noted that OA treatment significantly enhanced lipid droplet accumulation (Yousif *et al.* 2020). These findings shine light on the underlying lipid metabolism mechanism that may contribute to the protective effects of OA exposure on various cell types including the preimplantation embryo.

1.10.3 The Effects of OA on Other Cell Types

OA is described to have beneficial effects to many cell types. For example, it is protective against myocardial injuries, as demonstrated by Singh *et al.* (2020). After myocardial damage, rats that were pre-treated with OA showed a significant improvement in lipid profiles, as well as cardiac injury biomarkers compared to controls (Singh *et al.* 2020). It was identified that pre-treatment with OA prior to myocardial injury induction upregulated gene expression of a reactive oxygen species (ROS) regulator, UCP-2, as well as increased antioxidant activity in the cardiac tissues (Singh *et al.* 2020). One of the notable benefits of OA included its anti-tumor effects. In the search of a healthier diet, the Mediterranean diet was proposed as a cancer risk-reducing diet, due to its high content of antioxidant and anti-inflammatory properties from (though not limited to) OA-rich foods (Mentella *et al.* 2019). The inclusion of high OA in the diet significantly reduces the susceptibility to colon cancer in a male rat cancer model (Schwartz *et al.* 2004). Rats that were fed high OA diet had less cancerous lesions in the colon tissue compared to rats with low OA diet (Schwartz *et al.* 2004). It was further explained that high OA content significantly lowered expression of COX-2, an inflammatory marker, and increased apoptotic activity in the cancerous tissue (Schwartz *et al.* 2004). The combination of high OA diet and an anti-tumor drug even showed synergistic effects against colon cancer incidence, highlighting the advantages of including OA intake as a therapeutic option (Schwartz *et al.* 2004). A literature search on the anti-tumor effects of OA summarized the underlying effects of OA on oncogene

expression (Carrillo et al. 2012). Notably, Menendez *et al.* (2005) identified that OA suppressed the over-expression of HER2, an oncogene noted for progression and metastasis of numerous human cancers, in breast cancer cell lines. The addition of OA to Herceptin, a chemotherapy medication for cancer, had synergistic effects that reduced Her-2 expression and enhanced apoptosis in breast cancer cells (Menendez et al. 2005). These findings show strong support for the benefits of OA in cancer prevention and tumor suppression. In the liver, OA plays an important role in normal hepatic functioning. Inhibition of OA *de novo* synthesis in the liver, by genetic knockout of hepatic lipogenesis protein SCD1, demonstrated low lipid accumulation with severe hepatic damage in mice fed with low-fat diet (Flowers et al. 2006). These mice had increased levels of bilirubin and bile acid in the serum, demonstrating cholestasis phenotypes that are common in patients with jaundice and liver failure (Flowers et al. 2006). A follow-up analysis of gene expression in the liver identified an enhancement of ER stress and inflammation that contributed to the hepatic damage observed in those mice (Flowers et al. 2008). However, when supplemented with OA in the diet, hepatic function was restored and lipid accumulation, except for plasma cholesterol levels, returned to normal states (Flowers et al. 2006).

1.11 Palmitic Acid (PA) and Oleic Acid (OA) Co-treatment

1.11.1 PA and OA Co-treatment on Embryo Development

The protective ability of OA on embryo development has sparked interest in its effects when presented with saturated fatty acids that are generally believed to be harmful. Common consensus from the literature would suggest that a higher unsaturated-to-saturated fatty acid ratio should provide benefits to preimplantation embryo development. In bovine oocytes, Aardema *et al.* (2011) investigated the effect of OA co-treatment with saturated fatty acids, PA, and stearic acid (SA), on oocyte developmental competency and lipid metabolism. It was reported that although PA and SA, individually, had adverse effects on oocyte maturation in a dose-dependent manner, the addition of OA with each saturated fatty acid alleviated the adverse effects and restored developmental competency (Aardema et al. 2011). Furthermore, the combination of OA with each saturated fatty acid showed significantly greater lipid droplet accumulation (size and number), in bovine

oocytes than compared to PA and SA individually, highlighting the change in lipid storage as a potential mechanism of the compensatory effects of OA (Aardema et al. 2011). The hypothesis that OA counteracts PA-induced effects are also supported in murine embryos. Yousif *et al.* (2020) reported that incubation of mouse embryos in PA and OA combined, supplemented culture medium restored blastocyst development to control levels, compared to the significant developmental arrest observed in the PA-alone group. Furthermore, the rescuing effects of OA in the combination treatment beneficially affected ER stress pathway gene expression at the IRE1- α and PERK arm, lipid metabolism, as well as mitochondrial ROS levels, by reversing PA-induced effects to control levels (Yousif et al. 2020). Although OA is well-recognized for its protective effects, its abilities may be limited when exposed to a high proportion of saturated fatty acids. The study by Van Hoeck *et al.* (2011) investigated the effect of PA, SA, and OA co-treatment on bovine oocyte and embryo development. When bovine oocytes were treated with PA, SA, and OA in combination at a high saturated-to-unsaturated fatty acid ratio prior to fertilization, blastocyst development was significantly lower than the supplemented control (Van Hoeck et al. 2011). Additionally, the total cell number and apoptotic cell index of those embryos were significantly lower and higher, respectively, in the co-treatment (Van Hoeck et al. 2011). These findings support that OA can, in fact, counteract the effect of PA in early embryo development; however, the protective mechanism can still be overwhelmed, or even fail, when exposed to especially high proportions of saturated fatty acids.

1.11.2 PA and OA Co-treatment on Other Cell Types

The effects of PA and OA co-treatment on hepatocytes have been extensively studied as the liver is the main site of lipid metabolism. Chen *et al.* (2018) investigated the protective effects of PA and OA combination treatment on hepatocytes. In human HepG2 cells, the authors reported that *in vitro* culture with OA alleviated the PA-induced impact on hepatocyte viability at a 2:1 PA-to-OA molar ratio, which the presence of OA in PA culture media significantly reduced apoptosis compared to PA-alone treatment (Chen et al. 2018). Though, the benefit of OA inclusion was time-dependent where OA supplementation after 24 hours of PA-only treatment was unable to rescue hepatocyte

viability to control levels (Chen et al. 2018). It was suggested that OA exerts its protective mechanism on PA-induced effects by lowering cell stress, inflammation, and restoring mitochondrial functions (Chen et al. 2018). These findings were paralleled by primary rat hepatocytes under the same molar ratio of PA and OA co-treatment in the same study (Chen et al. 2018). Another major site of lipid metabolism is the skeletal muscle. A study by Peng *et al.* (2011) reported the changes in lipid metabolism by PA and OA treatments, *in vitro*, in mouse C2C12 myocytes. Like other studies, the authors reported that OA treatment resulted in larger lipid droplets than PA treatment alone (Peng et al. 2011). The outcomes indicated that significantly more PA was stored as TAG lipid droplet in the presence of OA compared to PA-alone treatment (Peng et al. 2011). Consistently, the conversion of PA into phospholipids and diacylglycerol (DAG) lipid droplets was significantly lowered in the presence of OA (Peng et al. 2011). Along with the findings that OA protects against ER stress in myocytes caused by PA effects, it was stated that OA prevents lipotoxicity of myocytes by mediating ER stress through alternate processing of excess lipids (Peng et al. 2011).

1.12 Cell Stress in Preimplantation Embryos

During embryogenesis, the growing embryo experiences various types of stress. These stress factors can be categorized into two main categories, local and environmental stress. The source of local stress on the embryo includes oxidative stress and inflammation among many others. Whereas environmental stress factors include maternal hormone and toxins (Puscheck et al. 2015). Embryo manipulation and growth *in vitro* also poses additional stress during embryogenesis through handling and culture conditions, to name a few. Ultimately, the embryo must utilize its capacity to adapt and offset exposure to stressors to achieve and maintain high developmental capacity.

One of the main factors for stress during embryogenesis is energy expenditure. A large amount of energy is required to support the exponential growth in cell number and division during the early cleavage stages. After fertilization, the developing embryo at the early stages utilize ATP from mitochondrial oxidative phosphorylation of pyruvate (Dumollard et al. 2007). Pyruvate is supplied by surrounding cumulus cells and follicular fluid to be taken up into the oocyte mitochondria (Bradley and Swann 2019). It is not

until after compaction at the 8-cell stage, in the mouse, that energy production from glucose via glycolysis is favored over pyruvate oxidation, with accompanying increased oxygen consumption (Leese and Barton 1984). Preimplantation embryo oxygen consumption is significantly lower in the early cleavage stages compared to the blastocyst stage, indicative of a low level of aerobic metabolism at the early stages (Leese et al. 2016). The quiet embryo hypothesis proposed by Leese (2002) suggests that instead of inactivity, mitochondria of the embryo at early stages function at a minimal level to provide just enough energy to meet its energy requirements. This hypothesis has been widely accepted as it nicely provides a sound reason behind low energy metabolism in early embryos – to minimize reactive oxygen species (ROS) production from direct pyruvate oxidation (Bradley and Swann 2019). ROS is an oxygen substrate that can cause oxidative damage to organelles and DNA. A study by Dumollard *et al.* (2017) reported that under high pyruvate environment in culture, mouse embryo blastocyst development was negatively impacted. It is further explained that the excess source of energy metabolite pyruvate may contribute to ROS production that disrupts blastocyst development (Dumollard et al. 2017).

Another source of energy expenditure comes from fatty acid oxidation. Fatty acids are taken up by embryos at the earliest stages as an energy source. In fact, fatty acids are taken up as early as an oocyte through the surrounding cumulus cells and follicular fluid. These lipids are converted into TAG by diacylglycerol acyltransferase (DGAT) enzyme to be stored as lipid droplets in the oocyte and embryo in the cytoplasm and endoplasmic reticulum (ER) (Bradley and Swann 2007). A study applied to porcine preimplantation embryos reported a significant decrease in lipid droplet volume at the blastocyst and late-blastocyst stages compared to other developmental stages (Romek et al. 2009), indicating a potential utilization of fatty acids as an energy source at the blastocyst stage.

Although embryos can metabolize lipids, a high fat environment is detrimental to preimplantation embryo development, as mentioned in the previous sections. Follicular fluids of mothers with high BMI levels tend to have higher concentrations of free fatty acids and triglycerides (Robker et al. 2009). High lipid contents taken up by the oocytes from the follicular fluid produce ROS and lipid peroxides that lead to lipotoxicity

(Igosheva et al. 2010). Many organelles including the mitochondria and ER experience structural remodeling and dysfunction due to lipotoxicity that ultimately induce apoptotic cell death (Wu et al. 2010). Lipotoxicity-induced dysregulation of the ER can also promote an imbalance in ER protein folding, resulting in the accumulation of unfolded proteins and activation of ER stress response mechanisms. The unfolded protein response (UPR) is activated to maintain ER homeostasis by removing unfolded proteins and preventing further protein production (Lin et al. 2019). Under prolonged ER stress, cells may opt to activate apoptosis to eliminate additional cell stress or perhaps autophagy (Lee et al. 2015), to restore ER homeostasis.

1.13 Autophagy

Autophagy is a cellular degradation pathway that is highly conserved in eukaryotes (Ravanan et al. 2017). In brief, it is a pathway in which cytoplasmic components in the cells are degraded by lysosomes for reuse in other cellular functions (Ravanan et al. 2017). Autophagy serves many different functions, including organelle clearance, regulation of development, as well as stress adaptation (Mizushima 2005). Autophagy is widely recognized as a pro-survival mechanism due to its protective functions and its involvement with mediating cell stress, specifically with ER stress (Lee et al. 2015). As mentioned, ER stress activates the UPR pathway that aims to maintain ER homeostasis. The UPR functions to upregulate the activity of protein degradation in the ER but would also upregulate autophagy to clear the ER from the accumulation of misfolded or unfolded proteins. Ogata *et al.* (2006) reported that inhibition of ER stress at the IRE1 and JNK pathway inhibited ER stress-induced autophagy in human neuroblasts cells, suggesting a strong link between ER stress and autophagy in cell survival. In addition to the ER stress mechanism mentioned earlier, autophagy can be triggered by many other factors like nutrient starvation and ROS buildup (Mizushima 2007). Autophagy can be described as a three-step process consisting of initiation, maturation, and degradation.

1.13.1 Initiation of Autophagy: Autophagosome Formation

Under normal conditions, autophagy induction is negatively regulated by the mammalian target of rapamycin (mTOR), in which mTOR phosphorylates its downstream UNC-51-

like kinase 1 (ULK1) complex to block autophagy initiation (Lee et al. 2015). Nutrient-rich environments and growth factor signaling converge on mTOR activation to promote growth (Saxton and Sabatini 2017). Summary of the process of inactivated autophagy is displayed in **figure 2**.

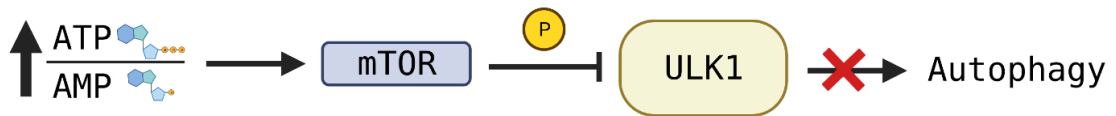


Figure 2. Summary of inactivated autophagy under nutrient-rich conditions.

Under nutrient-rich conditions, the ratio of ATP to AMP is high, which enables growth factor signaling to converge on mTOR activation. The activation of mTOR protein phosphorylates ULK1 complex and deactivates ULK1, inhibiting autophagy. Created with BioRender.com.

However, under nutrient-deprived or stress conditions, mTOR activity is suppressed (Lee et al. 2015). For example, the low energy condition is reflected by a high AMP-to-ATP ratio, which results in AMP-activating protein kinase (AMPK) inhibiting mTOR and activation of autophagy (Lee et al. 2015). Inhibition of mTOR dephosphorylates downstream ULK1 complex, leading to its activation. Activated ULK1 complex, along with autophagy-related protein ATG13, phosphorylate and activate downstream effectors of the class III phosphatidylinositol 3-kinase (PI3K) complex (Melia et al. 2020). The PI3K complex consist of factors like activating molecule in Beclin-1-regulated autophagy 1 (AMBRA1) and Beclin-1 (Bcln1). AMBRA1 is the connector protein that binds Beclin-1 and PI3K at the dynein complex until autophagy is initiated (Melia et al. 2020). The activation of ULK1 phosphorylates AMBRA1 to allow translocation of the PI3K complex to the ER for autophagosome formation (Cianfanelli et al. 2015). Additionally, Ambra1 regulates autophagy by stabilizing the activity of ULK1 (Nazio et al. 2013). Bcln-1 is an important mediator for autophagy as the chemical induction of Bcln-1 cleavage by caspase-3 inhibits autophagy as previously reported by Zhu *et al.* (2010). The activation of Bcln-1 dissociates itself from B-cell lymphoma 2 (Bcl-2), which activates Bcl-2 for anti-apoptotic functions to support the pro-survival nature of autophagy (Hill et al. 2018). The activation of PI3K complex produces phosphatidylinositol-3 phosphate (PI3P), which initiates the nucleation of a phagophore, a pre-autophagosome structure at the ER (Noda et al. 2010). The elongation of the phagophore involves recruitment of lipids to extend and form a double membrane autophagosome. The calculation by Melia *et al.* (2020) estimated that over 100 million lipid molecules are required per cell to support autophagosome formation. The presence of PI3P on the autophagosome membrane also recruits protein complexes for membrane elongation (Melia et al. 2020). The ATG5-ATG12-ATG16 complex is recruited to specific sites on the autophagosome membrane, though these binding sites are of unclear origin. Mizushima *et al.* (2001) identified these sites as crescent-like membrane-bound compartments in autophagosomes where ATG5 binds; nevertheless, very little is known about these structures. The ATG5-ATG12-ATG16 complexes on the autophagosome membranes contribute to autophagosome curvature and to recruit activated microtubule-associated protein light chain 3 (LC3) (Melia et al. 2020). LC3 is a marker for

autophagosome formation as it binds to both the inner and outer membranes of the autophagosome (Kabeya et al. 2000). LC3 is first translated in the cell as a precursor. Through ATG4 processing at the carboxylic terminal, LC3 is activated into its cytosolic form LC3-I (Agrotis et al. 2019). With ATG3 and ATG7, a phosphatidylethanolamine (PE) is conjugated onto LC3-I to create LC3-II, which can then be recruited onto autophagosome membranes by the ATG5-ATG12-ATG16 complex (Agrotis et al. 2019). LC3-II is widely accepted as a marker for autophagosome formation because its generation is initiated by autophagy induction, and it is degraded along with autophagosome contents (Singh and Bhaskar 2019). The elongation of the phagophore eventually seals the membranes and creates an autophagosome.

Autophagosome contents are quite random and non-discriminatory (Ravanan et al. 2017). However, some selective degradation products have been identified. It was proposed that LC3-II in the inner membrane can interact with and recognize P62/SQSTM1 adaptor proteins that bring in ubiquitinated proteins for degradation (Lamark et al. 2017). Additionally, neighbour of BRCA1 gene 1 (NBR1) is described to direct ubiquitinated protein aggregates into autophagosomes by binding to LC3-II of the inner membrane, independent of the P62 mechanism (Kirkin et al. 2009). Summary of the process of autophagosome formation is displayed in **figure 3**.

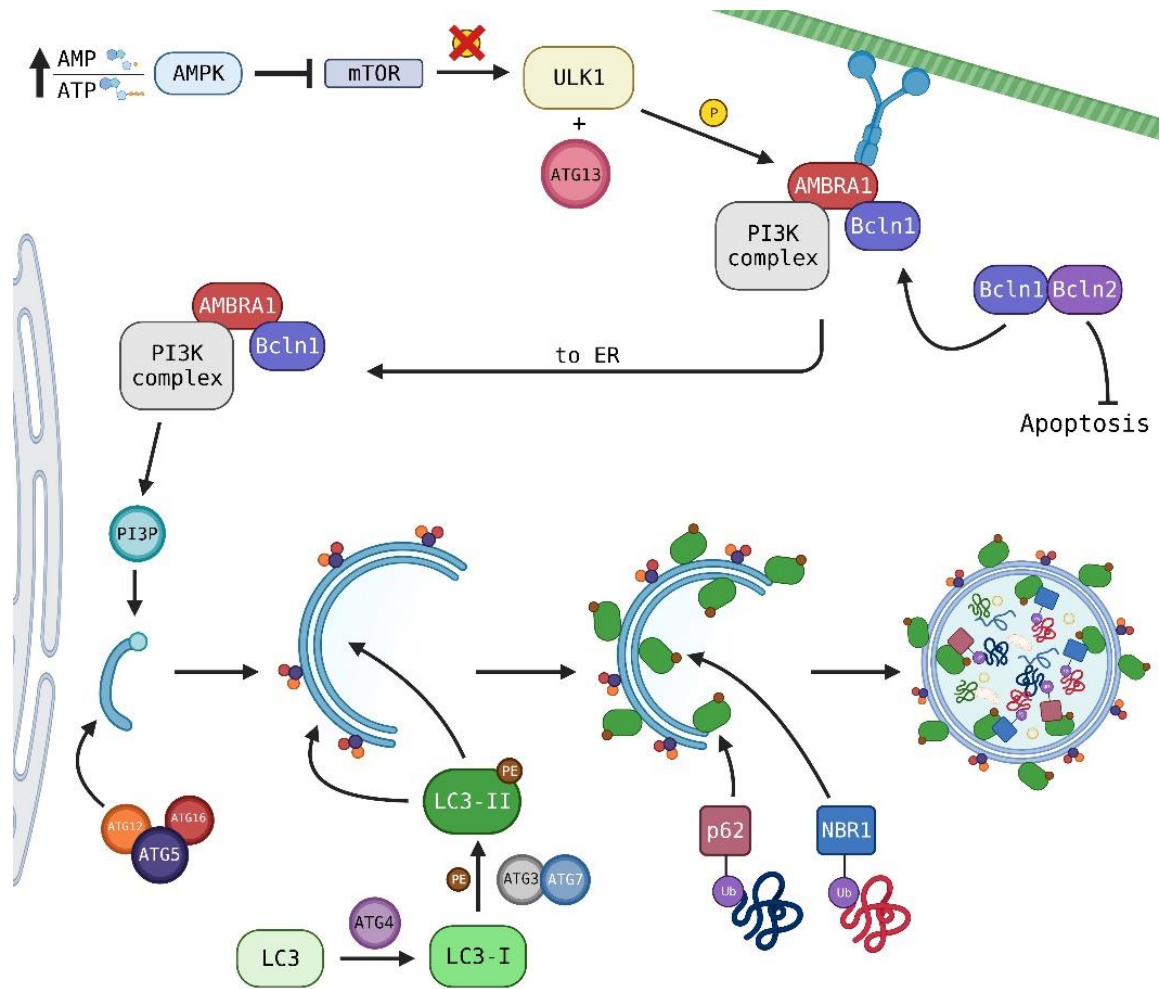


Figure 3. Summary of autophagosome formation.

Under nutrient-deprived conditions, the ratio of AMP to ATP is high, it activates AMPK to inhibit mTOR activity. Inhibition of mTOR prevents phosphorylation of ULK1 complex and activates autophagy. Activated ULK1, along with ATG13, phosphorylate AMBRA1 that is attached to the microtubule network via a dynein motor unit. The activation of autophagy also dissociates Bcln1 from Bcl-2, freeing Bcl-2 to prevent apoptosis and allow Bcln1 to join AMBRA1 and the rest of PI3K complex at the microtubule network. The phosphorylation of AMBRA1 frees the entire PI3K complex to translocate to the ER. Once at the ER, the PI3K complex produce PI3P that initiates nucleation of a phagophore. Then, the ATG5-ATG12-ATG16 complex associates and attaches onto the phagophore as the phagophore elongates to form an autophagosome.

The ATG5-ATG12-ATG16 complex then recruits activated LC3-II to both the outer and inner membranes of the autophagosome. Processing of LC3 via ATG proteins and lipidation with PE activates LC3 into LC3-II. LC3-II proteins on the inner membrane recruit p62 and NBR1 attached to ubiquitinated proteins to bring in autophagosome contents. As contents are directed into the phagophore, elongation of the membrane eventually seals the membrane and creates an autophagosome. Created with BioRender.com.

1.13.2 Autophagosome Maturation: Autolysosome

After the completion of the autophagosome, fusion with a lysosome is necessary for degradation of the contents. To do so, autophagosomes must dissociate from the ER and enter the cytoplasm to interact with a lysosome. The transport of an autophagosome in a mammalian cell requires the cytoskeletal microtubules (Zhao and Zhang 2019). Interestingly, in primary mouse dorsal root ganglion neurons, Maday *et al.* (2012) reported the unidirectional movement of distal autophagosomes towards the cell body via dynein units on microtubules. Another study by Köchl *et al.* (2006) chemically disrupted the microtubule network in primary rat hepatocytes and found a lower percentage of mature autophagosomes than control, as reflected by a lower co-localization rate of autophagosomes and lysosomes. These studies describe a role for microtubule networks in autophagosome transport. Two different hypotheses were proposed for the attachment of the autophagosomes to microtubules. One being that LC3-II on the outer autophagosome membrane directly binds onto microtubules, as antibodies against LC3-II N-terminus prevented autophagosome trafficking towards lysosomes (Kimura *et al.* 2008). Another hypothesis is that Rab7, a GTPase protein located on the late endosomes and lysosomes, recruits the dynein motor units attached to autophagosomes and thus contributes to its transport towards lysosomal structures (Jordens *et al.* 2001); however, evidence is scarce.

The autolysosome defines the structure of the autophagosome after lysosome fusion. This fusion occurs in a stepwise fashion, with acquisition of different lysosomal membrane proteins and hydrolases at each step (Zhao and Zhang 2019). First, autophagosomes fuse with early endosomes. Fusion of autophagosomes with early endosomes is required prior to fusion with lysosomes for proper content degradation to occur during autophagy; however, this fusion does not result in the formation of an acidic lumen or for the necessary proximity for degradation by proteases (Razi *et al.* 2009). Next, autophagosomes fuse with late endosomes and lysosomes. The fusion between autophagosomes and lysosomes require Rab GTPases, membrane-tethering proteins, and soluble N-ethylmaleimide-sensitive factor-attachment protein receptor (SNARE) proteins (Zhao and Zhang 2019). Rab7 protein is the main coordinator of the fusion process in

which it localizes onto specific sites of the autophagosome membrane (Zhao and Zhang 2019). Then, membrane-tethering proteins called the homotypic fusion and vacuolar protein sorting (HOPS) complex are recruited to Rab7 sites to attach the SNARE proteins on both the autophagosome and lysosome for the fusion event (Ganley 2013). The interaction of the SNARE proteins brings the autophagosome and lysosome together, allowing the fusion event to create the autolysosome. Summary of the process of autophagosome maturation is displayed in **figure 4**.

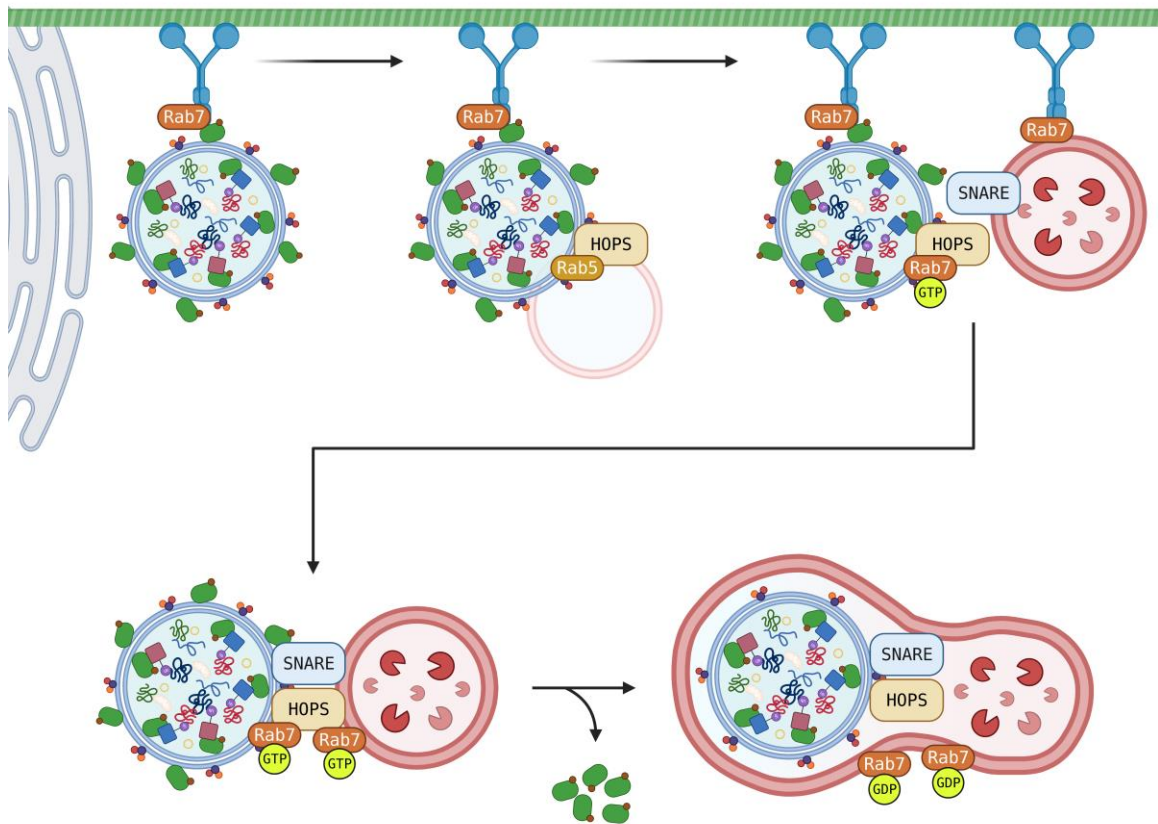


Figure 4. Summary of autophagosome maturation.

After autophagosome formation, the autophagosome is transported from the ER to the lysosome for maturation into an autolysosome. An autophagosome is transported through the cell via the microtubule network with a dynein motor protein. The autophagosome is first fused with an early endosome. Then, the autophagosome is transported towards the lysosome as Rab7 GTPase on the lysosome recruits the dynein protein. When the autophagosome is in near proximity of the lysosome, Rab7 GTPase localizes to the HOPS complex and recruits SNARE proteins to attach the autophagosome with the lysosome. After attachment, hydrolysis of the GTP to GDP on the Rab7 GTPase provides energy for the fusion of autophagosome and lysosome, creating an autolysosome. Created with BioRender.com.

1.13.3 Autophagosome Degradation with Lysosomes

After fusion of the autophagosome with a lysosome, autophagosome contents are degraded by lysosomal hydrolases. This degradation process degrades organelles and proteins into monomeric units like lipids and amino acids (Mizushima 2007). The degraded contents are then exported out into the cytoplasm for reuse in other cellular functions (Mizushima 2007). Little is known about lysosomal transporters in mammalian cells. So far, only the lysosomal amino acid transporter 1 (LYAAT-1) has been identified for the exportation of amino acids from lysosome to the cytoplasm (Sagné et al. 2001). Summary of the process of autophagosome degradation is displayed in **figure 5**.

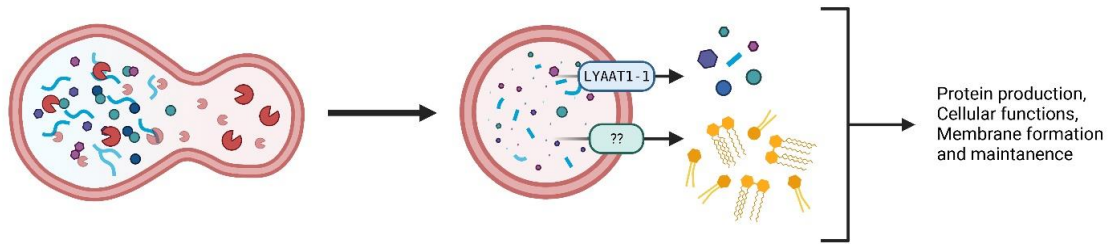


Figure 5. Summary of autophagosome degradation.

After the fusion event, autophagosome contents are degraded by lysosomal enzymes into monomeric units. The monomeric units are then transported out of the autolysosome via transporters like LYAAT-1. The monomeric units released into the cytosol are then reused for other cellular functions, like protein production, membrane formation, and cell maintenance. Created with BioRender.com.

1.14 Autophagy in Preimplantation Embryos

Autophagy was first reported to be essential for embryo preimplantation development by Tsukamoto *et al.* (2008). It was discovered that oocyte fertilization induces autophagy, and this induction is important for zygotic genome activation (ZGA) where maternal proteins are degraded as zygotic proteins are synthesized (Tsukamoto *et al.* 2008). In mouse embryos, deficient autophagic mechanisms arrest embryos at the 4- to 8-cell stages *in vitro*; whereas *in vivo* generation of *Atg5*-null mice die within one day of delivery (Tsukamoto *et al.* 2008). A study by Lee *et al.* (2011) investigated the effects of autophagy modulators on mouse preimplantation development. Under rapamycin (autophagy inducer) treatment, mouse embryos significantly increased apoptosis and displayed a significantly lower cell number than control, though blastocyst development was not impacted. Treatment of mouse embryos with 3-methyladenine (3-MA), an autophagy inhibitor, also resulted in a significant increase in apoptosis and lowered total cell count (Lee *et al.* 2011). Additionally, blastocyst development was decreased compared to control (Lee *et al.* 2011). Cell fate determination as reflected by ICM cell count was significantly higher after autophagy activation (Lee *et al.* 2011). These findings support that autophagy plays an essential role in early preimplantation embryo development, specifically in cell fate determination, achieving proper developmental competency, and even survival through the developmental stages. Some benefits following modulation of the autophagy pathway have been revealed in studies. For example, acute induction of autophagy with rapamycin significantly increased blastocyst development, TE cell number, as well as viability in *in vitro* produced bovine embryos (Song *et al.* 2012). Short-term induction of autophagy also relieved bovine embryos from ER stress, which may have contributed to the improvement in blastocyst viability observed in the study (Song *et al.* 2012). So far, no consensus is established regarding which direction of autophagy modulation is of most benefit for successful preimplantation embryo development and pregnancy. However, studies have highlighted the ability of autophagy modulation to improve early embryo development.

1.15 Autophagy in other cell types

Generally, autophagy acts to maintain homeostasis in a cell but its function and effects vary considerably across cell types and varying environmental conditions. Mizushima and Komatsu (2011) summarized the roles of autophagy in different organ systems. Autophagy exerts its function, ranging from preventing protein aggregation in the brain to preventing degeneration in the liver; as well as adaptation of heart cells to hemodynamic stress, to adaptation of pancreatic cells to high-fat diet, among many others (Mizushima and Komatsu 2011). Autophagy also has cytoprotective effects in various health conditions. In hepatocytes, a common genetic mutation of the hepatic glycoprotein, α -antitrypsin Z (α -ATZ), results in the accumulation of α -ATZ in the ER of the hepatocytes that eventually leads to chronic liver disease and even cancer (Kamimoto et al. 2006). It was suggested that autophagy plays a role in the clearance of the mutant α -ATZ protein from the ER in addition to other degradation pathways like the ubiquitin-proteasome system, and it contributes to alleviating hepatic injury from α -ATZ protein buildup (Kamimoto et al. 2006). In neurons, the neurodegenerative Huntington disease results from the polyglutamine tract mutation which accumulates huntingtin proteins as protein aggregates (Ravikumar et al. 2004). The study by Ravikumar *et al.* (2004) reported that mutation in the huntingtin protein induces autophagy in human and mouse brains as well as cell models of Huntington disease to clear toxic mutant fragments. The treatment of rapamycin, an inducer of autophagy, slows neurodegeneration in flies expressing the mutant huntingtin protein and resulted in smaller and less aggregate formation in a cell model expressing the mutant protein (Ravikumar et al. 2004). A mouse model of the Huntington disease also resulted in better performance in behavior and motor tasks when treated with a rapamycin analog compared to the placebo drug (Ravikumar et al. 2004). These findings show the direct effects of autophagy in neurodegenerative diseases and propose potential utilization of autophagy modulation as means of therapeutic options.

1.16 Lipotoxicity and Autophagy

The relationship between lipotoxicity and autophagy is a new research focus in that the first article investigating a connection between the two first appeared in 2009. The first

investigation assessed the effects of lipids on autophagy in skeletal muscle cells, though no effects were identified in altering apoptosis, autophagy, and lysosomal pathways (Turpin et al. 2009). Studies then shifted their interests in autophagic pathways of liver and pancreatic cells and identified that not only does autophagy play a role in regulating cell homeostasis, it also counteracts the lipotoxicity-induced stress in cells of diabetic mouse models, suggesting a potential protective mechanism of autophagy against lipotoxicity (Choi et al. 2009). However, evidence was conflicting as prolonged induction of autophagy can affect cell survival (Las and Shirihai 2010). Recent research efforts suggest that autophagy alleviates lipotoxicity effects, especially in the brain and the liver. In the brain, elevated fatty acid level accelerates oxidative stress that is associated with neurological disorders; but autophagy protects against this effect by eliminating ROS-generating organelles (Giordano et al. 2013). The study by Carotti *et al.* (2020) identified that non-alcoholic fatty liver disease (NAFLD) implicates lipophagy, a subset type of autophagy that specifically regulates lipid droplet degradation. This disruption is correlated with the abundance of autophagic marker expression of P62 as well as fibrosis stage in human and mouse with NAFLD (Carotti et al. 2020). Furthermore, exposure of hepatocytes to PA, triggered mTOR activation and induced expression of downstream targets that inhibit autophagy, whereas OA exposure had no effect on mTOR activity (Carotti et al. 2020). mTOR inhibitors initiate autophagy and attenuate PA-induced effects on hepatocytes including apoptotic cell death (Chen et al. 2020). It is therefore evident that lipotoxicity in hepatocytes following exposure to PA can be mediated by autophagic mechanisms.

1.17 Rationale

Previous studies have identified autophagy as an essential component to regulating cell homeostasis, cell growth and preimplantation development. Autophagy also has a protective mechanism against cytotoxic lipotoxicity in various cell types. Mouse preimplantation embryos display a dose dependent reduction in blastocyst development when exposed to PA treatment in culture and this effect of PA is reversed when co-treated with OA. Evidence suggests that autophagy may be beneficial in offsetting the negative effects of a high fat environment and may play a role in early preimplantation

embryo development where embryos are highly susceptible to environmental factors. To date, although some have investigated the effects of elevated NEFA exposure on autophagy in general, very few investigations were done specifically for the period of mouse preimplantation development.

1.17.1 Objectives and Hypotheses

Previous study from our lab group (Yousif et al. 2020) identified that NEFA exposure affects early mouse embryo development, which included PA-induced ER stress and impairment of blastocyst development. OA had no effects on development but reduced mitochondrial ROS and enhanced lipid droplet accumulation. It was also reported that the addition of OA to treatment media reversed PA-induced effects. The protective mechanisms of OA against PA effects are not exclusive to early embryo development but are observed in other cell types as well. My research project aimed to understand the underlying autophagic mechanisms impacted by the exposure to high levels of NEFA during early mouse preimplantation embryo development *in vitro*.

1.17.2 Specific Aims

- 1) To assess autophagy in NEFA-treated mouse embryos throughout preimplantation development. Autophagic markers were investigated in mouse preimplantation embryos after NEFA exposure times of 18, 24, 30, 40, and 48 hours.
- 2) To assess autophagosome formation in NEFA-treated mouse preimplantation embryos. Autophagic markers were investigated after NEFA exposure for 40 hours with chloroquine (autophagy inhibitor) treatment at the last two hours of incubation.
- 3) To assess autophagosome maturation and degradation in NEFA-treated mouse embryos. Autophagosome-lysosome localization as well as lysosomal activity was investigated after NEFA exposure for 40 hours.

1.17.3 Hypothesis

Overall, it was hypothesized that NEFA-induced lipotoxicity dysregulates autophagic mechanisms in mouse preimplantation development. Specifically, PA will disrupt autophagosome formation while the addition of OA will negate lipotoxic effects to enhance overall developmental success.

Chapter 2

2 Materials and Methods

2.1 Animals and Ethics Approval

All experiments were conducted using CD-1 mice from Charles River Laboratories (Senneville, QC). All mice were handled in accordance with the Canadian Council on Animal Care and Western University's Animal Care and Use Policies (Protocol # 2018-075; **Appendix E**). Mice were housed in conventional housing with 12-hour light-dark cycle and access to food and water *ad libitum*.

2.2 Mouse Embryonic Stem Cell (mESC)

R1 wild-type mouse embryonic stem cells (mESC) derived from CD1 mouse embryos (Nagy et al. 1993) were purchased from SickKids Hospital (Toronto, ON).

2.3 NEFA Preparation

Palmitic acid (PA) and oleic acid (OA) were purchased from Sigma-Aldrich (St. Louis, MO, USA). Free fatty acid-free (FFA-free) BSA was purchased from Sigma-Aldrich (St. Louis, MO, USA). FFA-free BSA was dissolved in PBS overnight and filter sterilized to create a 20 % BSA stock solution. The stock solution was stored at -20 °C until use. PA and OA stock solutions were prepared by solubilizing each fatty acid in RNAase-free water using NaOH at 70 °C to a stock concentration of 20 mM. The 20 % BSA solution was used to conjugate PA and OA stock solutions in a 2:1 fatty acid-to-BSA molar ratio to a final concentration of 500 μ M, then stored in 4 °C until use.

2.4 Embryo Culture

All experimental treatments were prepared with potassium simplex optimization media with amino acids (KSOMaa, Caisson Labs, Smithfield, UT). BSA culture media was prepared with the stock 20 % BSA solution to 1.5 % BSA in KSOMaa media. Culture dishes of 35 mm diameter (Corning, NY, USA) were used for embryo culture. Dishes were prepared with 20 μ L droplets of the treatment media and the treatment droplets

were covered with embryo-grade mineral oil (LiteOil, LifeGlobal, Guilford, CT, USA). Pools of embryos were placed into the appropriate treatment medium at the density of 1 embryo per μL of treatment medium. After which, embryos were cultured *in vitro* under 5 % CO_2 , 5 % O_2 , and 90 % N_2 environment at 37 °C for up to 48 hours.

Experiment 1: To assess autophagy in NEFA-treated embryos throughout preimplantation development

Experiment 1 identified the effects of NEFA exposure on early embryo autophagy. Embryos were treated *in vitro* with 100 μM PA, 250 μM OA, 100 μM PA and 250 μM OA, or KSOMaa medium alone (control) for 18, 24, 30, 40, and 48 hours.

Experiment 2: To assess autophagic flux in NEFA-treated embryos

Experiment 2 determined the changes in autophagic flux of early embryos under NEFA treatment. Embryos were treated *in vitro* with 100 μM PA, 250 μM OA, 100 μM PA and 250 μM OA, or KSOMaa medium alone (control) for 40 and 48 hours, with the addition of 75 μM of chloroquine (CQ) for 2 hours at the end of incubation period.

Experiment 3: To assess autophagosome-lysosome interaction in NEFA-treated mouse embryos

Experiment 3 determined the changes in autophagosome-lysosome interaction of early embryos under NEFA exposure. Embryos were treated *in vitro* with 100 μM PA, 250 μM OA, 100 μM PA and 250 μM OA, or KSOMaa medium alone (control) for 40 hours.

2.5 mESC Culture

R1 mouse embryonic stem cells (mESC) were maintained on 0.2 % gelatin-coated culture dishes. mESC culture medium consisted of KnockOut DMEM/F12 medium (49 %, Gibco, Thermo Fisher Scientific, USA), Neurobasal medium (49 %, Gibco, Thermo Fisher Scientific, USA), GlutaMax Supplement (1 %, Gibco, Thermo Fisher Scientific, USA), 2-mercaptoethanol (0.1 %, Gibco, Thermo Fisher Scientific, USA), N2 supplement (0.5 %, 100X, Gibco, Thermo Fisher Scientific, USA), B27 supplement (1 %, 50X, Gibco, Thermo Fisher Scientific, USA), mouse leukemia inhibitory factor (mLIF,

0.01 %, MilliporeSigma, USA), PD0325901 (0.01 %, 39-C68; Reagents Direct, Encinitas, CA, USA) and CHIR99021 (0.03 %, 27-H76; Reagents Direct, Encinitas, CA, USA). mESC medium was replaced daily and monitored for spontaneous differentiation. All experiments were cultured under 5 % CO₂ environment at 37 °C.

Supplementary experiment: To assess autophagy in NEFA-treated mouse embryonic stem cells

The supplementary experiment evaluates the changes in autophagy after NEFA exposure in mESC. mESC were treated with 1.5 % BSA (Cytiva, USA), 100 μM PA, 250 μM OA, 100 μM PA and 250 μM OA, or mESC culture medium alone (control) for 48 hours.

2.6 Mouse Superovulation and Mating

CD-1 female mice of 3-4 weeks old were gonadotrophin super-ovulated to prepare for mating. Female mice received intraperitoneal (IP) injections of pregnant mare serum gonadotrophin (PMSG, Merck Animal Health, Canada) at 5.0 IU to stimulate follicle growth and maturation. After 48 hours, the mice received IP injections of human chorionic gonadotrophin (hCG, Merck Animal Health, Canada) at 5.0 IU to stimulate follicle maturation and ovulation. After hCG injections, the female mice were placed in a cage with CD-1 male mice at 2:1 female-to-male ratio for mating overnight. The next morning, female mice were checked visually for vaginal plugs, which serves as an indication for successful mating. All female mice were returned to their original cage until embryo collection was performed.

2.7 Embryo Collection

Embryos were collected from female mice 48 hours post-hCG injections (hpi). An hour before collection, M2 flushing medium (Sigma-Aldrich, St. Louis, MO, USA) was prepared in 3 mL syringes and warmed up to 37 °C. All female mice were sacrificed via CO₂ asphyxiation and oviducts were dissected out. The pair of oviducts dissected from each mouse were placed into drops of warmed M2 flushing medium, under a heating lamp and a warm water flask to maintain culture temperature. Under a light microscope, oviducts were flushed using a needle (30 G) and a 3 mL syringe with warm M2 flushing

medium to isolate embryos from the oviducts. A 9" Pasteur pipette (Fisherbrand, Thermo Fischer Scientific, USA) was used to transfer embryos between media drops. Embryos were removed from M2 flushing medium and then washed four times with KSOMaa medium. After washing, 2-cell embryos were allocated to treatment groups at a density of 1 embryo per μL of treatment medium for the appropriate culture period.

2.8 Developmental Stage Analysis

After the designated culture period, embryos were collected for developmental stage analysis. Embryos were viewed under a light dissecting microscope and the cell stage progression for each embryo was classified. Embryos were identified as 2-cell, 4-cell, 8-cell, morula, blastocyst stage, or degraded. Two-cell staged embryos consisted of two equal-sized cells; 4-cell staged embryos consisted of three to four round cells; 8-cell staged embryos consisted of five to eight round cells; morula stage embryos consisted of more than eight cells after compaction; blastocyst stage embryos consisted of embryos after cavitation; and degraded embryos consisted of at least one degraded cell. **Figure 6** displays representative images of mouse embryos at different cell stages. Phase contrast images of embryos at various cell stages were captured using Leica DM IL LED microscope and Leica Application Suite V4.4 (Leica Microsystems, Canada).

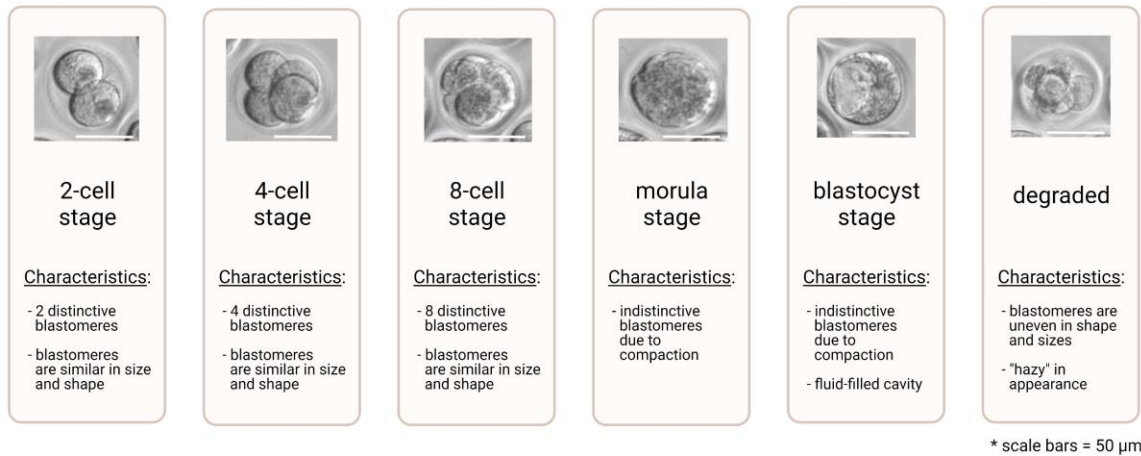


Figure 6. Representative images of mouse preimplantation embryo at each preimplantation stage.

Representative images of mouse preimplantation embryos at the 2-cell, 4-cell, 8-cell, morula, blastocyst stage, and degraded embryos. Inclusion criteria of each preimplantation stage is included. Created with BioRender.com.

2.9 mESC Cell Morphology

mESCs were viewed under a light microscope (Leica Microsystems, Canada) after the designated incubation period for cell morphology. Digital images of mESC were captured using a cell phone camera (Huawei P20) by Hailey Hunter.

2.10 RNA Extraction and Reverse Transcription (RT)

After embryo developmental stage analysis, mouse embryos were snap frozen at -80 °C to preserve mRNA integrity in the cells. On the day of mRNA extraction, samples were kept on ice to prevent thawing and degradation of mRNA samples. Arcturus PicoPure RNA Isolation Kit (Applied Biosystems, Thermo Fisher Scientific, USA) was used for RNA extraction of mouse embryos, according to manufacturer's instructions. Exogenous luciferase mRNA (Promega, USA) was added into RNA samples base on embryo number (0.025 pg per embryo) as a reference gene for mRNA transcript analysis. An RNase-free DNase set (Qiagen, KY, USA) was used to additionally remove genomic DNA from RNA samples, according to manufacturer's instructions. Reverse transcription was performed with Sensiscript RT Kit (Qiagen, KY, USA), according to manufacturer's instructions, to reverse transcribe RNA to cDNA. cDNA samples from mouse embryos were diluted to 0.5 to 1 embryo per μL with RNase-free water. cDNA samples were stored at -20 °C until mRNA transcript detection.

2.11 Polymerase Chain Reaction (PCR)

cDNA samples were subjected to reverse transcription--polymerase chain reaction (RT-PCR) to assess for cDNA quality. RT-PCR was performed for luciferase RNA control (*Luc*, L4561, Promega Corporation, Madison, WI, USA) and histone H2A (*Hist2h2aa1*). Each reaction consisted of 1 μL of cDNA sample with 24 μL of reaction mixture. Reaction mixture was prepared with 10X PCR Buffer (0.1 %), MgCl_2 (50 nM; 0.03 %), dNTP (10 mM; 0.02 %), forward and reverse primers (0.004 % each), Taq polymerase (0.004 %), and RNase free water. PCR was run in a thermocycler on these conditions: 94 °C for 2 minutes, then 44 cycles of: 94 °C for 30 seconds, 59 °C (*Luc*) or 61 °C (*Hist2h2aa1*) for 30 seconds, and 72 °C for 1 minute, then 72 °C for 10 minutes. PCR products were run on a 2 % agarose gel with ethidium bromide in 1X TAE running buffer

for transcript detection of *Luc* and *Hist2h2aa1*. Luciferase forward primer (5' TTGACAAGGATGGATGGCTAC 3') and reverse primer (5' TTCGGTACTTCGTCGTCCACAAAC 3') and histone H2A forward primer (5' CTCACCGCAGAGGTTACTTGAG 3') and reverse primer (5' ATGCAGAAATTTGGTTGGTTG 3') were obtained from Sigma-Aldrich (St. Louis, MO, USA). An embryo pool and RNase-free water were used as a positive and negative control, respectively. A DNA ladder (100 bp, Invitrogen, Thermo Fischer Scientific, USA) was used to confirm the presence of cDNA transcript of *Luc* and *Hist2h2aa1*. Gel electrophoresis was run at 115 V for 45 minutes. Gel was imaged using ChemiDoc XRS system (Laird Lab, UWO) for transcript detection.

2.12 Quantitative Polymerase Chain Reaction (qPCR)

Quantitative polymerase chain reaction (qPCR) was performed to assess relative mRNA transcript levels using TaqMan Universal PCR Master Mix (Applied Biosystems, Thermo Fisher Scientific, USA), according to manufacturer's instructions. A reaction mixture was prepared with 2X TaqMan Universal PCR Master Mix (MM; 50 %), TaqMan primer probes (5 %, Applied Biosystems, Thermo Fisher Scientific, USA), and RNase-free water (45 %). Each reaction was plated in triplicates of 20 μ L each with 1 μ L of cDNA into a 384-well plate. A non-transcript control of RNase-free water was included for each gene. The plate was centrifuged at 2000 rpm for 2 minutes prior to qPCR reaction. The BioRad CFX384 Touch Real-Time PCR Detection System was used to run the qPCR reaction with the following conditions: 95 $^{\circ}$ C for 5 minutes, then 50 cycles of: 95 $^{\circ}$ C for 15 seconds and 60 $^{\circ}$ C for 1 minute. Primer probes for *Luc* control (5'ACGTTTCGTCACATCTCAT3'), *Becn1* (Mm01265461_m1, Thermo Fisher Scientific, USA), *Atg3* (Mm00471287_m1, Thermo Fisher Scientific, USA), *Atg5* (Mm00504340_m1, Thermo Fisher Scientific, USA), and *Map1lc3b* (Mm00782868_sH, Thermo Fisher Scientific, USA) were used for analysis of autophagy-related genes.

2.13 Transcript Analysis

mRNA transcript levels were measured in cycle threshold (Ct) values through the CFX Maestro 1.1 (Bio-Rad; USA). Relative mRNA abundance was quantified using the delta

delta cycle threshold ($2^{-\text{ddCt}}$) method. Transcript analysis was performed on Excel (Microsoft, USA).

2.14 Immunofluorescence Staining

After the designated incubation period and developmental stage analysis, mouse embryos were placed in 2 % paraformaldehyde in PBS for 30 minutes for fixation. Then, mouse embryos were stored overnight in PHEM buffer (pH 6.9; Schliwa and van Blerkom 1981) containing PIPES (60 mM), HEPES (25 mM), EGTA (10 mM), and $\text{MgCl}_2 \cdot \text{H}_2\text{O}$ (1 mM) to preserve structural integrity of actin filaments. The embryos were washed once with PBS prior to blocking with a blocking buffer containing normal serum (5 %), Triton-X 100 (0.1 %), and NaN_3 (0.02 %) in PBS. An antibody dilution buffer (ADB) was prepared with normal serum (0.5 %), Triton-X 100 (0.05 %), and NaN_3 (0.02 %) in PBS for washes between incubation with antibody. Mouse embryos were washed with ADB once, then incubated in primary antibody overnight. Three washes with ADB were completed before placing embryos into secondary antibody for incubation overnight. DAPI and Phalloidin was used to stain for cellular structures of cell nucleus and f-actin, respectively. One hour of incubation with 4',6-diamidino-2-phenylindole (DAPI; 0.1 %; Sigma-Aldrich, St. Louis, MO, USA) and Phalloidin stain (5 %; Sigma-Aldrich, St. Louis, MO, USA) was followed by two washes with ADB. Normal donkey serum (Jackson ImmunoResearch, West Grove, PA, USA), anti-LC3A/LC3B polyclonal antibody (Invitrogen, Thermo Fisher Scientific, USA), and Alexa Fluor 488 Donkey anti-Rabbit IgG secondary antibody (Invitrogen, Thermo Fisher Scientific, USA) were used for protein localization of LC3-I and LC3-II.

2.15 Confocal Microscopy and Image Acquisition

Confocal microscopy was used to capture images of mouse embryos that were subjected to immunofluorescence staining. Mouse embryos were mounted on a 35 mm glass-bottom dish (MatTek, Ashland, MA, USA) with LiteOil-covered KSOMaa droplets for imaging. Z-stack images were captured of each embryo at 5 μm interval between images, using the 25X objective lens on a ZEISS LSM800 AiryScan confocal microscope

(Schulich Imaging Core Facility, UWO). Images for all treatment groups within the same replicate were captured using the same laser strength and intensity settings.

2.16 Image Analysis

Images captured from confocal microscopy were processed through ZEISS ZEN 3.1 (blue edition; Carl Zeiss Microscopy, Germany) for image export. Puncta structures were measured using the “analyze particle” function of ImageJ (National Institutes of Health, USA) based on pixel area of 9 pixel². Cell numbers were counted manually. Co-localization experiment measured overlapping signal from multi-channel images via the RG2B co-localization plug-in (Mauer 2004) on ImageJ. Fluorescence intensity was analyzed through ilastik (1.3.3; open source) and intensity was measured in arbitrary units.

2.17 Protein Extraction and Quantification

2.17.1 Protein Extraction and Quantification of Mouse Embryos

Protein extraction and quantification were carried out prior to detecting protein abundance. Mouse embryos were snap frozen at -80 °C with 100X protease inhibitor (1 %; Calbiochem, MilliporeSigma, USA) and 100X phosphatase inhibitor (1 %; Calbiochem, MilliporeSigma, USA) in Pierce RIPA buffer (Thermo Fisher Scientific, USA) to lyse cells and release proteins from the embryos. Extracted protein samples from mouse embryos were not quantified to measure total protein concentration due to the low protein abundance in the embryos. All extracted proteins were used for western blot in mouse embryo experiments.

2.17.2 Protein Extraction and Quantification of mESC

After incubation period, mESCs were washed briefly with PBS before collecting cells for protein extraction. Pierce RIPA buffer (Thermo Fisher Scientific, USA) was prepared with 100X protease inhibitor (1 %; Calbiochem, MilliporeSigma, USA) and 100X phosphatase inhibitor (1 %, Calbiochem, MilliporeSigma, USA) then added to the mESCs for collection with a cell scraper. mESCs collected were snap frozen at -80 °C before sonication. mESCs were disrupted with a sonicator (Misonix S-4000 Sonicator,

Qsonica, USA) at 30 A for 5 rounds of one second each to extract cell lysate. Cell lysates were then quantified using a BCA assay with the Pierce BCA Protein Assay Kit (Thermo Scientific, Thermo Fischer Scientific, USA) according to manufacturer's instruction. The SpectraMax M5 microplate reader (Molecular Devices, USA) and SoftMax Pro 5.2 software (Molecular Devices, USA) were used to measure total protein concentration of the cell lysate at 562 nm.

2.18 Western Blot

2.18.1 Sample Preparation of Mouse Embryos

Protein lysates derived from mouse embryos were added with NuPAGE 4X LDS sample buffer (25 %; Invitrogen, Thermo Fischer Scientific, USA) and NuPAGE 10X reducing agent (10 %; Invitrogen, Thermo Fischer Scientific, USA). Then, samples were warmed to 70 °C for 10 minutes to unfold extracted proteins.

2.18.2 Sample Preparation of mESC

Protein lysates derived from mESCs were added with NuPAGE 4X LDS sample buffer (25 %; Invitrogen, Thermo Fischer Scientific, USA), NuPAGE 10X reducing agent (10 %; Invitrogen, Thermo Fischer Scientific, USA), and biology-grade water (Cytiva, USA) to arrive at a concentration of 15 µg of protein per sample. Then, protein samples were heated at 70 °C for 10 minutes to unfold extracted proteins.

2.18.3 Polyacrylamide Gel Electrophoresis (PAGE) and Protein Transfer

Polyacrylamide gel electrophoresis (PAGE) was conducted to separate whole protein samples. Protein samples from mouse embryos or mESCs (15 µg protein in 20 µL sample) were separated in a NuPAGE 12 % Bis-Tris Mini Protein Gel (Invitrogen, Thermo Fischer Scientific, USA) in NuPAGE 1X MOPS SDS Running buffer (Invitrogen, Thermo Fischer Scientific, USA). NuPAGE Antioxidant (Invitrogen, Thermo Fischer Scientific, USA) was added into running buffer to maintain protein structure. The BLUelf Prestained Protein Ladder (FroggaBio, Concord, ON, Canada) was used to monitor protein separation based on molecular weight. Gel electrophoresis was

run at 75 V for 10 minutes then at 130 V for 1.5 hours. Separated protein samples from gel electrophoresis was transferred onto a PVDF membrane in 1X tris-glycine-methanol-based transfer buffer. Protein transfer was run at 100 V for 2 hours.

2.18.4 Ponceau S Staining and Antibody Incubation

Ponceau S was used to stain for total protein on PVDF membranes after protein transfer. For immunological detection, PVDF membranes were first blocked with 5 % BSA (Cytiva, USA) in 1X TBST (0.01 % Tween-20) for an hour and then incubated with primary antibody overnight. Membranes were washed thrice in 1X TBST prior to a one-hour incubation with secondary antibody. Membranes were incubated with anti-LC3A/LC3B polyclonal antibody (Invitrogen, Thermo Fisher Scientific, USA) and horseradish peroxidase- (HRP-) conjugated goat anti-rabbit IgG secondary antibody (Invitrogen, Thermo Fisher Scientific, USA) for LC3-I and LC3-II detection. HRP-conjugated anti- β -actin monoclonal antibody (Invitrogen, Thermo Fisher Scientific, USA) was incubated with the membranes for detection of β -actin.

2.19 Protein Detection and ECL Imaging

Protein abundance was detected on PVDF membranes using enhanced chemiluminescence (ECL). Immobilon Forte Western HRP Substrate (Millipore Sigma, Burlington, MA, USA) was used to incubate the membrane for ECL detection of target protein. The ChemiDoc Imaging System and Image Lab Touch Software (Bio-Rad, USA) were used to capture images of the membrane using the chemiluminescence settings.

2.20 Volumetric Analysis

Images of the western blot from ECL imaging were processed with volumetric analysis using ImageLab software (Bio-Rad, USA) to quantify for protein abundance.

2.21 Statistical Analysis

Statistical analysis for all experiments were performed on Prism 8 (GraphPad, USA). One-way ANOVA and if significant, Tukey's HSD post-hoc tests were performed to compare means between each treatment groups. Experiments were performed with a minimum of three biological replicates. P values less than 0.05 were considered statistically significant.

Chapter 3

3 Results

3.1 Effects of PA and OA on Preimplantation Development

Previously, it was established in our lab, that exposure to 100 μM of PA significantly reduced blastocyst development whilst co-culture with 250 μM of OA resulted in similar blastocyst formation as control levels (Yousif et al. 2020). My first experiment investigated the effects of 100 μM PA and 250 μM OA, individually and in combination, throughout mouse preimplantation embryo development. Representative images of 2-cell staged mouse embryos after 18, 24, 30, 40, and 48 hours of PA and OA exposure, individually and in combination, are shown in **Figure 7**.

Developmental progression was analyzed for each treatment group after 18, 24, 30, 40, and 48 hours of NEFA exposure beginning at the 2-cell stage. No significant differences were found between treatment groups for the developmental progression of embryos at the 4-cell, 8-cell, and morula stage after 18 and 24 hours of NEFA exposure (**Figure 8**, $P > 0.05$, Tukey's multiple comparisons test). No blastocyst formation was observed at these two timepoints. After 30 hours of NEFA exposure, the development of mouse embryos to the 4-cell and 8-cell stage embryos were similar between each treatment group (**Figure 8**, $P > 0.05$, Tukey's multiple comparisons test). Development to the morula stage after 30 hours of PA+OA co-culture was significantly lower than control group (**Figure 8**, $P < 0.05$, Tukey's multiple comparisons test); while morula development was similar in PA- and OA-alone groups. No blastocyst formation was observed at this the 30-hour time point as well in any treatment group including controls. At the 40-hour time point, no significant differences were observed across treatment groups for all cell stages, including the morula stage (**Figure 8**, $P > 0.05$, Tukey's multiple comparisons test). However, after 48 hours of incubation, exposure to PA alone resulted in a significantly higher proportion of 8-cell stage embryos than other treatment groups (**Figure 8**, $P < 0.001$, Tukey's multiple comparisons test). Development to the blastocyst stage in the PA-alone group was correspondingly significantly reduced

(**Figure 8**, $P < 0.01$, Tukey's multiple comparisons test). However, blastocyst development was similar in the PA+OA combination group to the control; OA-only group also showed no significant differences (**Figure 8**, $P > 0.05$, Tukey's multiple comparisons test).

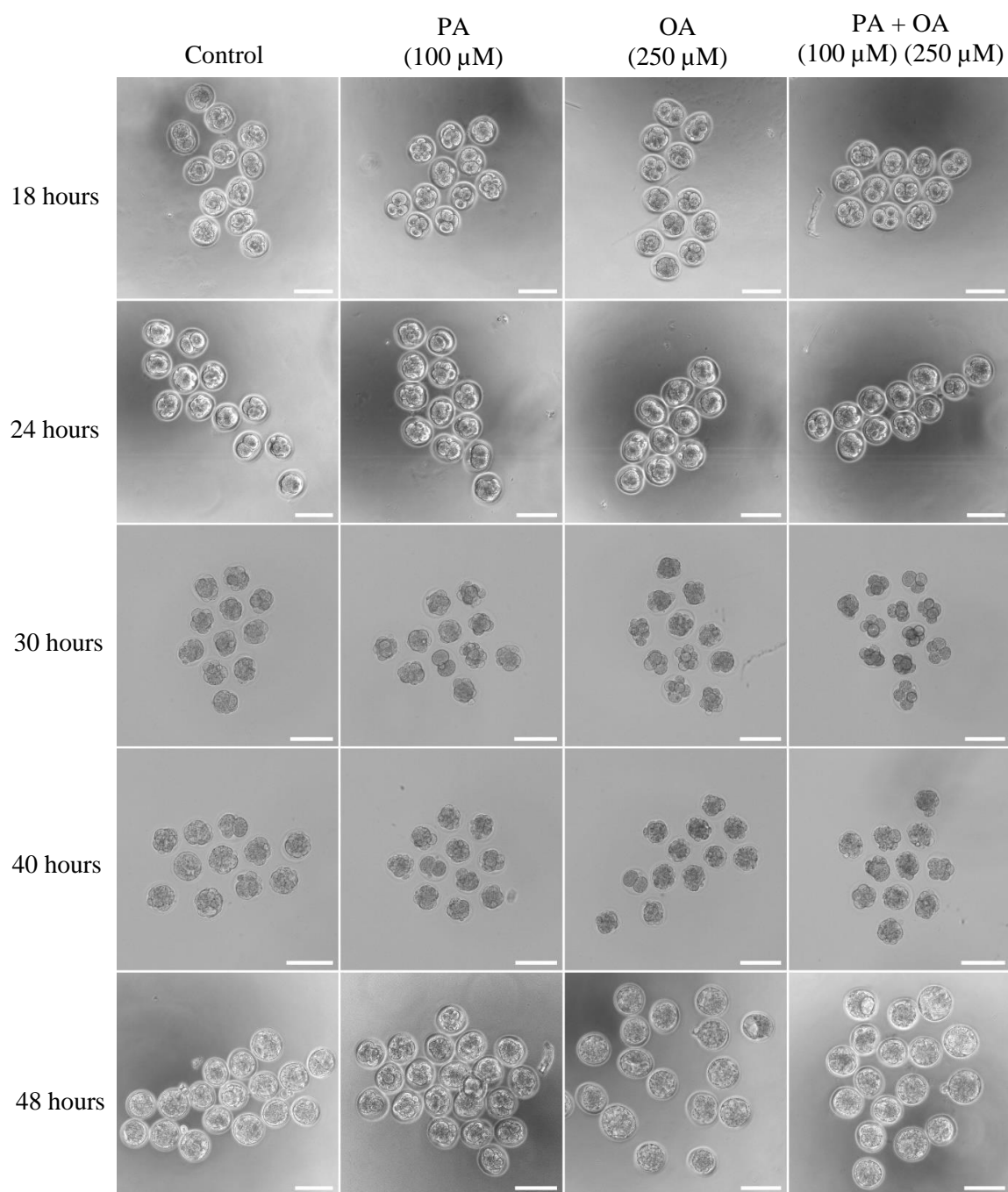


Figure 7. Representative images of embryos cultured in NEFA treatments

Representative images of mouse preimplantation embryos treated with 100 μ M PA, 250 μ M OA, 100 μ M PA and 250 μ M OA, or KSOMaa medium alone (control), beginning at the 2-cell stage for 18, 24, 30, 40, and 48 hours. Scale bar = 100 μ m.

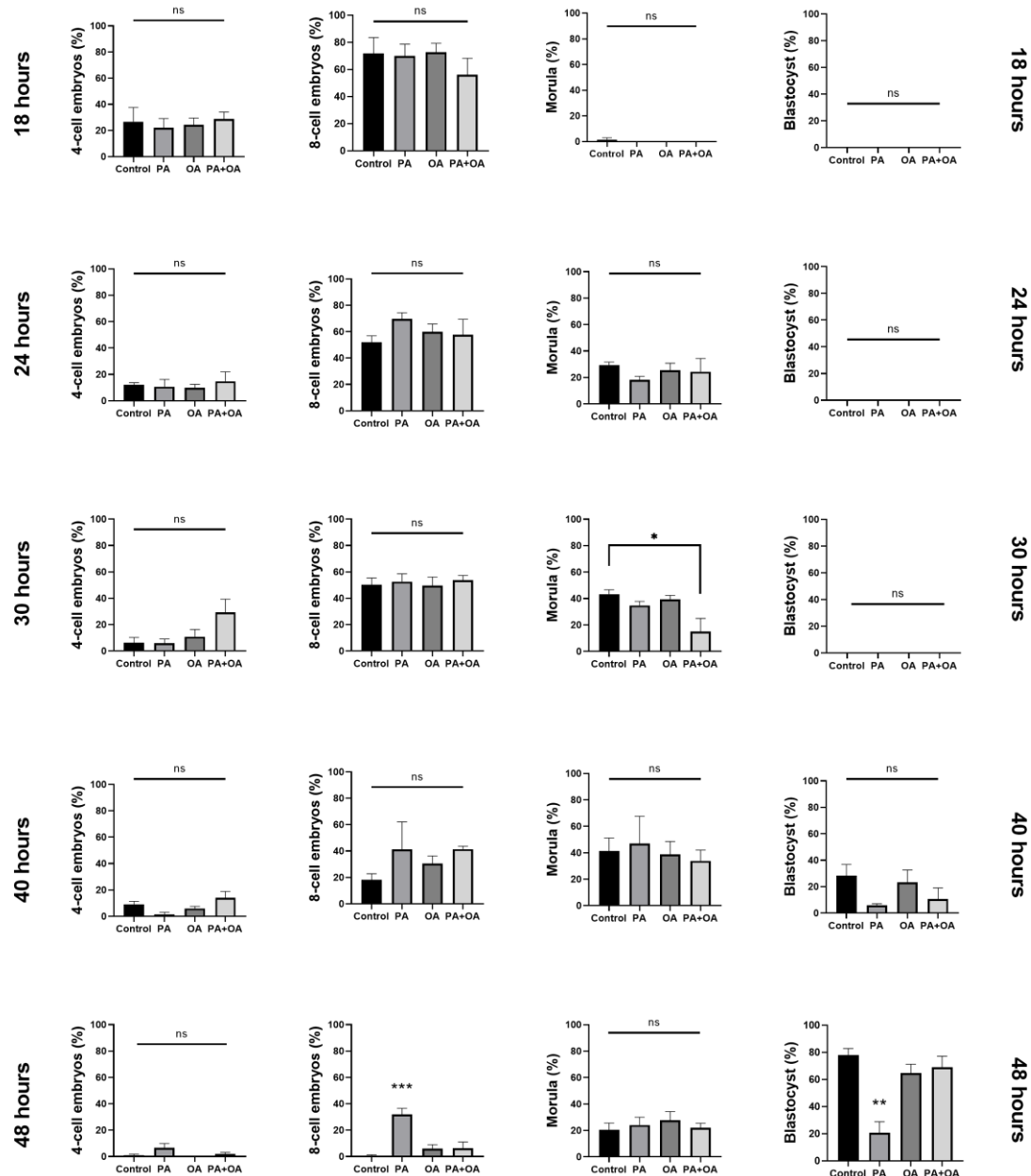


Figure 8. Developmental stage progression of embryos after NEFA treatments

Developmental stage progression (+ SEM) of mouse preimplantation embryos treated with 100 μ M PA, 250 μ M OA, 100 μ M PA and 250 μ M OA, or KSOMaa medium alone (control) beginning at the 2-cell stage for 18, 24, 30, 40, and 48 hours. N > 4, one-way ANOVA with Tukey's HSD post-hoc test. Significant differences are indicated by * p < 0.05, ** p < 0.01, and *** p < 0.001.

3.2 Autophagic profile throughout preimplantation development

The first primary objective aimed to assess autophagy onset throughout mouse preimplantation embryo development. To do so, I first characterized the expression of autophagy markers at the transcript and protein levels for all cell stages of mouse preimplantation development. The relative transcript abundance of Bcln1, ATG3, ATG5, and LC3 were evaluated. Bcln1 transcript abundance, normalized to internal standard luciferase mRNA levels, was significantly decreased at the first cleavage then maintained low levels until the morula stage (**Figure 9A**, $P < 0.05$, Tukey's multiple comparisons test). Relative Bcln1 transcript levels returned to zygote levels at the blastocyst stage (**Figure 9A**). In contrast, relative ATG3 transcript levels, normalized to luciferase mRNA levels, were not significantly different across all preimplantation development stages (**Figure 9B**, $P = 0.1266$, one-way ANOVA). Interestingly, relative ATG5 transcript levels, normalized to luciferase mRNA, significantly dropped from the zygote stage by more than 5-fold after first cleavage and stayed at a low relative level throughout preimplantation development (**Figure 9C**, $P < 0.05$, Tukey's multiple comparisons test). Lastly, relative LC3 transcript levels, normalized to luciferase mRNA, significantly increased from the zygote stage by approximately 15-fold at the blastocyst stage (**Figure 9D**, $P < 0.05$, Tukey's multiple comparisons test).

The analysis of LC3-II puncta, observed via fluorescence microscopy, is regarded as a specific marker for autophagosomes number (Mizushima et al. 2010, **Figure 10**). Relative levels of LC3-II puncta were evaluated at all stages of mouse preimplantation development. LC3-II puncta count per cell significantly decreased after the 2-cell stage, to represent a 100-fold decrease by the blastocyst stage (**Figure 10A**, $P < 0.05$, Tukey's multiple comparisons test). Representative images of LC3-II puncta at all preimplantation developmental stages are shown in **Figure 10B**.

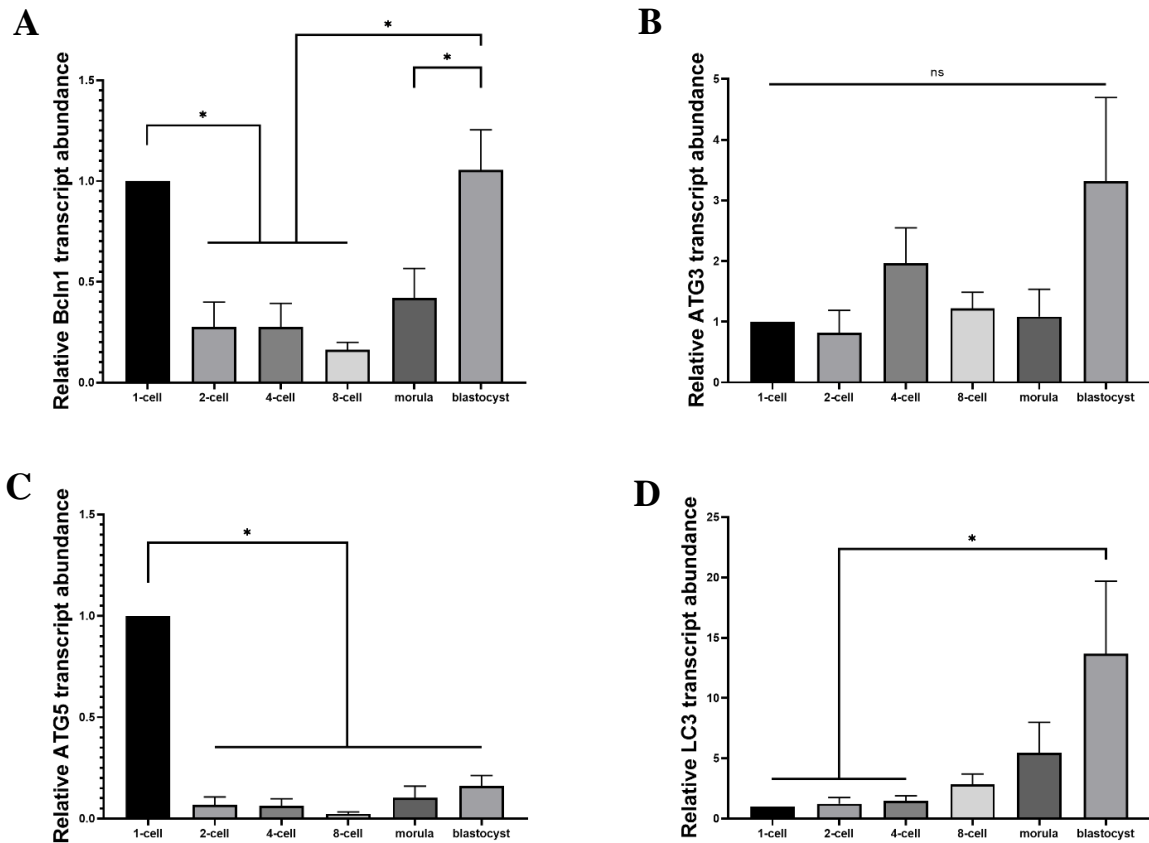


Figure 9. Autophagic marker transcript abundance in preimplantation development

Relative autophagic marker transcript levels (+ SEM) of preimplantation mouse embryos at 1-cell, 2-cell, 4-cell, 8-cell, morula, and blastocyst stage. $N > 3$, one-way ANOVA with Tukey's HSD post-hoc test. Significant differences are indicated by *, $p < 0.05$.

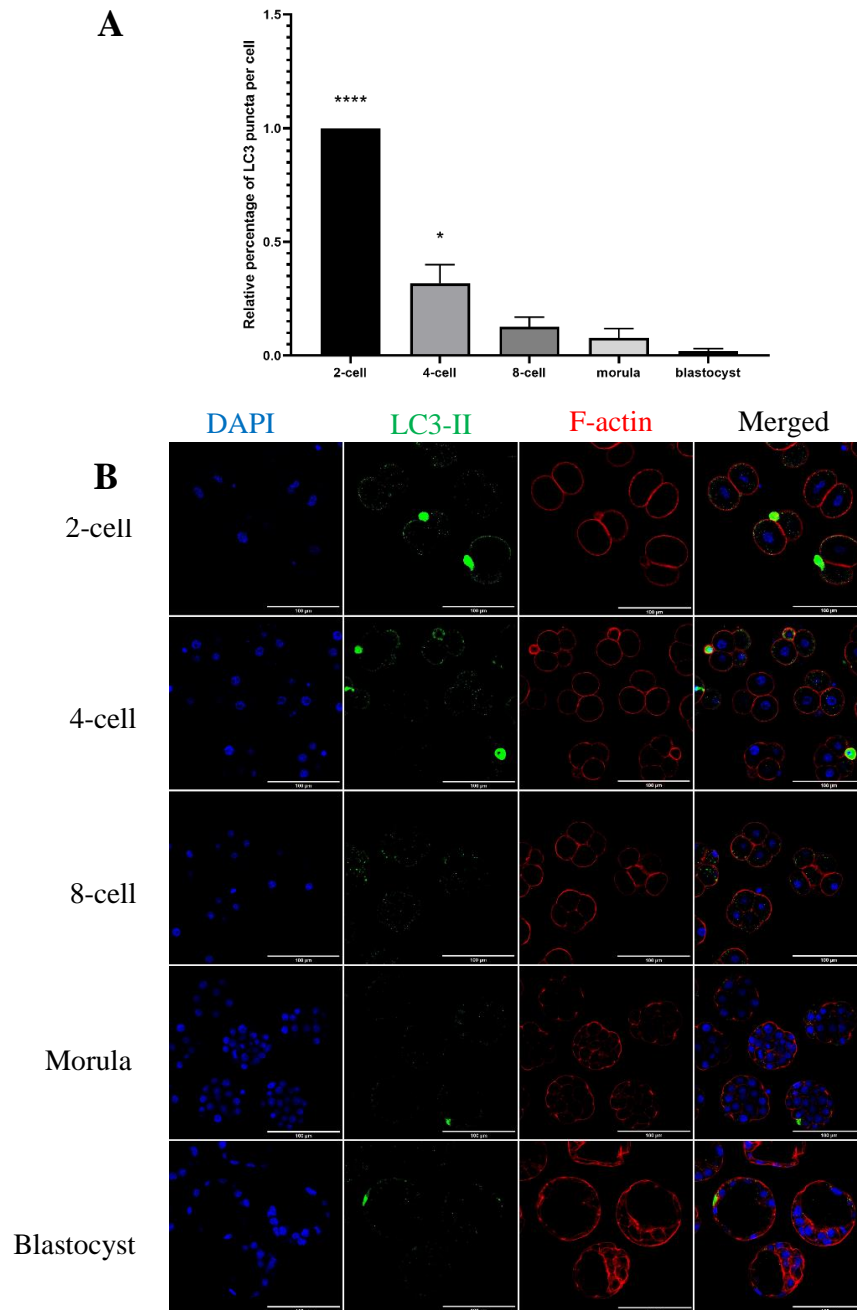


Figure 10. Autophagy marker LC3-II in preimplantation embryo development

Relative percent LC3-II aggregate puncta formation per cell (+ SEM) of preimplantation mouse embryos at 2-cell, 4-cell, 8-cell, morula, and blastocyst stage (A). $N > 3$, one-way ANOVA with Tukey's HSD post-hoc test. Significant differences are indicated by **** $p < 0.0001$ and * $p < 0.05$. Representative images of LC3-II aggregate puncta formation at each preimplantation stage (B).

3.3 Effects of PA and OA on overall autophagy

As mouse preimplantation development is negatively affected by PA treatment and rescued by PA and OA combination treatment, it is important to investigate whether exposures to PA and OA alters overall autophagy induction during this developmental period. Thus, I next characterized the pattern of relative autophagic marker transcript levels after 48 hours of NEFA exposure. The autophagic markers selected for investigation included Bcln1, ATG3, ATG5, and LC3. RT-qPCR transcript analysis revealed no significant differences in relative transcript abundance between control, 100 μ M PA, 250 μ M OA, and PA+OA co-treatment groups for all four autophagic markers (**Figure 11A**, $P = 0.9680$ (Bcln1); **Figure 11B**, $P = 0.9057$ (ATG3); **Figure 11C**, $P = 0.7418$ (ATG5); **Figure 11D**, $P = 0.9548$ (LC3), one-way ANOVA).

I then investigated whether autophagy is affected by NEFA exposure at the protein level, as reflected by the level of autophagosome detection via the characterization of LC3-II puncta levels using confocal microscopy. LC3-II puncta determination was applied to mouse preimplantation embryos following 18, 24, 30, 40, and 48 hours NEFA treatments. At both 18 and 24 hours NEFA treatment, no significant difference in LC3-II puncta per cell were observed in the PA and OA group, alone and in combination, from that observed in the control group (**Figure 12A**, **Figure 13A**, $P > 0.05$, Tukey's multiple comparisons test).

Significant variations in LC3-II puncta count per cell were first observed after 30 hours of NEFA exposure. Mouse embryos at the 2-cell stage were treated with 100 μ M of PA for 30 hours displayed a significant increase in LC3-II puncta count per cell compared to treatment with 250 μ M of OA for the same time interval (**Figure 14A**, $P < 0.05$, Tukey's multiple comparisons test). Likewise, treatment of 2-cell embryos with the PA+OA combination treatment for 30 hours also significantly increased LC3-II puncta count per cell compared to OA-alone treatment (**Figure 14A**, $P < 0.01$, Tukey's multiple comparisons test) as well as control (**Figure 14A**, $P < 0.05$, Tukey's multiple comparisons test). No significant differences were observed between PA-alone and PA+OA combination group (**Figure 14A**, $P = 0.9560$, Tukey's multiple comparisons test).

After 40 hours of NEFA treatment, variation in LC3-II puncta per cell counts across different treatment groups were enhanced. Two-cell mouse embryos treated with 100 μ M of PA for 40 hours displayed a significant increase in LC3-II puncta per cell by more than two-fold compared to the control (**Figure 15A**, $P < 0.0001$, Tukey's multiple comparisons test). The same relative increase in LC3-II puncta per cell was also observed in 2-cell mouse embryos treated with the PA+OA co-treatment for 40 hours (**Figure 15A**, $P < 0.001$). Treatment with 250 μ M of OA alone resulted in LC3-II puncta count per cell levels that were not significantly different than the control group (**Figure 15A**, $P > 0.9999$, Tukey's multiple comparisons test). Comparison of the PA-alone treatment and PA+OA combination treatment to the OA-alone treatment resulted in a significant increase in LC3-II puncta count per cell between groups (**Figure 15A**, $P < 0.001$, Tukey's multiple comparisons test).

I also assessed the effects of 48 hours of NEFA treatment on LC3-II puncta count per cell across all treatment groups. Consistent with other time intervals, treatment of 2-cell mouse embryos with 100 μ M of PA for 48 hours significantly increased LC3-II puncta per cell compared to treatment with 250 μ M of OA alone (**Figure 16A**, $P < 0.05$, Tukey's multiple comparisons test). However, in contrast to previous time points, 2-cell mouse embryo treatment with PA+OA in combination for 48 hours resulted in no significant difference in LC3-II puncta count per cell between this group and the OA-alone group (**Figure 16A**, $P = 0.9945$, Tukey's multiple comparisons test). Interestingly, PA+OA co-treatment for 48 hours resulted in a significant reduction in LC3-II puncta count per cell than that observed for the PA-only treatment, which was a unique outcome observed only in this time point (**Figure 16A**, $P < 0.05$, Tukey's multiple comparisons test).

Representative images of LC3-II puncta per cell of 2-cell mouse embryos following treatment with NEFAs for 18, 24, 30, 40, and 48 are shown (**Figure 12B, 13B, 14B, 15B, 16B**).

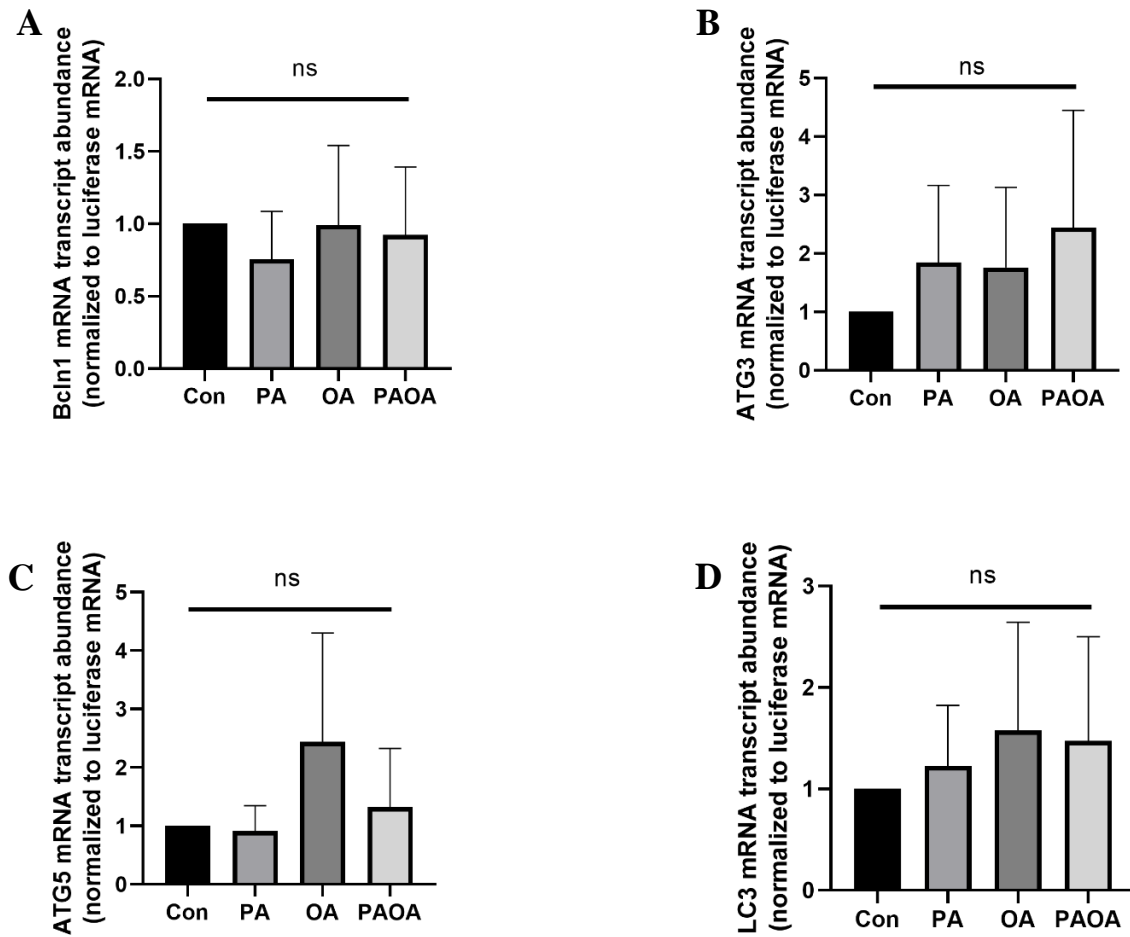


Figure 11. Autophagic marker transcript abundance in NEFA-treated embryos

Relative autophagic marker transcript levels (+ SEM) of preimplantation mouse embryos treated with 100 μ M PA, 250 μ M OA, 100 μ M PA and 250 μ M OA, or KSOMaa medium alone (control) for 48 hours. N=3, one-way ANOVA. Relative transcript levels for all 4 selected targets did not vary significantly across treatment from controls.

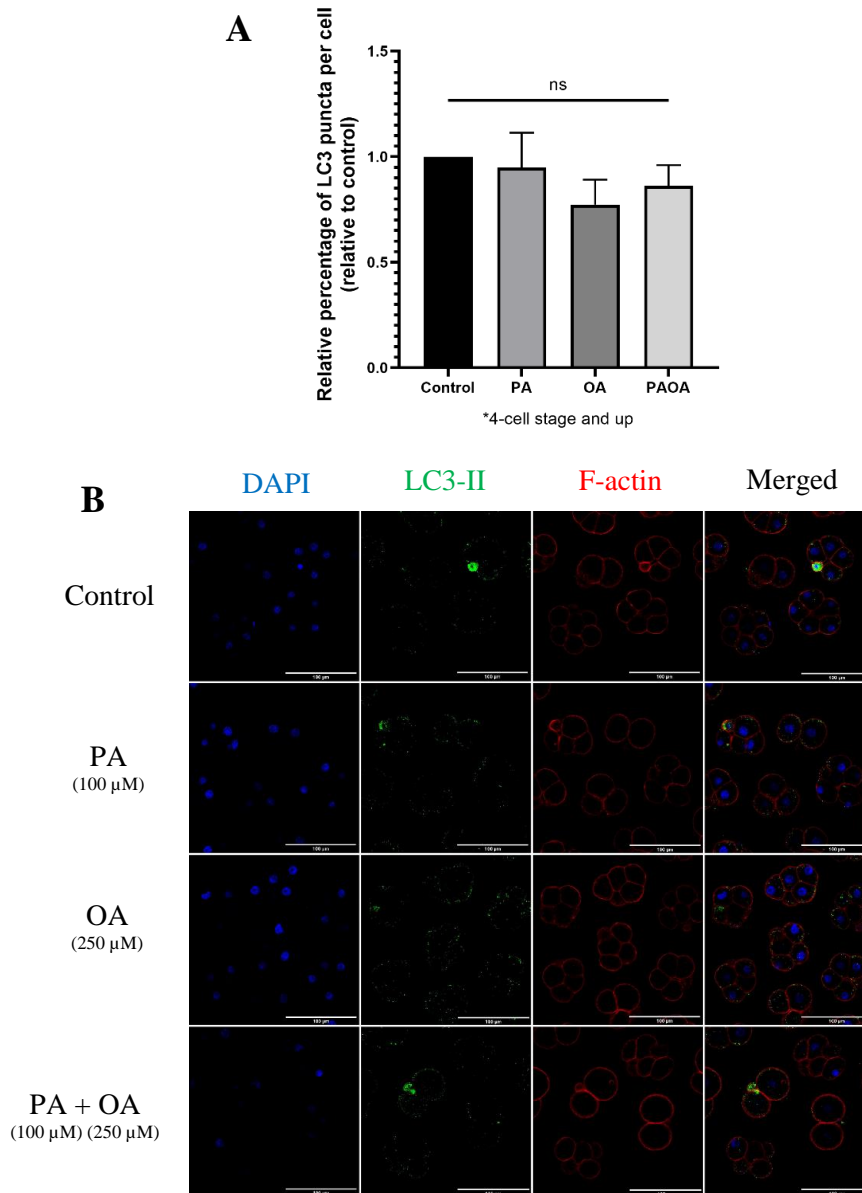


Figure 12. Autophagy marker LC3-II in NEFA-treated embryos after 18 hrs. of NEFA treatment

Relative percent aggregate puncta formation of LC3-II per cell (+ SEM) of 2-cell mouse embryos in 100 μ M PA, 250 μ M OA, 100 μ M PA and 250 μ M OA, or KSOMaa medium alone (control) for 18 hours (A). Only embryos past the 4-cell stage are included. N=3, two-way ANOVA with Tukey's HSD post-hoc test. Significant differences are indicated by *, $p < 0.05$. Representative images of LC3-II aggregate puncta formation after NEFA exposure (B). Scale bar = 100 μ m.

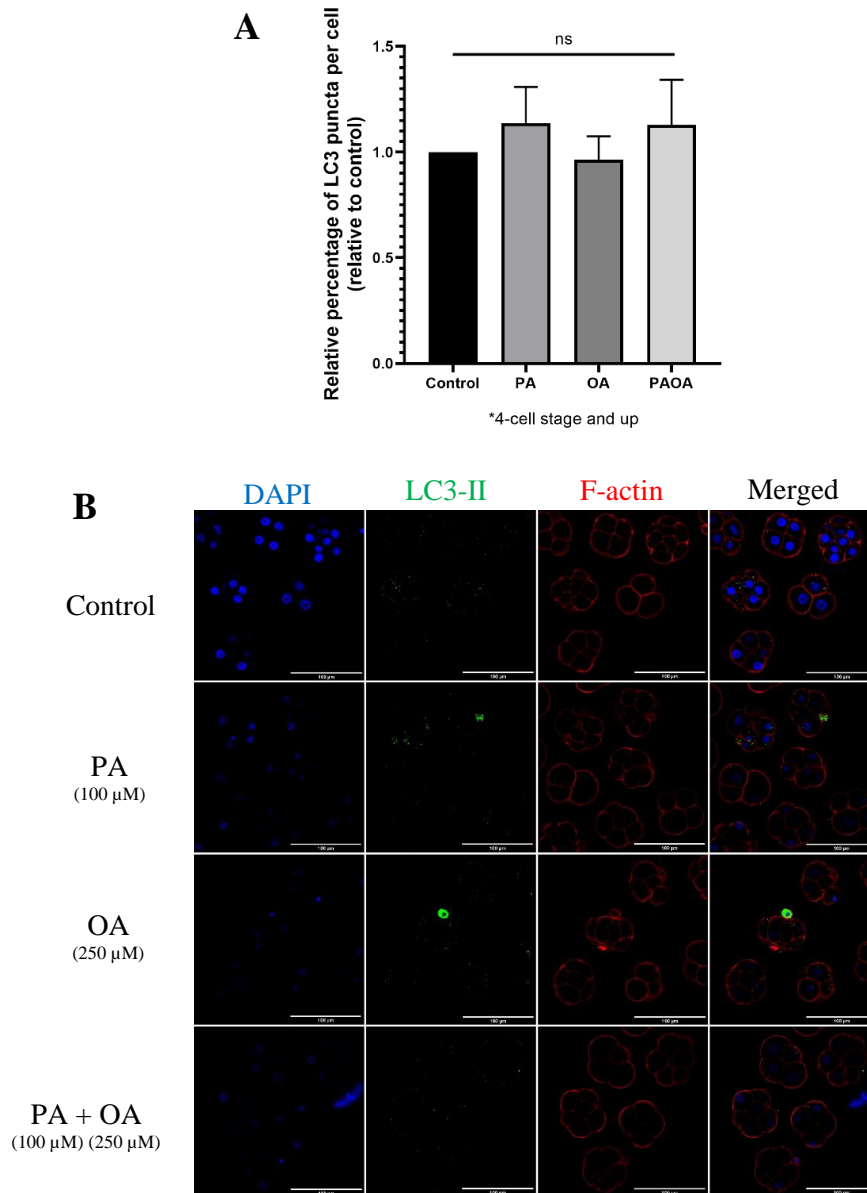


Figure 13. Autophagy marker LC3-II in NEFA-treated embryos after 24 hrs. of NEFA treatment

Relative percent aggregate puncta formation of LC3-II per cell (+ SEM) of 2-cell mouse embryos in 100 μ M PA, 250 μ M OA, 100 μ M PA and 250 μ M OA, or KSOMaa medium alone (control) for 24 hours (A). Only embryos past the 4-cell stage are included. N=3, two-way ANOVA with Tukey's HSD post-hoc test. Significant differences are indicated by *, $p < 0.05$. Representative images of LC3-II aggregate puncta formation after NEFA exposure (B). Scale bar = 100 μ m.

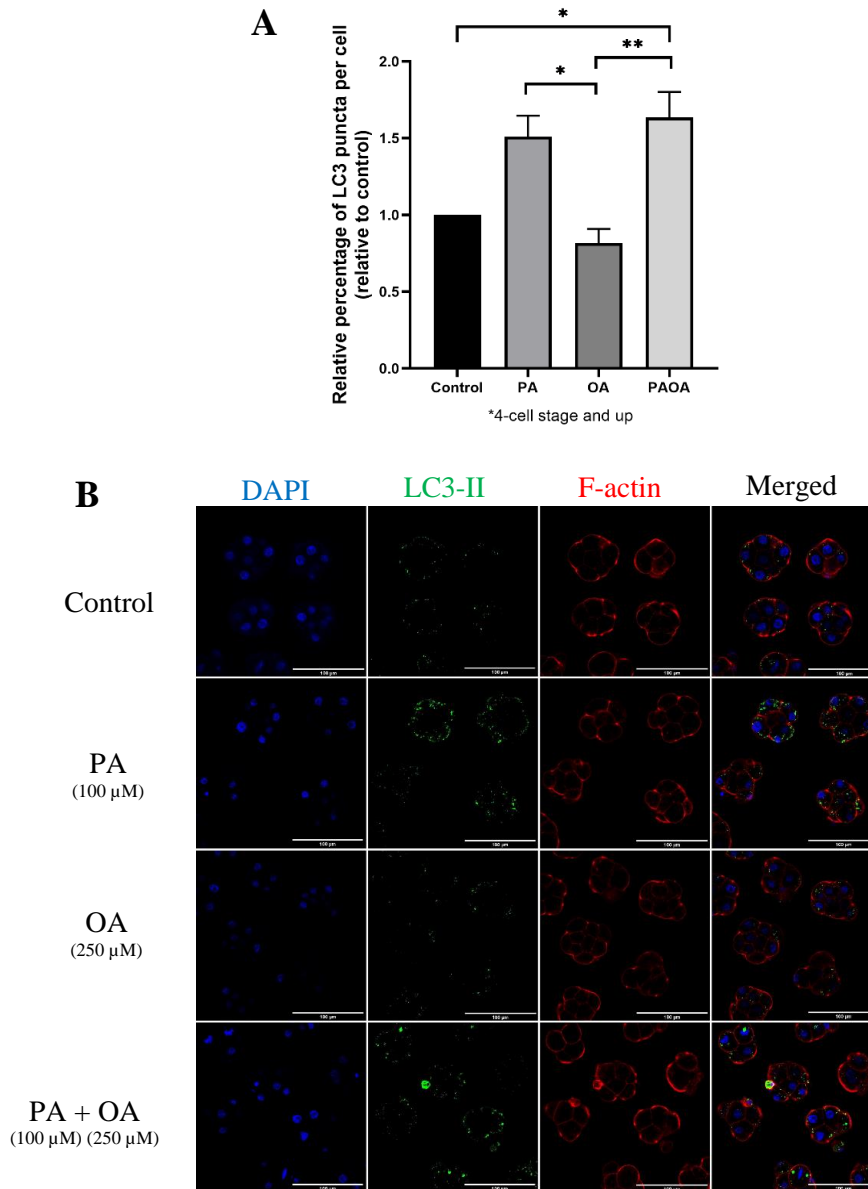


Figure 14. Autophagy marker LC3-II in NEFA-treated embryos after 30 hrs. of NEFA treatment

Relative percent aggregate puncta formation of LC3-II per cell (+ SEM) of 2-cell mouse embryos in 100 μM PA, 250 μM OA, 100 μM PA and 250 μM OA, or KSOMaa medium alone (control) for 30 hours (A). Only embryos past the 4-cell stage are included. N=3, two-way ANOVA with Tukey's HSD post-hoc test. Significant differences are indicated by *, $p < 0.05$. Representative images of LC3-II aggregate puncta formation after NEFA exposure (B). Scale bar = 100 μm.

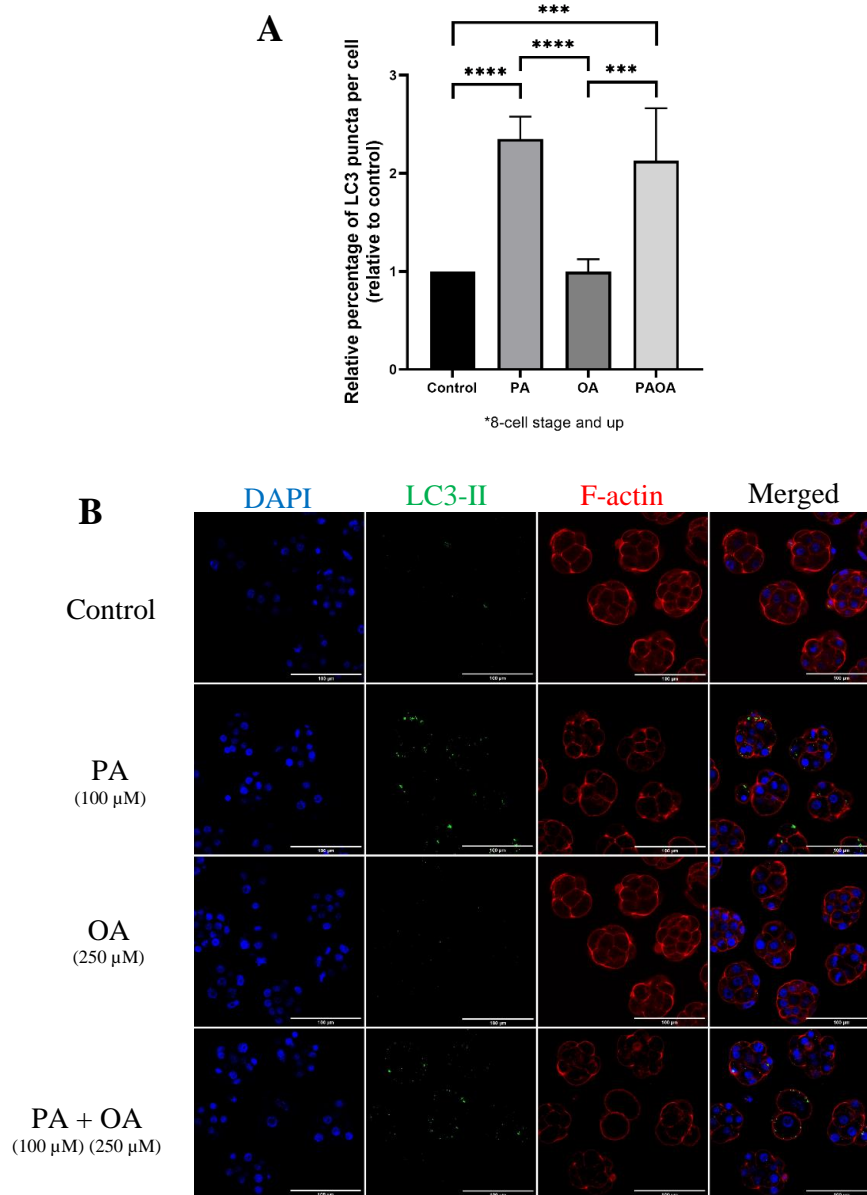


Figure 15. Autophagy marker LC3-II in NEFA-treated embryos after 40 hrs. of NEFA treatment

Relative percent aggregate puncta formation of LC3-II per cell (+ SEM) of 2-cell mouse embryos in 100 μM PA, 250 μM OA, 100 μM PA and 250 μM OA, or KSOMaa medium alone (control) for 40 hours (A). Only embryos past the 8-cell stage are included. N=3, two-way ANOVA with Tukey's HSD post-hoc test. Significant differences are indicated by *, $p < 0.05$. Representative images of LC3-II aggregate puncta formation after NEFA exposure (B). Scale bar = 100 μm.

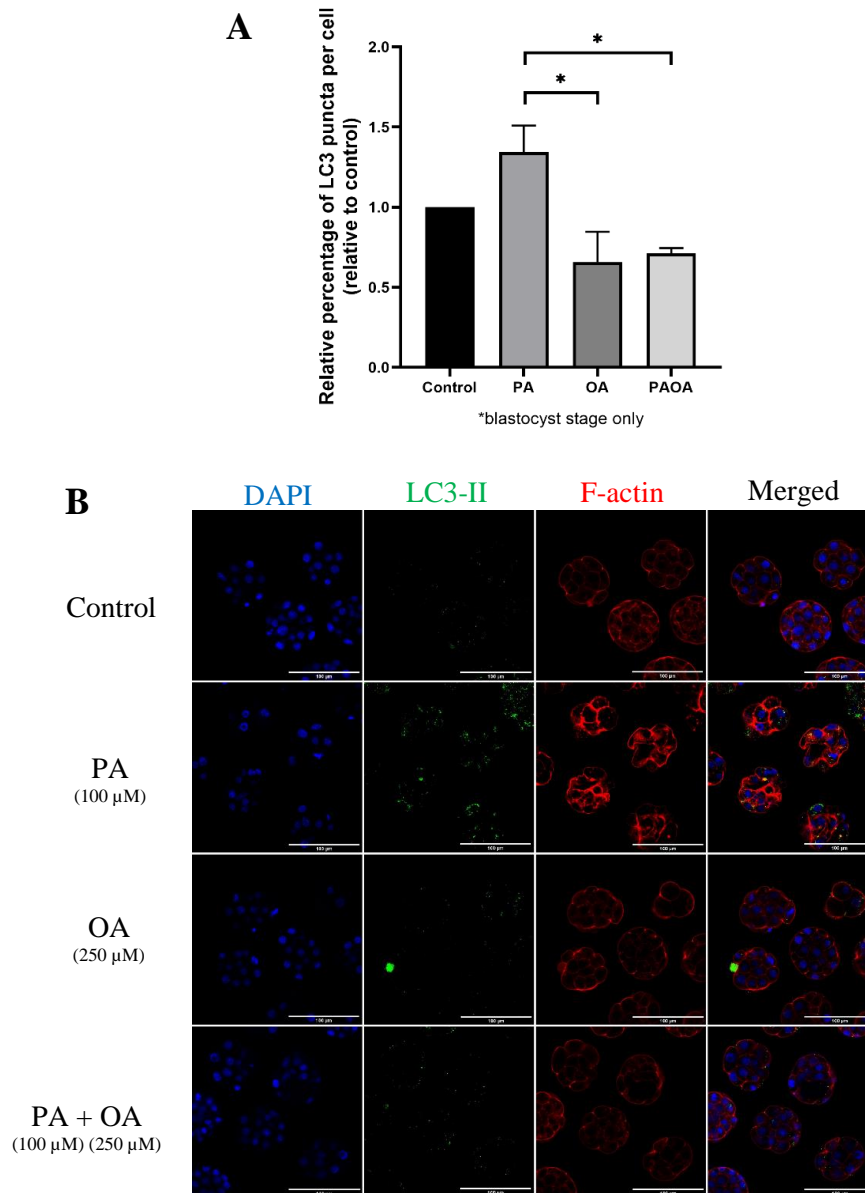


Figure 16. Autophagy marker LC3-II in NEFA-treated embryos after 48 hrs. of NEFA treatment

Relative percent aggregate puncta formation of LC3-II per cell (+ SEM) of 2-cell mouse embryos in 100 μM PA, 250 μM OA, 100 μM PA and 250 μM OA, or KSOMaa medium alone (control) for 48 hours (A). Only embryos of the blastocyst stage are included. N=3, two-way ANOVA with Tukey's HSD post-hoc test. Significant differences are indicated by *, $p < 0.05$. Representative images of LC3-II aggregate puncta formation after NEFA exposure (B). Scale bar = 100 μm.

3.4 Effects of PA and OA on autophagosome formation

Since autophagy is comprised of multiple steps (**figure 2 to 5**), my next objective was to assess autophagosome formation in NEFA-treated mouse embryos, employing an autophagy inhibitor, chloroquine (CQ). CQ inhibits autophagy by increasing the pH of lysosomes and thus preventing autophagosome-lysosome fusion (Mauthe et al. 2018). My preliminary data (**Appendix A and B**) determined that treatment of mouse embryos with CQ, at 75 μ M for two hours, allows for the detection of significant differences in LC3-II employing both western blot (**Supplementary Figure 3**) and LC3-II puncta cell counts by immunofluorescence (**Supplementary Figure 4**). This experimental protocol and design resulted in no observable changes in morphology between CQ-treated blastocysts and non-treated controls (**Supplementary Figure 2**). My preliminary data (**Appendix C**) confirms that CQ treatment inhibits autophagy in mouse preimplantation embryos.

Mouse embryos at the 2-cell stage were treated with NEFAs for 40 hours with a 75 μ M CQ treatment applied during the last two hours of the total treatment period. The immunofluorescence signal of LC3-II puncta aggregates per cell was analyzed for each treatment group. In all treatment groups with CQ, no significant difference in the levels of LC3-II puncta fluorescence per cell were observed compared to its corresponding treatment group without CQ control (**Figure 17**, $P > 0.05$, Tukey's multiple comparisons test). The PA+CQ group, displayed a significant increase in fluorescence signal of LC3-II puncta aggregates per cell than all other non-PA treatment groups (**Figure 17**, $P < 0.05$, Tukey's multiple comparisons test). Specifically, treatment of PA+CQ resulted in approximately a 2-fold increase in fluorescence signal of that observed for the CON+CQ group (**Figure 17**, $P < 0.01$, Tukey's multiple comparisons test) as well as OA+CQ and PAOA+CQ groups (**Figure 17**, $P < 0.05$, Tukey's multiple comparisons test). No significant differences in fluorescence intensity of LC3-II puncta aggregate per cell were observed between CON+CQ, OA+CQ, and PAOA+CQ groups (**Figure 17**, $P > 0.9999$, Tukey's multiple comparisons test). **Figure 18** displays representative images of LC3-II aggregate puncta formation after NEFA +/- CQ treatments for 40 hours.

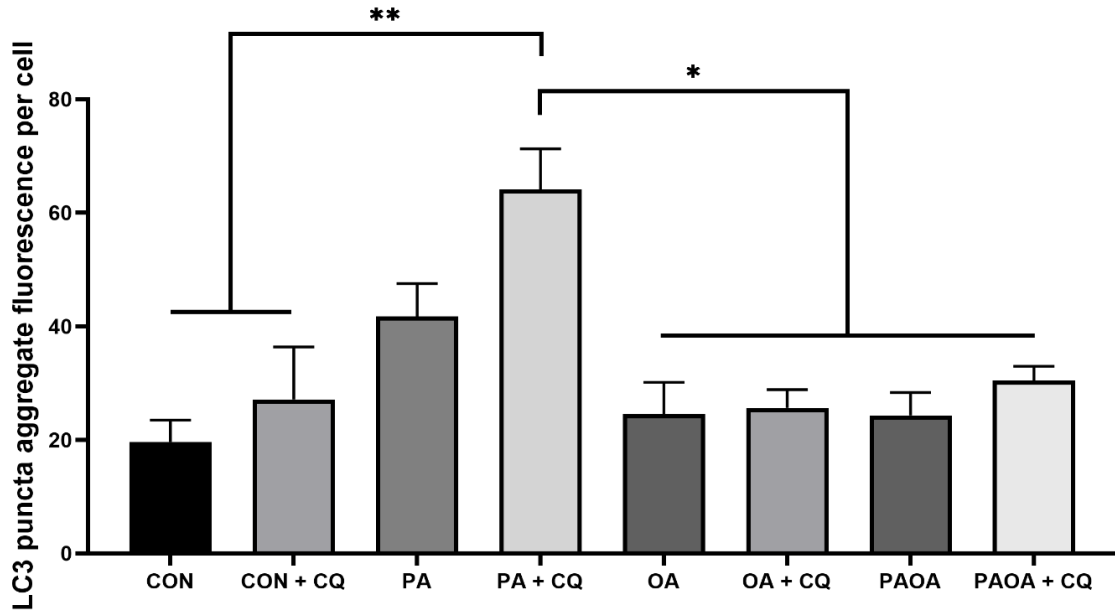


Figure 17. Autophagic flux of embryos after NEFA+/- CQ treatment for 40 hours.

Fluorescence signal of LC3-II puncta per cell after 40 hours of treatment with 100 μ M PA, 250 μ M OA, 100 μ M PA and 250 μ M OA, or KSOMaa medium alone (control), and 75 μ M of chloroquine exposure for the last 2 hours (+ SEM). Only embryos of 8-cell stage and up were included. N=3, one-way ANOVA and Tukey's HSD post-hoc test. Significant differences are indicated by * $p < 0.05$ and ** $p < 0.01$.

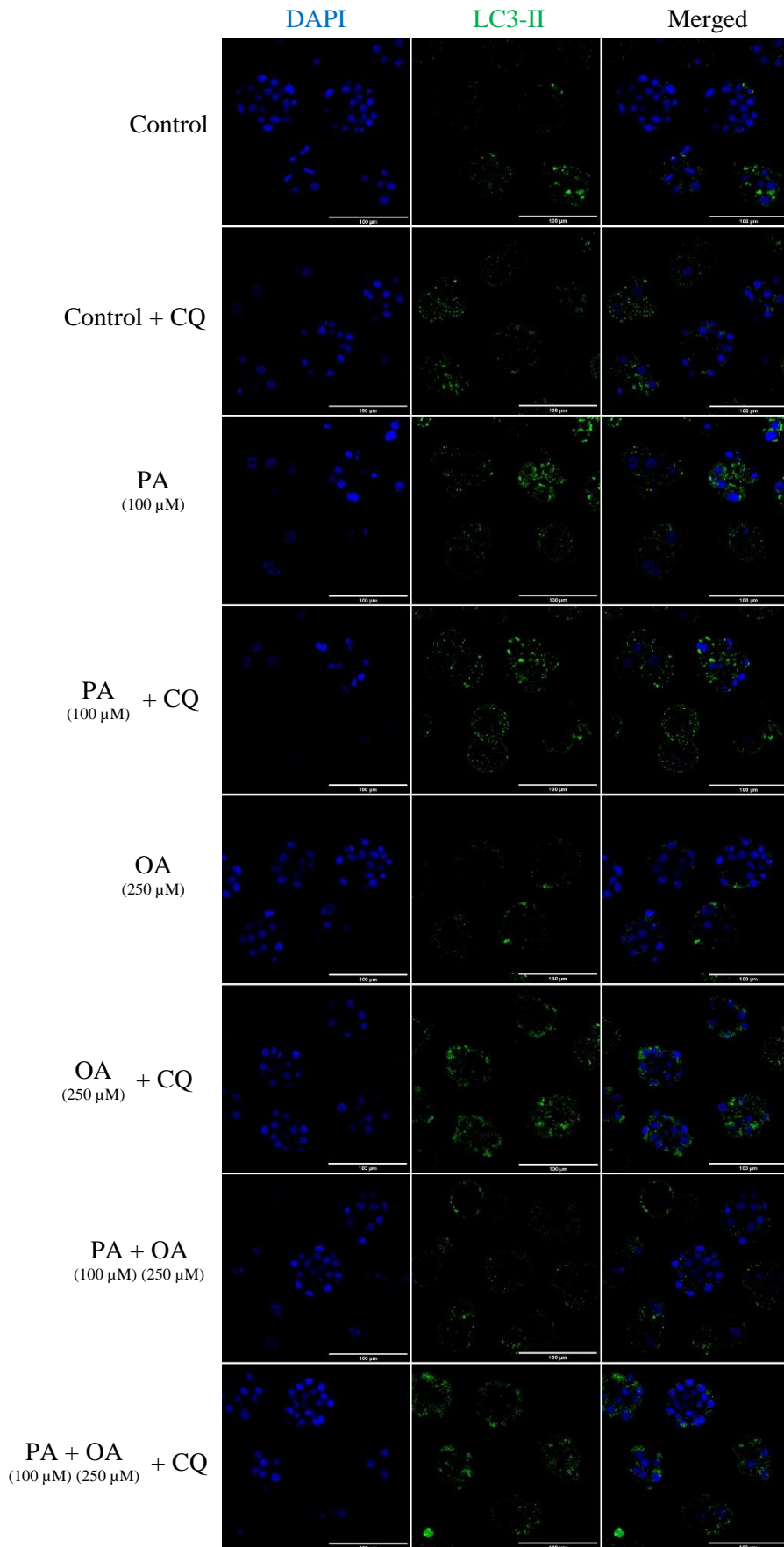


Figure 18. Representative images of LC3-II puncta in embryos after NEFA +/- CQ treatment for 40 hours.

Representative images of LC3-II aggregate puncta formation after NEFA +/- CQ treatments for 40 hours. Scale bar = 100 μ m.

3.5 Effects of PA and OA on autophagosome maturation and degradation

To investigate effects to additional key steps in the autophagic process I next assessed autophagosome-lysosome interactions in NEFA-treated mouse embryos. Mouse embryos at the 2-cell stage were exposed to NEFA for 40 hours then the co-localization of LC3-II puncta and lysosomes were analyzed.

Assessment of the average number of LC3-II-lysosome co-localized puncta per cell revealed that mouse embryos exposed to 250 μM of OA resulted in an approximately 3-fold significant increase of co-localized puncta than embryos treated with 100 μM of PA alone (**Figure 19A**, $P < 0.05$, Tukey's multiple comparisons test). Representative images of LC3-II-lysosome co-localized puncta after NEFA treatment is shown in **figure 19B**.

When the total LC3-II puncta count per cell were measured, the proportion of LC3-II-lysosome co-localized puncta per cell out of total LC3-II puncta per cell across each treatment group were also measured. This analysis demonstrated that treatment with 250 μM of OA resulted in a significantly higher proportion of autolysosome per cell than that observed in embryos treated with 100 μM of PA alone (**Figure 20**, $P < 0.05$, Tukey's multiple comparisons test).

Finally, an experiment was carried out to investigate the effects of PA and OA treatment on lysosomal activity. Mouse embryos at the 2-cell stage were exposed to NEFA for 40 hours then the fluorescence signal of LysoTracker Red, representing lysosomal activity, was analyzed. Comparison of the fluorescence signal across each treatment group revealed that after treatment with 100 μM of PA for 40 hours, LysoTracker Red fluorescence intensity was significantly lower compared to all other NEFA groups (**Figure 21A**, $P < 0.01$, Tukey's multiple comparisons test). Meanwhile, LysoTracker Red fluorescence intensity after 40 hours of treatment with 250 μM of OA alone or PA+OA co-treatment resulted in no significant differences from that observed in the control group (**Figure 21A**, $P > 0.05$, Tukey's multiple comparisons test). Representative images of LysoTracker Red fluorescence signal after NEFA exposure for 40 hours are shown in **figure 21B**.

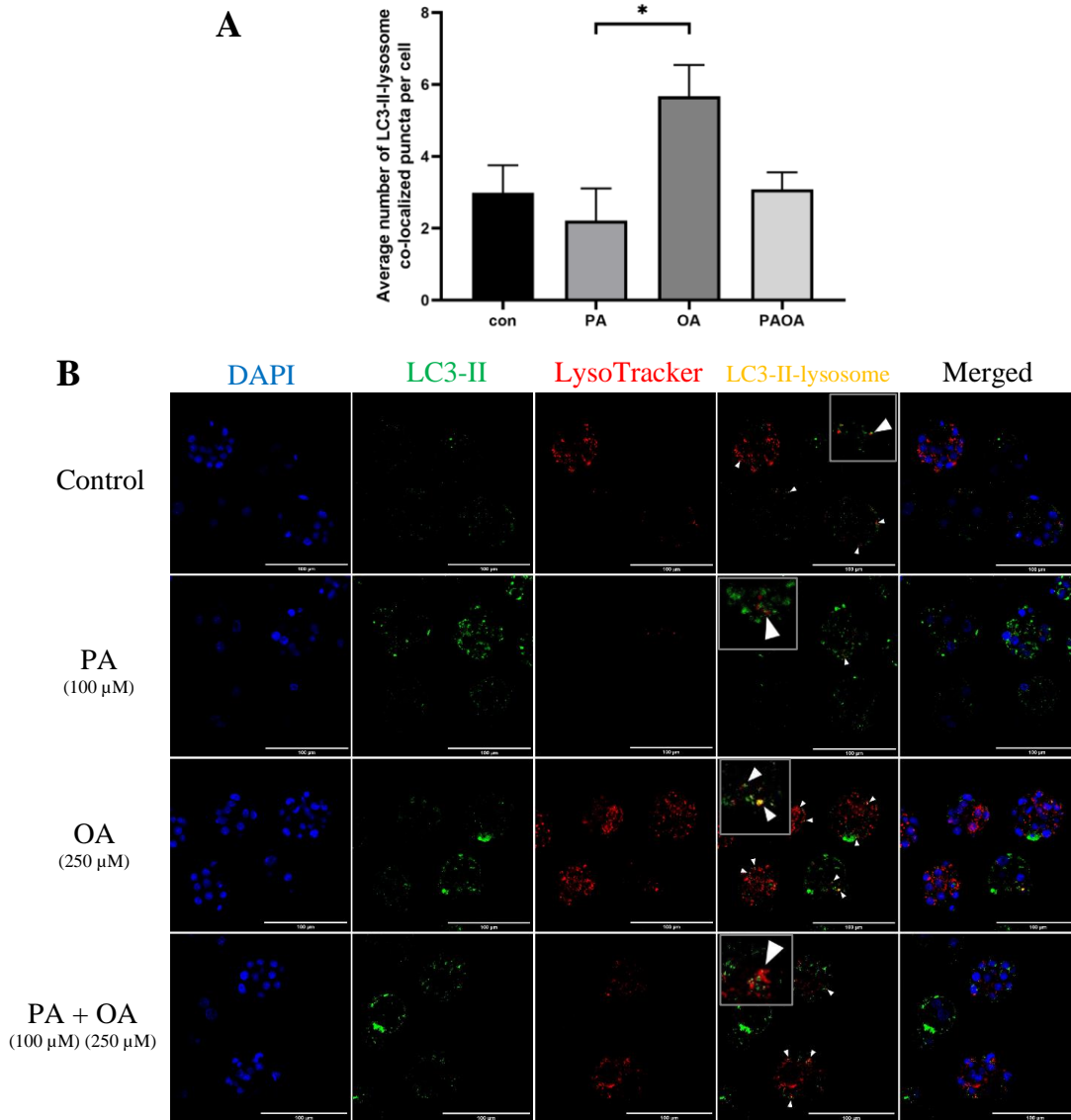


Figure 19. Autophagosome-lysosome co-localization in embryos after 40 hrs. of NEFA treatments

Average number of LC3-II-lysosome co-localized puncta per cell (+SEM) after treatment for 40 hours with 100 μ M PA, 250 μ M OA, 100 μ M PA and 250 μ M OA, or KSOMaa medium alone (control) (A). Only embryos of 8-cell stage and up were included. N=3, one-way ANOVA and Tukey's HSD post-hoc test. Significant differences indicated by *, $p < 0.05$. Representative images of LC3-II-lysosome co-localized puncta after NEFA exposure (B). Arrows indicate for LC3-II-lysosome co-localized puncta. Scale bar = 100 μ m.

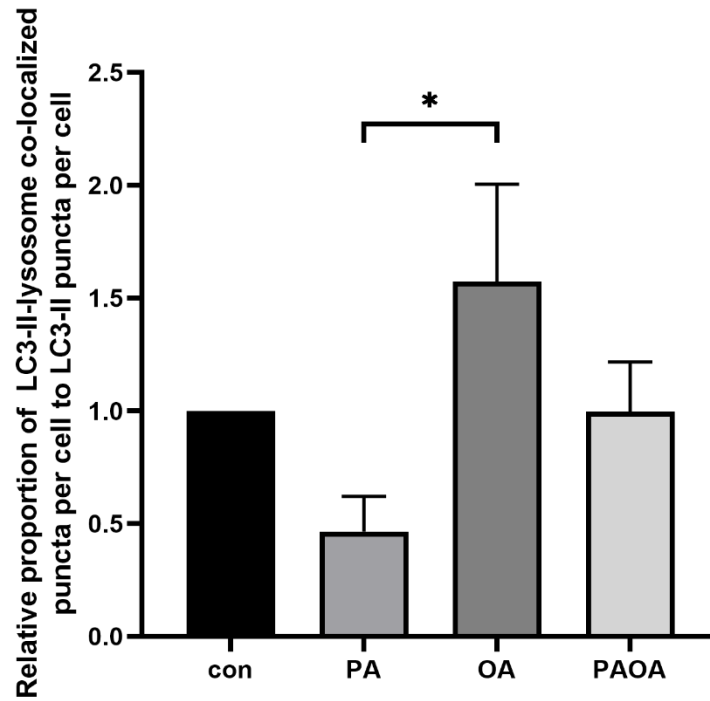


Figure 20. Autolysosome in embryos after 40 hrs. of NEFA treatments

Relative proportion of LC3-II-lysosome co-localized puncta per cell to total LC3-II puncta per cell (+SEM) following 40 hours of treatment with 100 μ M PA, 250 μ M OA, 100 μ M PA and 250 μ M OA, or KSOMaa medium alone (control). Only embryos of 8-cell stage and up were included. N=3, one-way ANOVA with Tukey's HSD post-hoc test. Significant differences are indicated by * $p < 0.05$.

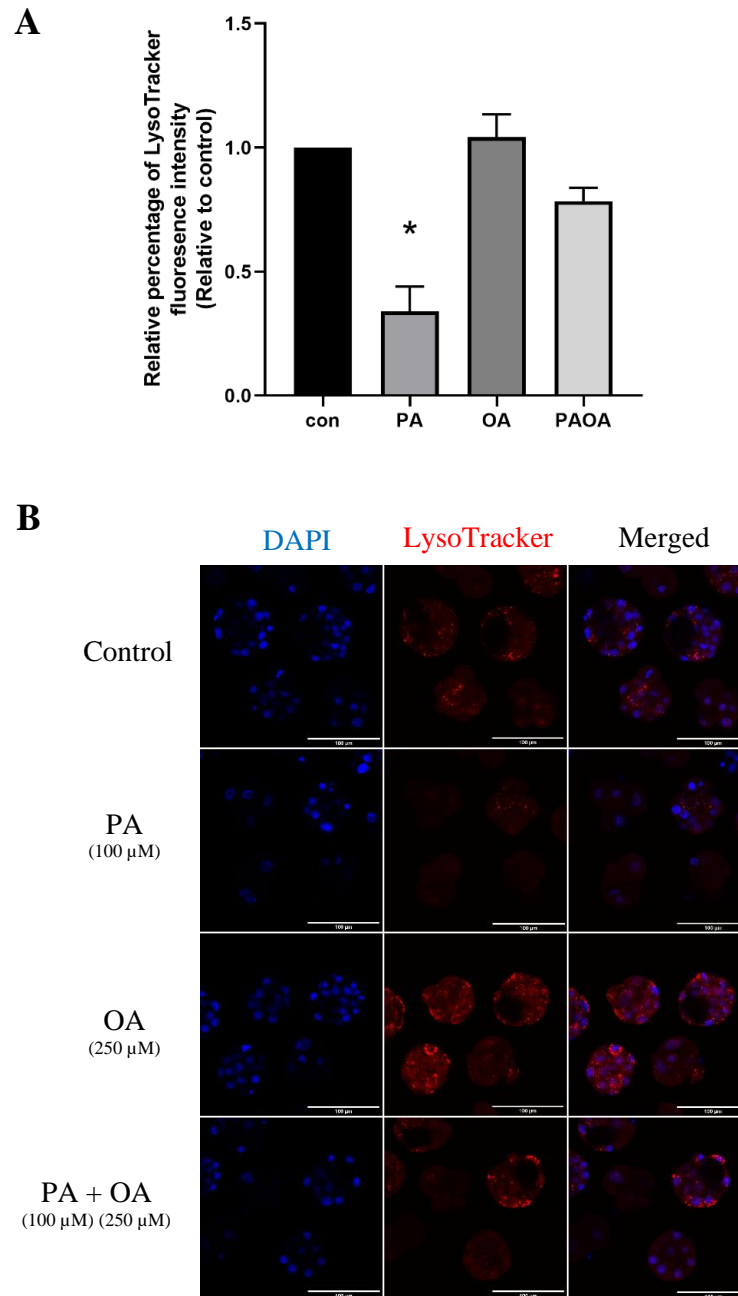


Figure 21. LysoTracker signal in embryos after NEFA treatments for 40 hrs.

Relative percentage of LysoTracker fluorescence signal (+SEM) under 40 hours treatment with 100 μ M PA, 250 μ M OA, 100 μ M PA and 250 μ M OA, or KSOMaa medium alone (control) (**A**). $N=4$, one-way ANOVA with Tukey's HSD post-hoc test. Significant differences are indicated by * $p < 0.05$. Representative images of 2-cell mouse embryos in NEFA treatments for 40 hours (**B**). Scale bars = 100 μ m.

Chapter 4

4 Discussion

A developing preimplantation embryo is highly vulnerable to the surrounding environment provided by the follicular and reproductive tract fluid(s). Profiling the follicular fluids of women undergoing ART identified the presence of NEFAs including PA and OA and determined that fatty acids are especially elevated in those women with a high BMI index (Valckx et al 2014). The effects of PA and OA treatments on a variety of cell types are the subject of intense investigation but very few have explored their effects on preimplantation embryos. Recently, our lab reported developmental impacts brought upon by PA and OA exposure during mouse preimplantation development. Our study uncovered several of the possible underlying mechanisms that contribute to the reduced developmental competency exhibited by PA treated embryos including the activation of ER stress pathway(s) (Yousif et al. 2020). ER stress activation initiates several cell survival mechanisms, with one being autophagy (Ogata et al. 2006). Autophagy is an evolutionarily conserved mechanism in eukaryotic organisms that acts as a “last resort” to maintain cellular homeostasis before initiating apoptosis (Lee et al. 2015). Despite its essential role in cell survival, the importance of autophagy in preimplantation development was only first indicated by Tsukamoto *et al.* (2008). This study demonstrated that autophagy activation, especially after fertilization, is required for proper mouse preimplantation development (Tsukamoto et al. 2008). However, the potential role that autophagy may contribute during preimplantation development following NEFA treatment was not considered. Thus, my thesis aimed to characterize and model the autophagic underpinnings impacted by obesity-induced hyperlipidemia during early mouse embryo development *in vitro*. Overall, it was hypothesized that NEFA-induced lipotoxicity would dysregulate autophagic mechanisms in mouse preimplantation development. Specifically, PA would disrupt autophagosome formation while the addition of OA would negate lipotoxic effects and enhance overall developmental success. To test this hypothesis, three objectives were investigated to first, assess autophagy in NEFA-treated mouse embryos throughout preimplantation development; second, to assess autophagosome formation in NEFA-treated embryos; and third, to

assess autophagosome-lysosome interactions in NEFA-treated mouse preimplantation embryos.

4.1 NEFA effects on mouse preimplantation development

To characterize the NEFA effects on preimplantation embryos, mouse preimplantation embryos were treated with 100 μ M PA, 250 μ M OA, 100 μ M PA and 250 μ M OA, or KSOMaa medium alone (control) beginning at the 2-cell stage for 18, 24, 30, 40, and 48 hours. This study presents outcomes from the first NEFA treatment time-course study that has characterized NEFA treatment effects on development of mouse early embryos. Developmental progression of treated 2-cell stage embryos was not affected by NEFA treatment during the first 24 hours of treatment. However, as the NEFA treatment time increases, important differential treatment effects on preimplantation development begin to appear. Consistent with our previous findings (Yousif et al. 2020), treatment of 2-cell stage mouse embryos with 100 μ M PA for 48 hours resulted in a significant decrease in blastocyst development as embryos were arrested at the 8-cell stage. As well, the treatment of mouse embryos beginning at the 2-cell stage with 250 μ M OA resulted in no beneficial effect nor impairment of preimplantation development, and this also consistent with our previous findings (Yousif et al. 2020). Similar results from PA and OA treatments were also reported in studies applied to bovine early embryos which suggests that both embryo species may employ similar adaptive mechanisms to adjust to changing NEFA level environments. Leroy et al. (2005) reported the addition of PA in oocyte maturation medium reduced cleavage rate and blastocyst yield of bovine embryos *in vitro*; while OA had no effects on developmental capacity compared to controls.

To our surprise, the treatment of 100 μ M PA and 250 μ M OA in combination resulted in a reduction in morula stage embryos at the 30-hour time point compared to the control group. This is the first report that a PA and OA combination treatment can slow preimplantation developmental progression. Although PA and OA combination treatment displayed a slower progression through the early cleavage stages, a “catch-up growth” effect occurred at the end of preimplantation development that resulted in no differences in blastocyst frequencies between the PA and OA combination treatment and untreated controls. I would propose that the slowed progression and catch-up growth effect could

potentially be due to differential uptake rates for each individual fatty acids at varying embryo cell stages. Wang and Tsujii (1999) reported significant differences in incorporation rate of PA and OA at different stages of preimplantation mouse development. The incorporation of PA into embryo lipids steadily increases throughout mouse preimplantation development, whereas OA is mostly incorporated into triacylglycerol (TAG) at an exponential rate at the morula and blastocyst stage (Wang and Tsujii 1999). Thus, PA uptake exceeds OA uptake at all preimplantation stages except at the blastocyst stage (Wang and Tsujii 1999). Early-stage preferential PA uptake and its possible conversion to diacylglycerol (DAG) and likely ceramide (Listenberger et al. 2003) could explain the detrimental effect of PA treatment resulting in developmental arrest between the 4- to 8-cell stages. The addition of OA in the combination treatment, despite having a delayed initial uptake during early cleavage stages, undergoes an exponential increase in uptake to more than 1.5-fold of PA uptake at the blastocyst stage (Wang and Tsujii 1999). As studies investigating OA treatment effects on cells generally conclude that OA is beneficial for regulating cell metabolism and inflammation (Fayezi et al. 2018), the surge of OA uptake at the later preimplantation stages could promote this “catch-up growth” that rescues blastocyst development levels in the PA and OA combined treatments. Additionally, the cellular conversion of OA to oxidative metabolism energy intermediates and phospholipids as demonstrated by Wang and Tsujii (1999) suggests OA treatment alone or in combination with PA can assist in regulating the required energy and cell membrane structural demands for accelerated growth to the blastocyst stage. My results also suggest that this process is well underway by 30 hour of combined treatment and is certainly well in place by 40 hours of co-treatment as developmental stage differences between the untreated control and PA and OA co-treatment were no longer observed at the 40-hour time point or beyond. In total, my results support that OA exerts an ability to offset PA treatment-induced developmental impairments. Uniquely my study has defined a developmental window between 30 to 40 hrs of treatment where OA fully engages in providing this beneficial outcome to the early embryo.

The dosage of PA and OA used in the experimental design was established based on Yousif *et al.* (2020). The dosage of PA and OA employed approximates the serum levels

of NEFAs found in individuals undergoing IVF treatments, whom BMI index averages at 25 (Jungheim et al. 2011). As reported by Jungheim *et al.* (2011), the mean serum PA concentration was 150 μM and mean serum OA concentration was 220 μM . Jungheim *et al.* (2011) also reported a three-fold reduction in NEFA concentrations in follicular fluids compared to serum levels at 56 μM for PA and 64 μM for OA. Another study by Valckx *et al.* (2014) reported total NEFA concentration of follicular fluids of obese individuals with BMI index over 35 averages at 315.5 μM ; levels of PA and OA in the follicular fluids was at 70.3 μM and 102.5 μM , respectively. It is important to note though, PA and OA exist in different forms in the follicular fluid, including triglycerides, cholesterol esters, and phospholipids in addition to non-esterified forms. PA and OA are both the most abundant fatty acids existing in all these forms regardless (Valckx et al. 2014). My studies were of course represented an *in vitro* model of PA and OA exposure on preimplantation development. They provide important outcomes that represent foundational discoveries that are required to understand the differential effects of PA and OA treatments on mouse preimplantation development. Thus, my outcomes have direct application to improving *in vitro* culture environments. OA treatment may become an important additional embryo culture medium constituent as it could improve blastocyst development of embryos that were maternally exposed to high fatty acid levels.

4.2 Autophagy throughout preimplantation development

Tsukamoto *et al.* (2008) observed that autophagy is induced after fertilization and that knockout of the autophagy-related gene 5 (ATG5) gene expression in early mouse embryos results in developmental arrest at the 4- to 8-cell stage, and even embryo lethality. ATG5 is essential for autophagosome membrane elongation and formation (Melia et al. 2020). Although autophagy is clearly important and necessary for normal preimplantation development to occur, the temporal pattern of key transcripts encoding key autophagic pathway constituents throughout mouse preimplantation development were not well known. Thus, to assess relative transcript level of autophagy pathway markers throughout preimplantation development, mouse embryos were cultured in KSOMaa medium and collected at 1-cell, 2-cell, 4-cell, 8-cell, morula, and blastocyst stages.

RT-qPCR analysis of mRNA transcript levels of autophagic markers *Becn1*, *Atg3*, *Atg5*, and *Map1lc3b* were conducted. Beclin-1 is an essential component of the PI3K complex that initiates for phagophore nucleation (Noda et al. 2010). It also plays a regulatory role in apoptosis by freeing Bcl-2 to inhibit pro-apoptotic protein BAX (Hill et al. 2019). The relative mRNA transcript level of Beclin-1 in preimplantation mouse embryos significantly declined after the 1-cell stage and then gradually restored the 1-cell level again by the blastocyst stage. This pattern of relative mRNA levels throughout mouse preimplantation development is very common for many other key developmental transcripts (Li et al. 2013). It reflects the well-known loss and degradation of maternal transcripts that occurs in fertilized 1-cell embryos and is largely completed by the 2-cell stage, followed by embryonic/zygotic genome activation (ZGA) and a stage specific increase in relative mRNA transcript level up to the blastocyst stage. A study by Lee *et al.* (2011) reported similar mRNA expression patterns for of Beclin-1 in mouse preimplantation embryos in which transcript levels gradually decreased from the zygote to the blastocyst stage; but no recovery of mRNA level was observed at the blastocyst stage (Lee et al. 2011). A study of Beclin-1 mRNA transcript abundance in porcine embryos also observed a gradual decrease as embryos progressed through preimplantation stages with no restoration of Beclin-1 mRNA levels (Xu et al. 2012). Thus, it is well understood that Beclin-1 mRNA expression during early preimplantation stages is of maternal genome origin. However, my discovery of a restoration of Beclin-1 mRNA transcript levels at the blastocyst stage is novel and one that suggests the embryonic genome is capable of transcribing Beclin-1 during preimplantation development. This difference between studies could simply be due to my investigation using later stage blastocysts and hatching blastocysts (E4.5) which are more advanced than those employed in other studies. An assessment of autophagy activity in rat embryos conducted by Ekizceli *et al.* (2017) found that autophagy increases in both trophoblast and inner cell mass during embryo implantation. Thus, the relative increase in Beclin-1 mRNAs at the blastocyst stage that I detected underlie the elevation of autophagy in the late blastocysts as they prepare for implantation. Further studies are required to determine if this possibility has merit.

ATG3 is an essential activator protein that attaches a phosphatidylethanolamine (PE) onto LC3-I to become activated LC3-II. This activation is required for autophagosome formation (Ravanan et al. 2017). The relative ATG3 mRNA transcript levels in preimplantation mouse embryos remained identical across all preimplantation stages. Although no significant differences were observed in relative ATG3 transcript levels between stages, it was readily detected in all embryo stages. This suggests the possibility that ATG3 mRNA has a relatively short half-life throughout mouse preimplantation development, and that its steady production throughout all stages is a functional autophagic pathway requirement for development and its consistent LC3-II activation pattern.

ATG5 orchestrates autophagosome formation by recruiting membrane-bound proteins to deliver cargo contents for degradation. My results showed that relative transcript abundance of ATG5 mRNA drops significantly after the 1-cell zygote stage. In agreement with these findings, Lee *et al.* (2011) reported a significant drop in ATG5 mRNA expression after the 1-cell stage in mouse embryos. Similarly, a study by Xu *et al.* (2012) also reported a significant decrease in ATG5 mRNA transcript after the 1-cell stage in porcine embryos. This relative transcript abundance pattern across preimplantation stages is highly suggestive of ATG5 transcripts being primarily of oogenetic genome origin. The gradual decrease observed post-1-cell stage likely arises due to maternal transcript turnover as early embryos progress through each subsequent developmental stage. Interestingly, normal levels of autophagy were observed in ATG5 knock-out 2-cell embryos derived from heterozygous ATG5 mice (Tsukamoto et al. 2008), which confirms that ATG5 transcripts are derived from the maternal genome and that while autophagy is necessary during preimplantation development, minimal levels of ATG5 are required to support autophagy during preimplantation development.

Activated LC3, LC3-II protein is critical for autophagosome formation as LC3-II acts as a binding site for cargo contents bound for degradation (Ravanan et al. 2017). LC3 is produced as a precursor prior to activation to LC3-I and -II (Ravanan et al. 2017). I observed that relative LC3 mRNA transcript abundance maintains similar levels throughout the early cleavage stages and then gradually increases as the embryos

progress to the blastocyst stage. Previously, the study by Lee *et al.* (2011) reported a gradual decrease of mRNA transcript of LC3 throughout mouse preimplantation stages and the study by Xu *et al.* (2012) also reported the same pattern in porcine embryos. Interestingly, Noguchi *et al.* (2020) reported that *in vitro* and *in vivo* produced bovine blastocysts displayed significant differences in the relative mRNA levels of PI3K-Akt-mTOR pathway constituents that support autophagy pathway activation. Since my studies were confined to stages resulting from the placement of 2-cell stage mouse embryos in culture up to the blastocyst stage, it is possible the increase in LC3 transcript I observed by the blastocyst stage, is a result of the prolonged culture period that my embryos were exposed to. Further experiments are required to determine if *in vitro* vs *in vivo* stage differences exist for these autophagy pathway constituent mRNAs in mouse preimplantation embryos.

LC3-II is a widely accepted marker for autophagy as it is present on the outer membranes of autophagosomes. Mizushima *et al.* (2010) described multiple assays for measuring autophagy and highlighted that the use of fluorescence microscopy to assess LC3-II puncta representing autophagosomes as an accessible and powerful method. In the current study, the relative percentage of LC3 puncta per cell significantly decreased from the 2-cell stage to the blastocyst stage. Lee *et al.* (2011) supported this finding as LC3 is observed in mouse preimplantation embryos at all cell stages via immunofluorescence staining, though the authors did not make quantitative comparisons between embryo stages. Interestingly, the significant decrease in LC3-II puncta counts per cell throughout preimplantation development was opposite to the increase LC3 relative mRNA transcript levels observed. This is partially explained by the way in which both methods were applied. While LC3-II puncta per cell decreased as development advanced, embryonic cell number dramatically increased during preimplantation development, so that total LC3-II puncta per embryo also increased as development proceeded. However, we were primarily interested in providing a measurement of autophagic activity per stage and this typically is measured by determining LC3-II puncta per cell. Thus, while puncta per cell decreased during mouse preimplantation development, suggesting a per cell decrease in autophagy, from a whole embryo perspective it actually increased per embryo as development proceeded, which conforms nicely with the relative increase in LC3 mRNA

observed by the blastocyst stage. Importantly, the activation of LC3 into LC3-II may be limited by the availability of ATG3 (Agrotis et al. 2019). ATG3 transcript levels remained relatively stable across all preimplantation stages. Activation of LC3 may therefore be limited by the turnover of ATG3 protein and the demand to initiate autophagy to maintain cell homeostasis. Another important aspect worth noting is that LC3 mRNA could have a short half-life and thus LC3 activation may be tightly regulated, resulting in the net low levels of LC3-II puncta per cell observed at the later stages of preimplantation development. My study and results are the first report demonstrating that autophagy activation per cell significantly decreases throughout preimplantation development.

4.3 NEFA effects on preimplantation embryo autophagy

Previous sections reported negative impacts of PA treatment on preimplantation development in mouse embryos and those PA-induced effects could be negated by OA treatments. As autophagy plays a role throughout development to maintain cell homeostasis, the primary objective of this thesis was to assess NEFA effects on autophagy in preimplantation embryos. Relative mRNA transcript analysis of autophagic markers (*Becn1*, *Atg3*, *Atg5*, and *Map1lc3b*) did not result in the detection of any significant differences at the transcript level following 48 hours of NEFA treatment, which suggests that NEFA treatment did not affect the relative transcriptional patterns and half-lives of the selected autophagic markers. In support of this outcome, studies applied to C2C12 mouse myoblast cells, observed no change in LC3 mRNA transcript levels after 48 hours of co-treatment of PA and OA at 250 μ M each (Bollinger et al. 2018). Furthermore, studies applied to mouse hepatic cells, observed no change in ATG5 mRNA levels after prolonged high-fat diet (Okada et al. 2017). NEFA exposure appears to have limited impact on autophagic pathway constituent at the mRNA level for various cell types, though more evidence is required to confirm our findings.

My thesis also presented, for the first time, the temporal pattern of protein expression of LC3-II after exposure to NEFA treatments throughout mouse preimplantation development. No significant changes in relative percentage of LC3-II puncta count per cell was observed between groups after 18 and 24 hours of NEFA treatment beginning at

the 2-cell stage. Wang and Tsujii (1999) reported significant differences in incorporation rate of PA and OA at different preimplantation stages in mouse embryos – the uptake of PA exceeds OA uptake specifically at the earlier stages. Though, the treatment of PA did not result in significant changes in autophagy during the first 24 hours of preimplantation development. These results certainly suggest that the effects of PA and OA treatment at the doses employed in this study require longer than 24 hrs of exposure to affect autophagy activation. The temporal pattern of autophagy in nerve cells after stressors like spinal cord injury summarized that the activation of autophagy is delayed for hours to even days after the injury, regardless of the types of nerve cells (Zhou et al. 2017). Although the level of autophagy is likely dependent on the severity of the stressor, non-immediate activation of autophagic activity was a common element across several divergent cell systems and tissues (Zhou et al. 2017).

Importantly, 2-cell mouse embryos exposed to PA-only and PA and OA co-treatment for 30 hours did show a significant increase in percentage of LC3-II puncta per cell than OA-alone treatment. This outcome appears to define a treatment period required using the NEFA doses employed in this study to activate autophagy in an effort re-establish embryo homeostasis. The induction of autophagy, as reflected by LC3-II puncta count, likely occurred between 24 and 30 hours of PA exposure. I speculate that PA treatment disrupted ER homeostasis and induced ER stress, which led to the initiation of UPR as well as the activation of autophagy to maintain homeostasis. Yousif *et al.* (2020) reported that PA treatment induces ER stress pathway constituents in preimplantation mouse embryos. Notably, the treatment of 2-cell mouse embryos with PA increased x-box binding protein 1 (XBP1) mRNA splicing in the inositol-requiring protein 1 α (IRE1 α) arm of the ER stress pathway (Yousif et al. 2020). Such mRNA splicing of the XBP1 creates the active XBP1 protein that acts as a nuclear transcription factor to induce gene expression of autophagy-related proteins like Beclin-1 in endothelial cells (Margariti et al. 2013). Additionally, autophagy can also be initiated by AMPK activity via direct activation of ULK1 (Kim et al. 2011). The elevated transcription of autophagy-related genes by PA-induced effects potentially contributes to the elevated presence of autophagosomes (as reflected by the elevated level of LC3-II puncta count per cell) in the PA group after 30 hours of treatment. In contrast, OA treatment had no effect on the

percentage LC3-II puncta per cell than control. The presence of LC3-II puncta in the OA treatment group immunofluorescence images likely represents basal levels of autophagy.

The same overall outcome was observed after 40 hours of NEFA exposure, but to a greater extent. Exposure of 2-cell mouse embryos to PA-only and PA and OA co-treatment for 40 hours resulted in a significantly greater percentage of LC3-II puncta per cell than control and OA groups. The OA treatment group remained the same as control in terms of percentage LC3-II puncta per cell after 40 hours of treatment.

However, after exposure to 48 hours of NEFA treatments, the percentage of LC3-II puncta per cell dropped for the PA and OA co-treatment group. To our surprise, two-cell mouse embryos that were exposed to PA and OA co-treatment for 48 hours resulted in a significantly lower percentage of LC3-II puncta per cell than the PA-alone group. Additionally, PA and OA co-treatment resulted in similar levels of LC3-II puncta per cell as the OA-alone group. This result suggests that the addition of OA in the co-culture group relieved PA-treated embryos from the elevated level of autophagy seen at the 30 and 40 hours. I would propose that this outcome is again related to the differential uptake kinetics that PA and OA display during mouse preimplantation development (Wang and Tsujii 1999). Akoumi *et al.* (2017) reported that treatment of cardiomyocytes with PA and OA preferentially stored fatty acids as DAG and TAG, respectively. The exponential increase in OA uptake during the morula-blastocyst phase of preimplantation development likely contributes to altered energy metabolism that negates PA individual effects and restores appropriate embryonic homeostasis at the later stages of preimplantation development. Aardema *et al.* (2011) reported significantly larger and increased number of lipid droplets in bovine oocytes that were co-treated with PA and OA in comparison to PA-alone treatment. Furthermore, a study of Chinese hamster ovary cells suggested that the addition of OA in PA treatment re-directed lipid storage of PA into triglycerides instead of generating reactive species like ceramides, thus preventing cytotoxicity effects from PA accumulation (Listenberger *et al.* 2003). Mouse preimplantation embryos also respond to PA and OA co-treatment similarly, where the presence of OA in PA treatment alters lipid metabolic pathway and PA uptake into long-term storage as triglycerides (Yousif *et al.* 2020). It is likely that the redirection of PA

into lipid droplets (as triglycerides) reduces PA metabolism to DAG and ceramide in the cytosol that induces ER stress to thus lower autophagy required to maintain embryo homeostasis. My study is the first report of this temporal aspect of OA rescuing effects in mouse preimplantation embryos and the restoration of autophagic activity occurring between 40 and 48 hours of NEFA treatment during mouse preimplantation development.

It is important to note that the OA-alone treatment for 48 hours beginning at the 2-cell stage had no significant effect on the percentage of LC3-II puncta per cell compared to controls, even though OA uptake should be significantly increased (Wang and Tsujii 1999; Yousif et al. 2020). Lee *et al.* (2019) reported no change in LC3-II protein expression in hepatocytes after treatment of up to 200 μ M OA. Similarly, in bovine embryos, OA-alone treatment had no detrimental effects on preimplantation development; OA treatment even significantly increased cleavage rates and blastocyst development (Karaşahin and Arıkan 2015). Although OA beneficial effects in mouse embryos were not observed, it is agreed in the literature that OA treatment does not impose negative effects on preimplantation development (Aardema et al. 2011; Karaşahin and Arıkan 2015; Lee et al. 2019). The LC3-II puncta observed in the immunofluorescence images of the OA group likely represent basal levels of autophagy.

At the 48 hours time point, the relative percentage of LC3-II puncta per cell was maintained at a high level in the PA treated group. The relatively high percentage of LC3-II puncta per cell is suggestive of autophagosome accumulation in the PA-treated embryos. If left in this condition it is likely that the accumulation of autophagosomes in PA-treated embryos would result in a cytotoxic response in the embryos, that may underlie the early developmental arrest observed in PA-treated embryos. Autophagosome accumulation has a close relationship to cytotoxicity (Button et al. 2017). Button *et al.* (2017) showed the buildup of autophagosomes in various cell lines with little lysosomal activity results in a significant reduction in cell viability. In contrast, the reduction in autophagosome formation to prevent autophagosome accumulation could alleviate cellular toxicity (Button et al. 2017).

Although quantification of LC3-II puncta is considered a gold-standard assay as a measurement for autophagosome formation, there is a limitation to this method of measurement. Runwal *et al.* (2019) reported that when HeLa cells were inhibited from autophagy activation, LC3-I and p62 can aggregate and accumulate in the cytosol as prominent LC3-positive structures. The study warns of potential misinterpretation of LC3-I-p62 aggregates as LC3-II puncta and thus the confusion of autophagosome structures when this method of measurement is employed (Runwal et al. 2019). We cannot rule out the possibility that LC3-I-p62 aggregation may confound our findings in the current study, but it highlights the need for future experiments to validate our findings. Potentially through an alternate method of measuring autophagosomes formation, for example, LC3-II protein expression analysis through western blot, may confirm the effects of NEFA treatment on autophagosome accumulation in the present study.

4.4 NEFA effects on autophagosome formation

The second primary objective was to characterize the effects of NEFAs on autophagosome formation in preimplantation mouse embryos. In the first objective, it was identified that 100 μ M PA treatment results in a significant increase of relative percentage of LC3-II puncta per cell after 30 hours of treatment. The observation that more LC3-II puncta per cell was present in the PA group is reflective of autophagosome accumulation at that treatment time point. Autophagy, however, is a dynamic process consisting of autophagosome formation, maturation, and degradation. The accumulation of autophagosomes is therefore a balance between the rate of autophagosome formation and autophagosome degradation (Mizushima et al. 2010). Thus, it is important to investigate autophagy at several different levels to characterize the underlying effects brought upon by NEFA exposure on mouse preimplantation embryo autophagy. In the present objective, the effects of NEFA treatments on autophagosome formation in preimplantation mouse embryos were investigated by employing treatment with an autophagy inhibitor chloroquine (CQ) that blocks autophagosome binding to lysosomes (Mauthe et al. 2018).

Mouse preimplantation embryos at the 2-cell stage were treated with NEFA treatments for 40 hours with 75 μ M CQ for the last two hours of treatment period. Although no significant differences were found between each NEFA treatment groups with its respective CQ-treated groups, treatment of PA with CQ resulted in a significantly greater fluorescence of LC3-II puncta aggregate per cell than all other non-PA groups. Amongst all groups, it is important to highlight that treatment of PA with CQ for 40 hours resulted in a significantly greater fluorescence in LC3-II puncta aggregate per cell than CQ-only group. After inhibiting autophagosome degradation for two hours using CQ, the difference of LC3-II puncta fluorescence between PA+CQ group and CQ-only group is likely indicative of a significant increase in autophagosome formation in the PA treatment than that of controls. A previous study by Dhayal *et al.* (2019) reported that in pancreatic β -cells, a significant increase in the number of autophagosome puncta was observed after PA and Bafilomycin A1 (BafA1; autophagy inhibitor) treatment compared to inhibitor-alone treatment. Similarly, Las *et al.* (2011) also reported increased autophagosome formation in a PA treatment group with ammonium chloride and leupeptin ($\text{NH}_4\text{Cl}/\text{Leu}$) as autophagy inhibitors in INS-1 pancreatic β -cells. These studies and mine show that PA treatment consistently results in the accumulation of autophagosomes, by increasing autophagosome formation, in a variety of different cell types.

Another crucial finding is that both OA+CQ and PAOA+CQ treatment for 40 hours resulted in similar levels of fluorescence as the CQ-only group. This is suggestive of that following blockade of autophagosome degradation for two hours with CQ, OA treatment for 40 hours showed no independent effect on autophagosome formation from the control group. Furthermore, the addition of OA in PA treatment also negated PA-induced elevated levels of autophagosome formation. Very few other studies have investigated the effects of OA treatment on autophagosome accumulation. OA treatment of MIN6 pancreatic β -cells for 24 and 48 hours significantly increased autophagosome formation after inhibition of autophagosome degradation with CQ (Chu *et al.* 2019). It is interesting that OA effects on autophagosome formation may differ depending on the cell-type. Certainly, further experimentation is required to support my findings.

However, these findings must be interpreted with caution as I am the first to employ CQ treatment as an approach to investigate effects of autophagic inhibition on early mammalian development. CQ treatment has of course been employed in many other studies applied to various cell types, including primary neurons (Redmann et al. 2017) and cancer cell lines (Mauthe et al. 2018; Leung et al. 2021), to name a few. However, no consensus on dosage and treatment time was established between these studies as CQ dosage can range from 25 μM to 100 μM while treatment time ranges from 5 to 24 hours. The 2-hour CQ treatment time I employed arose from an assessment of the literature and preliminary dose and treatment time experiments I conducted (see **appendix A and B**) that identified 75 μM CQ treatment for 2 hours would resolve detectable differences in LC3-II puncta if differences existed. However, the preliminary experiments were applied to mouse blastocysts, which are at different stages than most of the embryos after 40 hours of NEFA treatment. Embryos of different preimplantation stages could exhibit different rates of autophagosome formation. Further investigations are required to test this concept.

It is also important to note that the current experiment quantified LC3-II “puncta aggregate” per cell as fluorescence signals instead of puncta count (as previously reported in objective 1). The reason behind this change in quantification method was because the use of autophagy inhibitors (BafA1 and CQ) results in increased number and sizes of LC3-II puncta aggregate, which likely represent autophagosome-autophagosome fusions (Mauthe et al. 2018). The quantification of LC3-II based on fluorescent signals considers the possible increase of sizes and number of LC3-II aggregates, which serves as a more accurate assessment LC3-II after CQ treatment.

4.5 NEFA effects on autophagosome maturation and degradation

My third objective assessed the effects of NEFAs on autophagosome maturation and degradation in preimplantation mouse embryos. Autophagy consists of autophagosome formation, maturation, and degradation so the net accumulation of autophagosomes is a balance between the processes of autophagosome formation and autophagosome degradation. It is important to investigate autophagy processes at several different levels

to fully characterize the underlying effects brought upon by NEFA exposure on preimplantation embryos.

Two-cell mouse embryos were treated with NEFA treatments for 40 hours then immunolabelled to identify for autophagosome-lysosome fusion based on autophagosome-lysosome co-localization. The co-localization of LC3-II-lysotracker puncta were analyzed to determine autophagosome maturation. My results indicate a significantly greater average number of LC3-II-lysotracker co-localized puncta per cell in the OA group than in the PA group, which suggests that treatment with 250 μ M OA results in greater autophagosome maturation than treatment with 100 μ M PA. I also observed that 250 μ M OA treatment resulted in a significantly higher proportion of LC3-II-lysosome co-localized puncta per cell (relative to the number of LC3-II puncta per cell) than 100 μ M PA treatment. Altogether, my results strongly suggest that a higher number and proportion of autolysosomes was observed in the OA treatment group compared to the PA group. Induction of autophagosome maturation by OA treatment was reported in tongue squamous cell carcinoma cell lines (Jiang et al. 2017); however, this was not observed in a study employing HepG2 cells (Lee et al. 2019). I would suggest that, as mentioned previously, it is likely that OA effects differ among cell types.

Interestingly, I did not detect a change in autophagosome maturation in mouse embryos after treatment of PA compared to control. Similarly, exposure of hypothalamic neuronal cells to PA treatment also showed no difference in autolysosome number from control (Hernández-Cáceres et al. 2020). Studies of pancreatic β -cells, however, have reported significant increases in autophagosome maturation, reflected by a higher percentage of autophagosome-lysosome fusion, after treatment with PA (Dhayal et al. 2019; Choi et al. 2009). It is important to note that limited studies have investigated the effects of PA on autophagosome maturation in embryos as well as the effects of PA and OA in combination on autophagosome maturation.

Next, I investigated the effects of NEFA treatment on autophagosome degradation in mouse preimplantation embryos. Fluorescence intensity of a lysosomal dye, LysoTracker Red, as to reflect lysosomal activity, were analyzed in NEFA-treated mouse embryos

with references to the protocol by Albrecht *et al.* (2020). No significant differences in lysosomal activity were found between control, OA, and PA and OA co-treatment groups. Though, compared to the other treatment groups, treatment of 100 μ M PA resulted in significantly less LysoTracker fluorescence, which could suggest a significantly lower level of lysosomal activity. In support of the previous findings, the accumulation of autophagosomes observed after PA treatment could be due to a reduction of lysosomal activity and thus lower level of autophagosome degradation in PA-treated mouse preimplantation embryos. The disruption of autophagy mechanisms by lowering lysosomal activity could contribute to developmental incompetency in PA-treated embryos. Chu *et al.* (2019) previously reported that, in contrast to our findings, both PA and OA treatments do not affect lysosome size and numbers in MIN6 pancreatic β -cells; however, both PA and OA treatments increased lysosomal acidity, which the authors considered was an improvement in lysosomal activity. Regardless, lysosomal activity is an important aspect of autophagosome degradation in preimplantation embryo development that requires further experimentation.

The role of the lysosome in autophagy shines light on the potential mechanistic changes by PA treatment. A study by Hernández-Cáceres *et al.* (2020) reported that PA disrupts autophagic flux by decreasing autophagosome-lysosome fusion in hypothalamic neuronal cells. Though, PA does not lower lysosomal activity; instead, it lowers the motility of lysosomal compartments by accumulating of Rab7 GTPase (Hernández-Cáceres *et al.* 2020). Rab7 GTPase is located on lysosomes that attaches to a motor unit to facilitate the transport of autophagosome towards a lysosome (Jordens *et al.* 2001). Additionally, it facilitates autophagosome-lysosome fusion by recruiting tethering proteins like SNARE proteins (Ganley 2013). However, the activation of Rab7 GTPase require hydrolysis of the attached GTP to GDP to utilize the energy for its function. The accumulation of Rab7 GTPase after treatment of PA results in reducing autophagosome movement towards lysosomes, thus lowering autophagosome-lysosome fusion and disrupting autophagy in the hypothalamic neuronal cells (Hernández-Cáceres *et al.* 2020). It is unknown whether Rab7 GTPase is affected by PA treatment in preimplantation mouse embryos, but such a mechanism would be interesting and important to investigate in future experiments. It is postulated that PA may similarly disrupt the hydrolysis of Rab7 GTPase in the mouse

preimplantation embryos, thereby preventing autophagosome-lysosome fusion necessary for autophagosome degradation and thus resulting in impairments in development to the blastocyst stage.

Although OA resulted in no effects in development or autophagy, OA treatment has been previously described to promote the accumulation of lipid droplets during mouse preimplantation development (Yousif et al. 2020). Nakajima *et al.* (2019) reported an induction of lipid droplet accumulation after OA treatment in astrocytes that contributes to offsetting PA-induced lipotoxicity. A similar mechanism is likely in place in preimplantation mouse embryos as well, as the addition of OA to PA treatment successfully negated PA-induced reduction in lysosomal activity. With the high levels of lysosomal activity observed in the OA group in my study, it is possible that lysosomes take part in the break down of the accumulated lipid droplets via autophagy, a mechanism specifically described as lipophagy (Schulze et al. 2020), to produce energy to counteract PA effects. Further investigations, of lipophagy, would be beneficial to generating a full understanding the OA treatment effects in alleviating PA-effects.

My outcome interpretations must be made with caution as the analysis of LysoTracker fluorescence signal of NEFA-treated embryos as a measurement of lysosomal activity is novel. The use of LysoTracker Red is primarily employed for live cell imaging although it can be readily applied to fixed cells (Raben et al. 2009). My preliminary investigations with this method, defined appropriate LysoTracker dye concentration and treatment times for application to fixed preimplantation stage embryos. I observed that LysoTracker fluorescence signal rapidly declines in mouse preimplantation embryos after fixation and time progression. Thus, I modified the current standardized method to employ a higher concentration of LysoTracker (500 μ M vs. 50 μ M of LysoTracker for 30 mins). This novel approach did not have any observable morphological effects but there is a possibility of some lysosome alkalinization happening caused by the slightly basic nature of LysoTracker (pH=9). Alternative methods to immunolabel lysosomal proteins with LAMP1 and LAMP2, for example, could be included in future experiments to confirm the current findings.

Overall, my results provide important insight on the consequences of PA and OA treatment effects on autophagosome-lysosome fusion during mouse preimplantation development for the first time.

4.6 Conclusion and Significance

This thesis presents new outcomes from experiments that investigated the effects of PA and OA treatment on preimplantation development, autophagy, autophagosome formation, and autophagosome degradation in mouse preimplantation embryos.

PA treatment beginning at the 2-cell stage impaired blastocyst development by arresting mouse embryos at the 4- 8-cell stage. The significant accumulation of autophagosomes in the later stages of embryo development observed was likely a result of elevated autophagosome formation as well as lowered levels of autophagosome maturation and degradation modulated by adjustments in lysosomal activity. OA treatment beginning at the 2-cell stage had no significant effects on preimplantation development, autophagosome formation, or autophagosome degradation.

The effects of PA and OA co-treatment of mouse preimplantation embryos beginning at the 2-cell stage was time-dependent. A delay in development was identified at the early cleavage stages but affected embryos restored blastocyst development frequency to control levels. A correlation was observed between development and autophagy as the restoration of blastocyst formation coincided with the restoration of control autophagy levels at the later stages of preimplantation embryo development. Interestingly, although high levels of autophagosome accumulation was observed after 40 hours of PA and OA co-treatment, levels of autophagosome formation, maturation, and degradation were not significantly different than control at that time point. Perhaps autophagosome accumulation observed after 40 hours of co-treatment was a result of aberrant early cleavage stage embryo buildup overseen by rapid PA effects that were alleviated by OA rescue and adjustment of the autophagic pathway back to control levels at 48 hrs of co-treatment. The 40-hour time point could likely be within the period of the “catch-up growth” mentioned in the first experiment, thus further experimentation is required to

fully understand NEFA effects on autophagy at a shorter time interval between 30- and 48-hour treatment of 2-cell embryos, potentially of 6-hour time intervals.

The general objective of my thesis was to understand the underlying autophagic mechanisms impacted by NEFA treatments during early mouse embryo development *in vitro*. My findings are summarized in **Figure 22**.

Overall, this thesis reports the effects of NEFA treatments on embryo development and autophagic mechanisms throughout preimplantation development. The results demonstrated a correlation between embryo development and autophagy, and that autophagic mechanisms are likely altered by NEFA treatments. Future experiments shall include embryonic stem cells as an alternate model for preimplantation embryos when investigating the effects of NEFAs on early mammalian autophagy, as ES cells nicely replicate ICM cells of blastocyst stage embryos. Some preliminary experiments of NEFA effects on autophagy of mESC were completed (**Appendix D**). These findings will advance our understanding of the effects of NEFAs on preimplantation embryo autophagy. They will also guide future investigations that may eventually employ autophagic modulation, perhaps by OA treatment, as a therapeutic option to enhance developmental success. It is our goal to assist patients who are seeking ARTs for their fertility needs, especially of those who are obese.

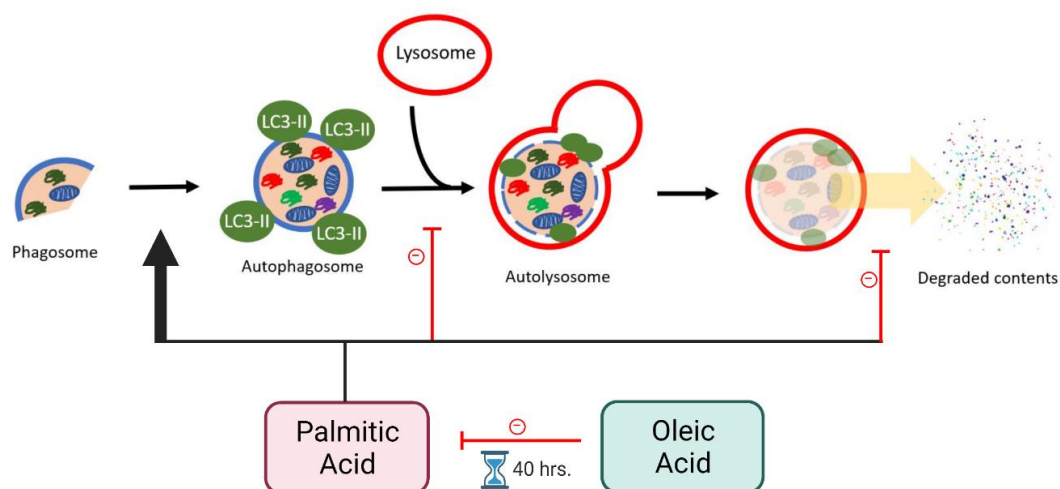


Figure 22. Summary Figure: Effects of PA and OA on autophagy in mouse preimplantation embryos.

Autophagy begins when a phagosome is initiated to form an autophagosome. A phagosome recruits autophagy-related proteins to direct degradation contents into the phagosome as it elongates and seal off to become an autophagosome. After autophagosome formation is completed, autophagosome is transported to a lysosome for autophagosome maturation. Fusion of autophagosome and lysosome creates an autolysosome. Acidic contents of the lysosomes degrade the autophagosome, then releasing the degraded contents into the cytosol for reuse in other cellular functions. PA treatment of mouse preimplantation embryos was observed to increase autophagosome accumulation by elevating autophagosome formation, reducing autophagosome maturation, and reducing autophagosome degradation by disruption of lysosomal activity. In contrast, OA-alone treatment of mouse preimplantation embryos has no effects on autophagy. The addition of OA in PA treatment was observed to inhibit PA-induced effects on preimplantation embryo autophagy, but only after 40 hours of co-treatment. Created with BioRender.com.

References

- Aardema, H., et al. "Oleic Acid Prevents Detrimental Effects of Saturated Fatty Acids on Bovine Oocyte Developmental Competence." *Biol Reprod* 85.1 (2011): 62-9.
- Aardema, H., H. T. A. van Tol, and P. L. A.M Vos. "An Overview on How Cumulus Cells Interact with the Oocyte in a Condition with Elevated Nefa Levels in Dairy Cows." *Anim Reprod Sci* 207 (2019): 131-37.
- Agrotis, A., et al. "Redundancy of Human Atg4 Protease Isoforms in Autophagy and Lc3/Gabarap Processing Revealed in Cells." *Autophagy* 15.6 (2019): 976-97.
- Akoumi, A., et al. "Palmitate Mediated Diacylglycerol Accumulation Causes Endoplasmic Reticulum Stress, Plin2 Degradation, and Cell Death in H9c2 Cardiomyoblasts." *Exp Cell Res* 354.2 (2017): 85-94.
- Albrecht, L. V., N. Tejada-Muñoz, and E. M. De Robertis. "Protocol for Probing Regulated Lysosomal Activity and Function in Living Cells." *STAR Protoc* 1.3 (2020): 100132.
- Ameer, F., et al. "De Novo Lipogenesis in Health and Disease." *Metabolism* 63.7 (2014): 895-902.
- Boden, G. "Obesity, Insulin Resistance and Free Fatty Acids." *Curr Opin Endocrinol Diabetes Obes* 18.2 (2011): 139-43.
- Bollinger, L. M., M. S. Campbell, and J. J. Brault. "Palmitate and Oleate Co-Treatment Increases Myocellular Protein Content Via Impaired Protein Degradation." *Nutrition* 46 (2018): 41-43.
- Bornstein, S. R., H. Rutkowski, and I. Vrezas. "Cytokines and Steroidogenesis." *Mol Cell Endocrinol* 215.1-2 (2004): 135-41.
- Bradley, J., and K. Swann. "Mitochondria and Lipid Metabolism in Mammalian Oocytes and Early Embryos." *Int J Dev Biol* 63.3-4-5 (2019): 93-103.
- Brewer, C. J., and A. H. Balen. "The Adverse Effects of Obesity on Conception and Implantation." *Reproduction* 140.3 (2010): 347-64.
- Broughton, D. E., and K. H. Moley. "Obesity and Female Infertility: Potential Mediators of Obesity's Impact." *Fertil Steril* 107.4 (2017): 840-47.
- Button, R. W., et al. "Accumulation of Autophagosomes Confers Cytotoxicity." *J Biol Chem* 292.33 (2017): 13599-614.
- Buyuk, E., et al. "Serum and Follicular Fluid Monocyte Chemotactic Protein-1 Levels Are Elevated in Obese Women and Are Associated with Poorer Clinical Pregnancy Rate after In vitro Fertilization: A pilot Study." *Fertil Steril* 107.3 (2017): 632-40.e3.

Canadian Assisted Reproductive Technologies Registry (CARTR) Plus. "Preliminary Treatment Cycle Data For 2019." 2021. Presentation.

Canadian Fertility & Andrology Society. *PRESS RELEASE*. 2019. Web. 18 Aug. 2021 . <https://cfas.ca/_Library/CARTR/2019_CARTR_Press_Release_PDF.pdf>.

Carotti, S., et al. "Lipophagy Impairment Is Associated with Disease Progression in Nafld." *Front Physiol* 11 (2020): 850.

Carrillo, C., M.el M Cavia, and S. R. Alonso-Torre. "Antitumor Effect of Oleic Acid; Mechanisms of Action: A Review." *Nutr Hosp* 27.6 (2012): 1860-5.

Carta, G., et al. "Palmitic Acid: Physiological Role, Metabolism and Nutritional Implications." *Front Physiol* 8 (2017): 902.

Chazaud, C., and Y. Yamanaka. "Lineage Specification in the Mouse Preimplantation Embryo." *Development* 143.7 (2016): 1063-74.

Chen, X., et al. "Oleic Acid Protects Saturated Fatty Acid Mediated Lipotoxicity in Hepatocytes and Rat of Non-Alcoholic Steatohepatitis." *Life Sci* 203 (2018): 291-304.

Chen, Y., et al. "Inositol-Requiring Enzyme 1 α Links Palmitate-Induced Mtor Activation and Lipotoxicity in Hepatocytes." *Am J Physiol Cell Physiol* 319.6 (2020): C1130-C40.

Choi, S. E., et al. "Protective Role of Autophagy in Palmitate-Induced Ins-1 Beta-Cell Death." *Endocrinology* 150.1 (2009): 126-34.

Chu, K. Y., et al. "Oleate Disrupts Camp Signaling, Contributing to Potent Stimulation of Pancreatic B-Cell Autophagy." *J Biol Chem* 294.4 (2019): 1218-29.

Chu, S. G., et al. "Palmitic Acid-Rich High-Fat Diet Exacerbates Experimental Pulmonary Fibrosis by Modulating Endoplasmic Reticulum Stress." *Am J Respir Cell Mol Biol* 61.6 (2019): 737-46.

Cianfanelli, V., et al. "Ambra1 at a Glance." *J Cell Sci* 128.11 (2015): 2003-8.

Conway, B., and A. Rene. "Obesity as a Disease: No Lightweight Matter." *Obes Rev* 5.3 (2004): 145-51.

Corbould, A. "Chronic Testosterone Treatment Induces Selective Insulin Resistance in Subcutaneous Adipocytes of Women." *J Endocrinol* 192.3 (2007): 585-94.

Dhayal, S., et al. "Differential Effects of Saturated and Unsaturated Fatty Acids on Autophagy in Pancreatic B-Cells." *J Mol Endocrinol* 63.4 (2019): 285-96.

Dumollard, R., et al. "Regulation of Redox Metabolism in the Mouse Oocyte and Embryo." *Development* 134.3 (2007): 455-65.

Dunning, K. R., et al. "Beta-Oxidation Is Essential for Mouse Oocyte Developmental Competence and Early Embryo Development." *Biol Reprod* 83.6 (2010): 909-18.

Eijkemans, M. J., et al. "Too Old to Have Children? Lessons from Natural Fertility Populations." *Hum Reprod* 29.6 (2014): 1304-12.

Ekizceli, G., et al. "Assessment of Mtor Pathway Molecules During Implantation in Rats." *Biotech Histochem* 92.6 (2017): 450-58.

Fayezi, S., et al. "Oleic Acid in the Modulation of Oocyte and Preimplantation Embryo Development." *Zygote* 26.1 (2018): 1-13.

Flowers, M. T., et al. "Cholestasis and Hypercholesterolemia in Scd1-Deficient Mice Fed a Low-Fat, High-Carbohydrate Diet." *J Lipid Res* 47.12 (2006): 2668-80.

Flowers, M. T., et al. "Liver Gene Expression Analysis Reveals Endoplasmic Reticulum Stress and Metabolic Dysfunction in Scd1-Deficient Mice Fed a Very Low-Fat Diet." *Physiol Genomics* 33.3 (2008): 361-72.

Frankenberg, S. R., et al. "The Mammalian Blastocyst." *Wiley Interdiscip Rev Dev Biol* 5.2 (2016): 210-32.

Franks, S. "Polycystic Ovary Syndrome in Adolescents." *Int J Obes (Lond)* 32.7 (2008): 1035-41.

Ganley, I. G. "Autophagosome Maturation and Lysosomal Fusion." *Essays Biochem* 55 (2013): 65-78.

Giordano, S., V. Darley-USmar, and J. Zhang. "Autophagy as an Essential Cellular Antioxidant Pathway in Neurodegenerative Disease." *Redox Biol* 2 (2014): 82-90.

Gonzalez, R. R., and P. Leavis. "Leptin Upregulates Beta3-Integrin Expression and Interleukin-1beta, Upregulates Leptin and Leptin Receptor Expression in Human Endometrial Epithelial Cell Cultures." *Endocrine* 16.1 (2001): 21-8.

Hernández-Cáceres, M. P., et al. "Palmitic Acid Reduces the Autophagic Flux in Hypothalamic Neurons by Impairing Autophagosome-Lysosome Fusion and Endolysosomal Dynamics." *Mol Cell Oncol* 7.5 (2020): 1789418.

Hill, S. M., L. Wrobel, and D. C. Rubinsztein. "Post-Translational Modifications of Beclin 1 Provide Multiple Strategies for Autophagy Regulation." *Cell Death Differ* 26.4 (2019): 617-29.

Hou, Y. J., et al. "Both Diet and Gene Mutation Induced Obesity Affect Oocyte Quality in Mice." *Sci Rep* 6 (2016): 18858.

Igosheva, N., et al. "Maternal Diet-Induced Obesity Alters Mitochondrial Activity and Redox Status in Mouse Oocytes and Zygotes." *PLoS One* 5.4 (2010): e10074.

- Jain, A., et al. "Pulsatile Luteinizing Hormone Amplitude and Progesterone Metabolite Excretion Are Reduced in Obese Women." *J Clin Endocrinol Metab* 92.7 (2007): 2468-73.
- Jastreboff, A. M., et al. "Obesity as a Disease: The Obesity Society 2018 Position Statement." *Obesity (Silver Spring)* 27.1 (2019): 7-9.
- Jiang, L., et al. "Oleic Acid Induces Apoptosis and Autophagy in the Treatment of Tongue Squamous Cell Carcinomas." *Sci Rep* 7.1 (2017): 11277.
- Jones, H. W., et al. "International Federation of Fertility Societies Surveillance 2010: Preface." *Fertil Steril* 95.2 (2011): 491.
- Jordens, I., et al. "The Rab7 Effector Protein Rilp Controls Lysosomal Transport by Inducing the Recruitment of Dynein-Dynactin Motors." *Curr Biol* 11.21 (2001): 1680-5.
- Joshi-Barve, S., et al. "Palmitic Acid Induces Production of Proinflammatory Cytokine Interleukin-8 from Hepatocytes." *Hepatology* 46.3 (2007): 823-30.
- Jukam, D., S. A. M. Shariati, and J. M. Skotheim. "Zygotic Genome Activation in Vertebrates." *Dev Cell* 42.4 (2017): 316-32.
- Jungheim, E. S., et al. "Associations between Free Fatty Acids, Cumulus Oocyte Complex Morphology and Ovarian Function During in Vitro Fertilization." *Fertil Steril* 95.6 (2011): 1970-4.
- Jungheim, E. S., et al. "Preimplantation Exposure of Mouse Embryos to Palmitic Acid Results in Fetal Growth Restriction Followed by Catch-up Growth in the Offspring." *Biol Reprod* 85.4 (2011): 678-83.
- Kabeya, Y., et al. "Lc3, a Mammalian Homologue of Yeast Apg8p, Is Localized in Autophagosome Membranes after Processing." *EMBO J* 19.21 (2000): 5720-8.
- Kamimoto, T., et al. "Intracellular Inclusions Containing Mutant Alpha1-Antitrypsin Z Are Propagated in the Absence of Autophagic Activity." *J Biol Chem* 281.7 (2006): 4467-76.
- Karaşahin, T., and Ş. Arikan. "The Effect Of Oleic And Linoleic Acids On In Vitro Bovineembryonic Development And Embryo Quality." *Turkish J Vet Anim* 39 (2015): 154-159. Web.
- Karpe, F., J. R. Dickmann, and K. N. Frayn. "Fatty Acids, Obesity, and Insulin Resistance: Time for a Reevaluation." *Diabetes* 60.10 (2011): 2441-9.
- Kenchaiah, S., et al. "Obesity and the Risk of Heart Failure." *N Engl J Med* 347.5 (2002): 305-13.

- Kim, J., et al. "Ampk and Mtor Regulate Autophagy through Direct Phosphorylation of Ulk1." *Nat Cell Biol* 13.2 (2011): 132-41.
- Kimura, S., T. Noda, and T. Yoshimori. "Dynein-Dependent Movement of Autophagosomes Mediates Efficient Encounters with Lysosomes." *Cell Struct Funct* 33.1 (2008): 109-22.
- Kirkin, V., et al. "A Role for Nbr1 in Autophagosomal Degradation of Ubiquitinated Substrates." *Mol Cell* 33.4 (2009): 505-16.
- Köchli, R., et al. "Microtubules Facilitate Autophagosome Formation and Fusion of Autophagosomes with Endosomes." *Traffic* 7.2 (2006): 129-45.
- Kojima, Y., O. H. Tam, and P. P. Tam. "Timing of Developmental Events in the Early Mouse Embryo." *Semin Cell Dev Biol* 34 (2014): 65-75.
- Lamark, T., S. Svenning, and T. Johansen. "Regulation of Selective Autophagy: The P62/Sqstm1 Paradigm." *Essays Biochem* 61.6 (2017): 609-24.
- Las, G., and O. S. Shirihai. "The Role of Autophagy in B-Cell Lipotoxicity and Type 2 Diabetes." *Diabetes Obes Metab* 12 Suppl 2 (2010): 15-9.
- Las, G., et al. "Fatty Acids Suppress Autophagic Turnover in B-Cells." *J Biol Chem* 286.49 (2011): 42534-44.
- Lauterbach, M. A., and F. T. Wunderlich. "Macrophage Function in Obesity-Induced Inflammation and Insulin Resistance." *Pflugers Arch* 469.3-4 (2017): 385-96.
- Lee, D. H., et al. "Oleic Acid-Induced Defective Autolysosome Shows Impaired Lipid Degradation." *Biochem Biophys Res Commun* 513.3 (2019): 553-59.
- Lee, M. T., A. R. Bonneau, and A. J. Giraldez. "Zygotic Genome Activation During the Maternal-to-Zygotic Transition." *Annu Rev Cell Dev Biol* 30 (2014): 581-613.
- Lee, S. E., et al. "Modulation of Autophagy Influences Development and Apoptosis in Mouse Embryos Developing in Vitro." *Mol Reprod Dev* 78.7 (2011): 498-509.
- Lee, W. S., W. H. Yoo, and H. J. Chae. "Er Stress and Autophagy." *Curr Mol Med* 15.8 (2015): 735-45.
- Leese, H. J. "Quiet Please, Do Not Disturb: A Hypothesis of Embryo Metabolism and Viability." *Bioessays* 24.9 (2002): 845-9.
- Leese, H. J., and A. M. Barton. "Pyruvate and Glucose Uptake by Mouse Ova and Preimplantation Embryos." *J Reprod Fertil* 72.1 (1984): 9-13.
- Leese, H. J., et al. "Biological Optimization, the Goldilocks Principle, and How Much Is Lagom in the Preimplantation Embryo." *Mol Reprod Dev* 83.9 (2016): 748-54.

- Leroy, J. L., et al. "Non-Esterified Fatty Acids in Follicular Fluid of Dairy Cows and Their Effect on Developmental Capacity of Bovine Oocytes in Vitro." *Reproduction* 130.4 (2005): 485-95.
- Leung, E., et al. "Identification of Novel Atg3-Atg8 Inhibitors Using Virtual Screening for Autophagy Modulation." *Bioorg Chem* 114 (2021): 105092.
- Li, L., X. Lu, and J. Dean. "The Maternal to Zygotic Transition in Mammals." *Mol Aspects Med* 34.5 (2013): 919-38.
- Li, S., and W. Winuthayanon. "Oviduct: Roles in Fertilization and Early Embryo Development." *J Endocrinol* 232.1 (2017): R1-R26.
- Lin, T., et al. "Endoplasmic Reticulum (Er) Stress and Unfolded Protein Response (Upr) in Mammalian Oocyte Maturation and Preimplantation Embryo Development." *Int J Mol Sci* 20.2 (2019).
- Listenberger, L. L., et al. "Triglyceride Accumulation Protects against Fatty Acid-Induced Lipotoxicity." *Proc Natl Acad Sci U S A* 100.6 (2003): 3077-82.
- Louie, J. K., et al. "A Novel Risk Factor for a Novel Virus: Obesity and 2009 Pandemic Influenza a (H1n1)." *Clin Infect Dis* 52.3 (2011): 301-12.
- Maday, S., K. E. Wallace, and E. L. Holzbaur. "Autophagosomes Initiate Distally and Mature During Transport toward the Cell Soma in Primary Neurons." *J Cell Biol* 196.4 (2012): 407-17.
- Mansbach, C. M., and S. A. Siddiqi. "The Biogenesis of Chylomicrons." *Annu Rev Physiol* 72 (2010): 315-33.
- Marcelino, G., et al. "Effects of Olive Oil and Its Minor Components on Cardiovascular Diseases, Inflammation, and Gut Microbiota." *Nutrients* 11.8 (2019).
- Margariti, A., et al. "Xbp1 Mrna Splicing Triggers an Autophagic Response in Endothelial Cells through Beclin-1 Transcriptional Activation." *J Biol Chem* 288.2 (2013): 859-72.
- Mauer, C. P. (2004) RG2B Colocalization (Version 1) [ImageJ Plug-in]. <https://imagej.nih.gov/ij/plugins/rg2bcolocalization.html>
- Mauthe, M., et al. "Chloroquine Inhibits Autophagic Flux by Decreasing Autophagosome-Lysosome Fusion." *Autophagy* 14.8 (2018): 1435-55.
- McQuaid, S. E., et al. "Downregulation of Adipose Tissue Fatty Acid Trafficking in Obesity: A Driver for Ectopic Fat Deposition?" *Diabetes* 60.1 (2011): 47-55.
- Melia, T. J., A. H. Lystad, and A. Simonsen. "Autophagosome Biogenesis: From Membrane Growth to Closure." *J Cell Biol* 219.6 (2020).

Mena, G. P., G. I. Mielke, and W. J. Brown. "Prospective Associations between Physical Activity and Bmi with Irregular Periods and Heavy Menstrual Bleeding in a Large Cohort of Australian Women." *Hum Reprod* 36.6 (2021): 1481-91.

Menendez, J. A., et al. "Oleic Acid, the Main Monounsaturated Fatty Acid of Olive Oil, Suppresses Her-2/Neu (ErbB-2) Expression and Synergistically Enhances the Growth Inhibitory Effects of Trastuzumab (Herceptin) in Breast Cancer Cells with Her-2/Neu Oncogene Amplification." *Ann Oncol* 16.3 (2005): 359-71.

Mentella, M. C., et al. "Cancer and Mediterranean Diet: A Review." *Nutrients* 11.9 (2019).

Metwally, M., et al. "Does High Body Mass Index Increase the Risk of Miscarriage after Spontaneous and Assisted Conception? A Meta-Analysis of the Evidence." *Fertil Steril* 90.3 (2008): 714-26.

Mizushima, N. "Autophagy: Process and Function." *Genes Dev* 21.22 (2007): 2861-73.

Mizushima, N. "The Pleiotropic Role of Autophagy: From Protein Metabolism to Bactericide." *Cell Death Differ* 12 Suppl 2 (2005): 1535-41.

Mizushima, N., and M. Komatsu. "Autophagy: Renovation of Cells and Tissues." *Cell* 147.4 (2011): 728-41.

Mizushima, N., et al. "Dissection of Autophagosome Formation Using Apg5-Deficient Mouse Embryonic Stem Cells." *J Cell Biol* 152.4 (2001): 657-68.

Mizushima, N., T. Yoshimori, and B. Levine. "Methods in Mammalian Autophagy Research." *Cell* 140.3 (2010): 313-26.

Nagy, A., et al. "Derivation of Completely Cell Culture-Derived Mice from Early-Passage Embryonic Stem Cells." *Proc Natl Acad Sci U S A* 90.18 (1993): 8424-8.

Nakajima, S., et al. "Oleic Acid Is a Potent Inducer for Lipid Droplet Accumulation through Its Esterification to Glycerol by Diacylglycerol Acyltransferase in Primary Cortical Astrocytes." *Brain Res* 1725 (2019): 146484.

Nazio, F., et al. "Mtor Inhibits Autophagy by Controlling Ulk1 Ubiquitylation, Self-Association and Function through Ambra1 and Traf6." *Nat Cell Biol* 15.4 (2013): 406-16.

Nguyen, P., et al. "Liver Lipid Metabolism." *J Anim Physiol Anim Nutr (Berl)* 92.3 (2008): 272-83.

Noda, T., et al. "Regulation of Membrane Biogenesis in Autophagy Via Pi3p Dynamics." *Semin Cell Dev Biol* 21.7 (2010): 671-6.

Noguchi, T., et al. "Comparison of Gene Expression and Mitochondria Number between Bovine Blastocysts Obtained *in Vitro* and *in Vivo*." *J Reprod Dev* 66.1 (2020): 35-39.

Nteeba, J., S. Ganesan, and A. F. Keating. "Progressive Obesity Alters Ovarian Folliculogenesis with Impacts on Pro-Inflammatory and Steroidogenic Signaling in Female Mice." *Biol Reprod* 91.4 (2014): 86.

O'Farrell, P. H., J. Stumpff, and T. T. Su. "Embryonic Cleavage Cycles: How Is a Mouse Like a Fly?" *Curr Biol* 14.1 (2004): R35-45.

Ogata, M., et al. "Autophagy Is Activated for Cell Survival after Endoplasmic Reticulum Stress." *Mol Cell Biol* 26.24 (2006): 9220-31.

Okada, H., et al. "Peretinoin, an Acyclic Retinoid, Suppresses Steatohepatitis and Tumorigenesis by Activating Autophagy in Mice Fed an Atherogenic High-Fat Diet." *Oncotarget* 8.25 (2017): 39978-93.

Opie, L. H., and P. G. Walfish. "Plasma Free Fatty Acid Concentrations in Obesity." *N Engl J Med* 268 (1963): 757-60.

Peng, G., et al. "Oleate Blocks Palmitate-Induced Abnormal Lipid Distribution, Endoplasmic Reticulum Expansion and Stress, and Insulin Resistance in Skeletal Muscle." *Endocrinology* 152.6 (2011): 2206-18.

Poddar, M., Y. Chetty, and V. T. Chetty. "How Does Obesity Affect the Endocrine System? A Narrative Review." *Clin Obes* 7.3 (2017): 136-44.

Public Health Agency of Canada. "Fertility - Canada.Ca." *Canada.ca*. N.p., 2021. Web. 18 Aug. 2021 . <<https://www.canada.ca/en/public-health/services/fertility/fertility.html>>.

Puscheck, E. E., et al. "Molecular Biology of the Stress Response in the Early Embryo and Its Stem Cells." *Adv Exp Med Biol* 843 (2015): 77-128.

Raben, N., et al. "Monitoring Autophagy in Lysosomal Storage Disorders." *Methods Enzymol* 453 (2009): 417-49.

Ravanan, P., I. F. Srikumar, and P. Talwar. "Autophagy: The Spotlight for Cellular Stress Responses." *Life Sci* 188 (2017): 53-67.

Ravikumar, B., et al. "Inhibition of Mtor Induces Autophagy and Reduces Toxicity of Polyglutamine Expansions in Fly and Mouse Models of Huntington Disease." *Nat Genet* 36.6 (2004): 585-95.

Razi, M., E. Y. Chan, and S. A. Tooze. "Early Endosomes and Endosomal Coatomer Are Required for Autophagy." *J Cell Biol* 185.2 (2009): 305-21.

Redmann, M., et al. "Inhibition of Autophagy with Bafilomycin and Chloroquine Decreases Mitochondrial Quality and Bioenergetic Function in Primary Neurons." *Redox Biol* 11 (2017): 73-81.

Rhee, J. S., et al. "Diet-Induced Obesity Impairs Endometrial Stromal Cell Decidualization: A Potential Role for Impaired Autophagy." *Hum Reprod* 31.6 (2016): 1315-26.

Richani, D., et al. "Metabolic Co-Dependence of the Oocyte and Cumulus Cells: Essential Role in Determining Oocyte Developmental Competence." *Hum Reprod Update* 27.1 (2021): 27-47.

Richani, D., et al. "Participation of the Adenosine Salvage Pathway and Cyclic Amp Modulation in Oocyte Energy Metabolism." *Sci Rep* 9.1 (2019): 18395.

Robker, R. L., et al. "Obese Women Exhibit Differences in Ovarian Metabolites, Hormones, and Gene Expression Compared with Moderate-Weight Women." *J Clin Endocrinol Metab* 94.5 (2009): 1533-40.

Roman Lay, A. A., A. Pereira, and M. L. Garmendia Miguel. "Association between Obesity with Pattern and Length of Menstrual Cycle: The Role of Metabolic and Hormonal Markers." *Eur J Obstet Gynecol Reprod Biol* 260 (2021): 225-31.

Romek, M., et al. "Lipid Content of Non-Cultured and Cultured Pig Embryo." *Reprod Domest Anim* 44.1 (2009): 24-32.

Runwal, G., et al. "Lc3-Positive Structures Are Prominent in Autophagy-Deficient Cells." *Sci Rep* 9.1 (2019): 10147.

Sacks, F. M., et al. "Dietary Fats and Cardiovascular Disease: A Presidential Advisory from the American Heart Association." *Circulation* 136.3 (2017): e1-e23.

Sagné, C., et al. "Identification and Characterization of a Lysosomal Transporter for Small Neutral Amino Acids." *Proc Natl Acad Sci U S A* 98.13 (2001): 7206-11.

Sattar, N., I. B. McInnes, and J. J. V. McMurray. "Obesity Is a Risk Factor for Severe Covid-19 Infection: Multiple Potential Mechanisms." *Circulation* 142.1 (2020): 4-6.

Saxton, R. A., and D. M. Sabatini. "Mtor Signaling in Growth, Metabolism, and Disease." *Cell* 169.2 (2017): 361-71.

Schliwa, M., and J. van Blerkom. "Structural Interaction of Cytoskeletal Components." *J Cell Biol* 90.1 (1981): 222-35.

Schoeler, M., and R. Caesar. "Dietary Lipids, Gut Microbiota and Lipid Metabolism." *Rev Endocr Metab Disord* 20.4 (2019): 461-72.

- Schulze, R. J., et al. "Direct Lysosome-Based Autophagy of Lipid Droplets in Hepatocytes." *Proc Natl Acad Sci U S A* 117.51 (2020): 32443-52.
- Schwartz, B., et al. "Nutritional-Pharmacological Combinations--a Novel Approach to Reducing Colon Cancer Incidence." *Eur J Nutr* 43.4 (2004): 221-9.
- Seif, M. W., K. Diamond, and M. Nickkho-Amiry. "Obesity and Menstrual Disorders." *Best Pract Res Clin Obstet Gynaecol* 29.4 (2015): 516-27.
- Shah, D. K., et al. "Effect of Obesity on Oocyte and Embryo Quality in Women Undergoing in Vitro Fertilization." *Obstet Gynecol* 118.1 (2011): 63-70.
- Shi, L., and J. Wu. "Epigenetic Regulation in Mammalian Preimplantation Embryo Development." *Reprod Biol Endocrinol* 7 (2009): 59.
- Singh, B., and S. Bhaskar. "Methods for Detection of Autophagy in Mammalian Cells." *Methods Mol Biol* 2045 (2019): 245-58.
- Singh, P. K., et al. "Oleic Acid Prevents Isoprenaline-Induced Cardiac Injury: Effects on Cellular Oxidative Stress, Inflammation and Histopathological Alterations." *Cardiovasc Toxicol* 20.1 (2020): 28-48.
- Skaznik-Wikiel, M. E., et al. "High-Fat Diet Causes Subfertility and Compromised Ovarian Function Independent of Obesity in Mice." *Biol Reprod* 94.5 (2016): 108.
- Song, B. S., et al. "Induction of Autophagy Promotes Preattachment Development of Bovine Embryos by Reducing Endoplasmic Reticulum Stress." *Biol Reprod* 87.1 (2012): 8, 1-11.
- Staiger, H., et al. "Palmitate-Induced Interleukin-6 Expression in Human Coronary Artery Endothelial Cells." *Diabetes* 53.12 (2004): 3209-16.
- Statistics Canada. *Overweight And Obese Adults, 2018*. Statistics Canada, 2019. Web. 18 Aug. 2021 . <<https://www150.statcan.gc.ca/n1/pub/82-625-x/2019001/article/00005-eng.htm>>. Health Fact Sheets.
- Strable, M. S., and J. M. Ntambi. "Genetic Control of De Novo Lipogenesis: Role in Diet-Induced Obesity." *Crit Rev Biochem Mol Biol* 45.3 (2010): 199-214.
- Sun, H., et al. "Global, Regional, and National Prevalence and Disability-Adjusted Life-Years for Infertility in 195 Countries and Territories, 1990-2017: Results from a Global Burden of Disease Study, 2017." *Aging (Albany NY)* 11.23 (2019): 10952-91.
- Tosti, V., B. Bertozzi, and L. Fontana. "Health Benefits of the Mediterranean Diet: Metabolic and Molecular Mechanisms." *J Gerontol A Biol Sci Med Sci* 73.3 (2018): 318-26.

- Tsatsanis, C., et al. "The Impact of Adipose Tissue-Derived Factors on the Hypothalamic-Pituitary-Gonadal (Hpg) Axis." *Hormones (Athens)* 14.4 (2015): 549-62.
- Tsukamoto, S., et al. "Autophagy Is Essential for Preimplantation Development of Mouse Embryos." *Science* 321.5885 (2008): 117-20.
- Turpin, S. M., et al. "Examination of 'Lipotoxicity' in Skeletal Muscle of High-Fat Fed and Ob/Ob Mice." *J Physiol* 587.Pt 7 (2009): 1593-605.
- Ubags, N. D., et al. "Hyperleptinemia Is Associated with Impaired Pulmonary Host Defense." *JCI Insight* 1.8 (2016).
- Vahratian, A. "Utilization of Fertility-Related Services in the United States." *Fertil Steril* 90.4 (2008): 1317-9.
- Valckx, S. D. M., et al. "Fatty Acid Composition of the Follicular Fluid of Normal Weight, Overweight and Obese Women Undergoing Assisted Reproductive Treatment: A Descriptive Cross-Sectional Study." *Reprod Biol Endocrinol* 12 (2014): 13.
- Van Hoeck, V., et al. "Elevated Non-Esterified Fatty Acid Concentrations During Bovine Oocyte Maturation Compromise Early Embryo Physiology." *PLoS One* 6.8 (2011): e23183.
- Vander Borght, M., and C. Wyns. "Fertility and Infertility: Definition and Epidemiology." *Clin Biochem* 62 (2018): 2-10.
- Wang, Gongjin, and Hirotada Tsujii. "Metabolism Of Exogenous Palmitic And Oleic Acids By Preimplantation Mouse Embryos.." *Journal of Mammalian Ova Research* 16.1 (1999): 10-15. Web.
- Warzych, E., and P. Lipinska. "Energy Metabolism of Follicular Environment During Oocyte Growth and Maturation." *J Reprod Dev* 66.1 (2020): 1-7.
- Wei, S., et al. "Obesity and Menstrual Irregularity: Associations with Shbg, Testosterone, and Insulin." *Obesity (Silver Spring)* 17.5 (2009): 1070-6.
- Wiley, L. M. "Cavitation in the Mouse Preimplantation Embryo: Na/K-Atpase and the Origin of Nascent Blastocoele Fluid." *Dev Biol* 105.2 (1984): 330-42.
- Wilson, P. W., et al. "Overweight and Obesity as Determinants of Cardiovascular Risk: The Framingham Experience." *Arch Intern Med* 162.16 (2002): 1867-72.
- World Health Organization. "Infertility." *Who.int*. N.p., 2021. Web. . <<https://www.who.int/news-room/fact-sheets/detail/infertility>>.
- World Health Organization. "Obesity And Overweight." *Who.int*. N.p., 2021. Web. 18 Aug. 2021 . <<https://www.who.int/news-room/fact-sheets/detail/obesity-and-overweight>>.

Wu, L. L., et al. "High-Fat Diet Causes Lipotoxicity Responses in Cumulus-Oocyte Complexes and Decreased Fertilization Rates." *Endocrinology* 151.11 (2010): 5438-45.

Xu, Y. N., et al. "Autophagy Influences Maternal Mrna Degradation and Apoptosis in Porcine Parthenotes Developing in Vitro." *J Reprod Dev* 58.5 (2012): 576-84.

Yoo, R. Y., et al. "Increased Luteinizing Hormone Pulse Frequency in Obese Oligomenorrheic Girls with No Evidence of Hyperandrogenism." *Fertil Steril* 85.4 (2006): 1049-56.

Yousif, M. D., et al. "Oleic Acid Counters Impaired Blastocyst Development Induced by Palmitic Acid During Mouse Preimplantation Development: Understanding Obesity-Related Declines in Fertility." *Reprod Sci* 27.11 (2020): 2038-51.

Zeng, X., et al. "Polycystic Ovarian Syndrome: Correlation between Hyperandrogenism, Insulin Resistance and Obesity." *Clin Chim Acta* 502 (2020): 214-21.

Zhao, Y. G., and H. Zhang. "Autophagosome Maturation: An Epic Journey from the ER to Lysosomes." *J Cell Biol* 218.3 (2019): 757-70.

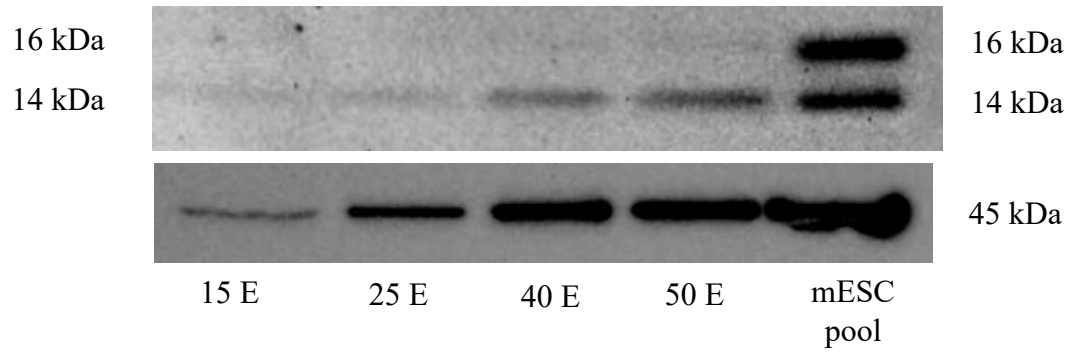
Zhou, K., et al. "The Temporal Pattern, Flux, and Function of Autophagy in Spinal Cord Injury." *Int J Mol Sci* 18.2 (2017).

Zhu, Y., et al. "Beclin 1 Cleavage by Caspase-3 Inactivates Autophagy and Promotes Apoptosis." *Protein Cell* 1.5 (2010): 468-77.

Appendices

Appendix A: Western blot assay for preimplantation embryos

Western blot is an effective assay for the quantification of protein levels in cell and tissue samples. However, there are very few studies that utilize western blot for the quantification of protein expression in preimplantation embryos due to the low total protein levels and thus high number of embryos required to apply this type of analysis. However, as an important alternate assay for the analysis of autophagic markers like LC3-I and LC3-II, it is essential to include western blot data as part of the analysis. I adapted the mESCs western blot protocol for application to detecting these proteins in preimplantation mouse embryos. With the goal of measuring autophagic markers in preimplantation embryos, I explored the number of mouse blastocysts required per lane that is sufficient to measure protein abundance of LC3-I and LC3-II. Mouse embryos at the 2-cell stage were cultured in KSOMaa medium for 48 hours and collected at the blastocyst stage. After which, a western blot consisting of different numbers of blastocysts per lane was conducted for the detection of LC3-I and LC3-II. An mESCs pool sample was included as a positive control. Thus, it was established that at least 40 blastocyst stage embryos are required for the detection of LC3-I and LC3-II in mouse preimplantation embryos via western blot. Representative image of the western blot is shown in **supplementary figure 1**.



Supplementary figure 1. Representative image of a western blot using mouse preimplantation blastocyst embryos of various number of embryos per lane for the detection of LC3-I (16 kDa), LC3-II (14 kDa), and β -actin (45 kDa; loading control). Mouse embryos at the 2-cell stage were cultured in KSOMaa medium for 48 hours and collected at the blastocyst stage prior to western blot analysis.

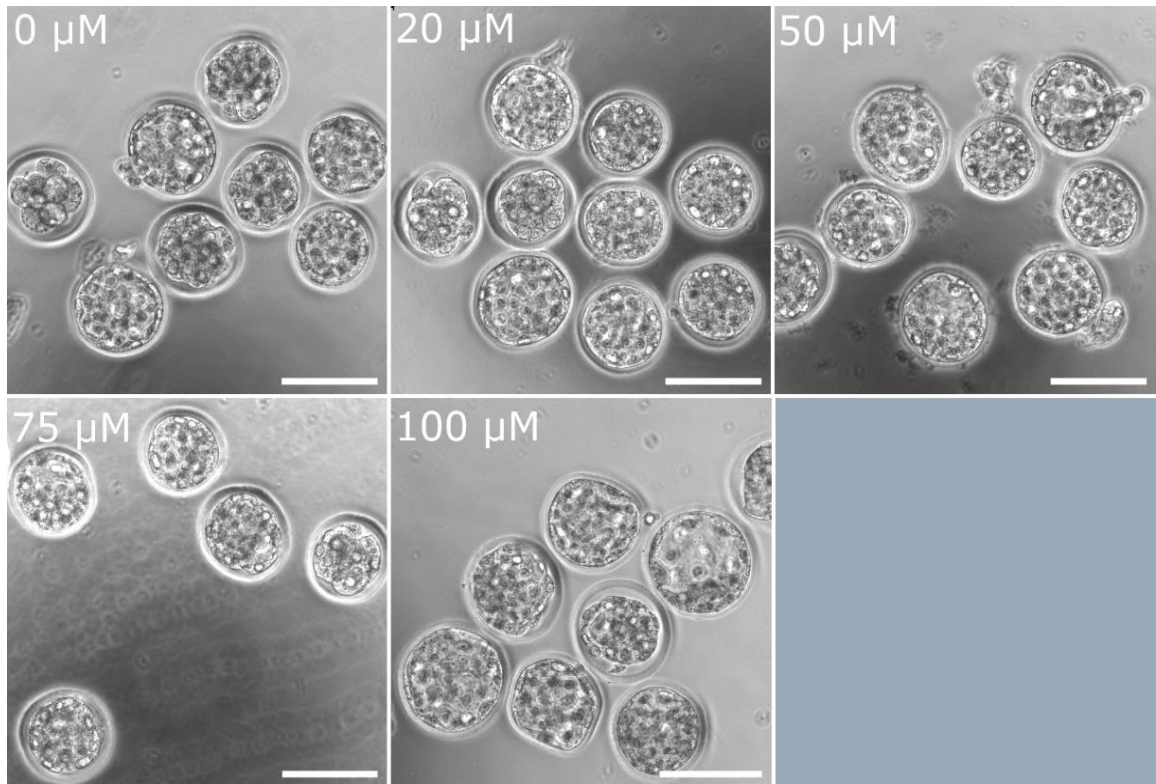
Appendix B: Chloroquine assay to measure autophagic flux

Chloroquine (CQ) is an autophagy inhibitor that alters the acidity of lysosomal compartments thus preventing the fusion of autophagosomes to lysosomes for degradation (Mauthe et al. 2018). Very few studies have used CQ as an autophagy inhibitor in mouse preimplantation embryos; and for the studies that used CQ in other cell types, no common consensus were established for treatment concentration and time periods. Thus, with consideration of published studies that used CQ in their respective cell types, I investigated the dosage response of 2-hour treatment of CQ on mouse preimplantation embryos. Mouse embryos at the 2-cell stage were cultured in KSOMaa medium for 48 hours and treated with 0, 20, 50, 75, or 100 μM of CQ at the last two hours of treatment period. Then, embryos were collected at the end of the treatment period for the analysis of LC3-II expression through western blot and for the analysis of LC3-II puncta count through immunofluorescence.

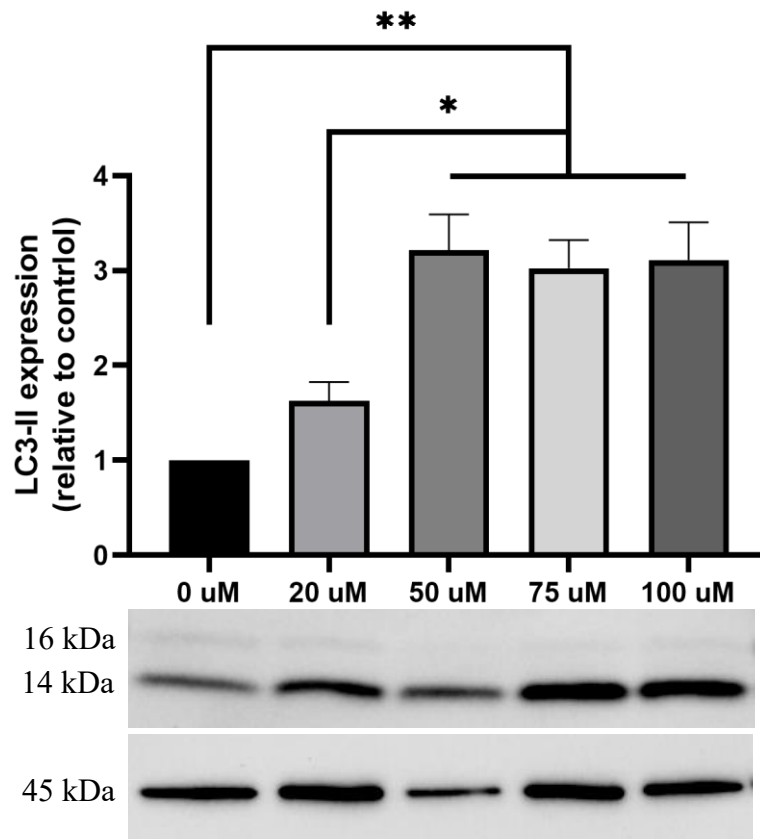
After two hours of CQ treatment post-culture incubation, morphological changes in the mouse preimplantation embryos were visually assessed under a phase contrast microscope. Exposure to CQ up to 100 μM for two hours did not result in visible morphological changes compared to non-treated control. **Supplementary figure 2** displays the representative images of the mouse embryos post-CQ exposure.

Mouse embryos collected after morphological evaluation were subjected to protein extraction for western blot analysis of LC3-I and LC3-II or immunofluorescence staining for LC3-II puncta. It was revealed that at least 50 μM of CQ for two hours is required for detectable differences in LC3-II expression via western blot analysis (**Supplementary figure 3**, $P < 0.05$, Tukey's multiple comparisons test). On the other hand, it was found that at least 75 μM of CQ for two hours is required for detectable differences in LC3-II puncta count via immunofluorescence staining technique (**Supplementary figure 4A**, $P < 0.05$, Tukey's multiple comparisons test). Representative images of embryos after CQ exposure for two hours are shown in **supplementary figure 4B**.

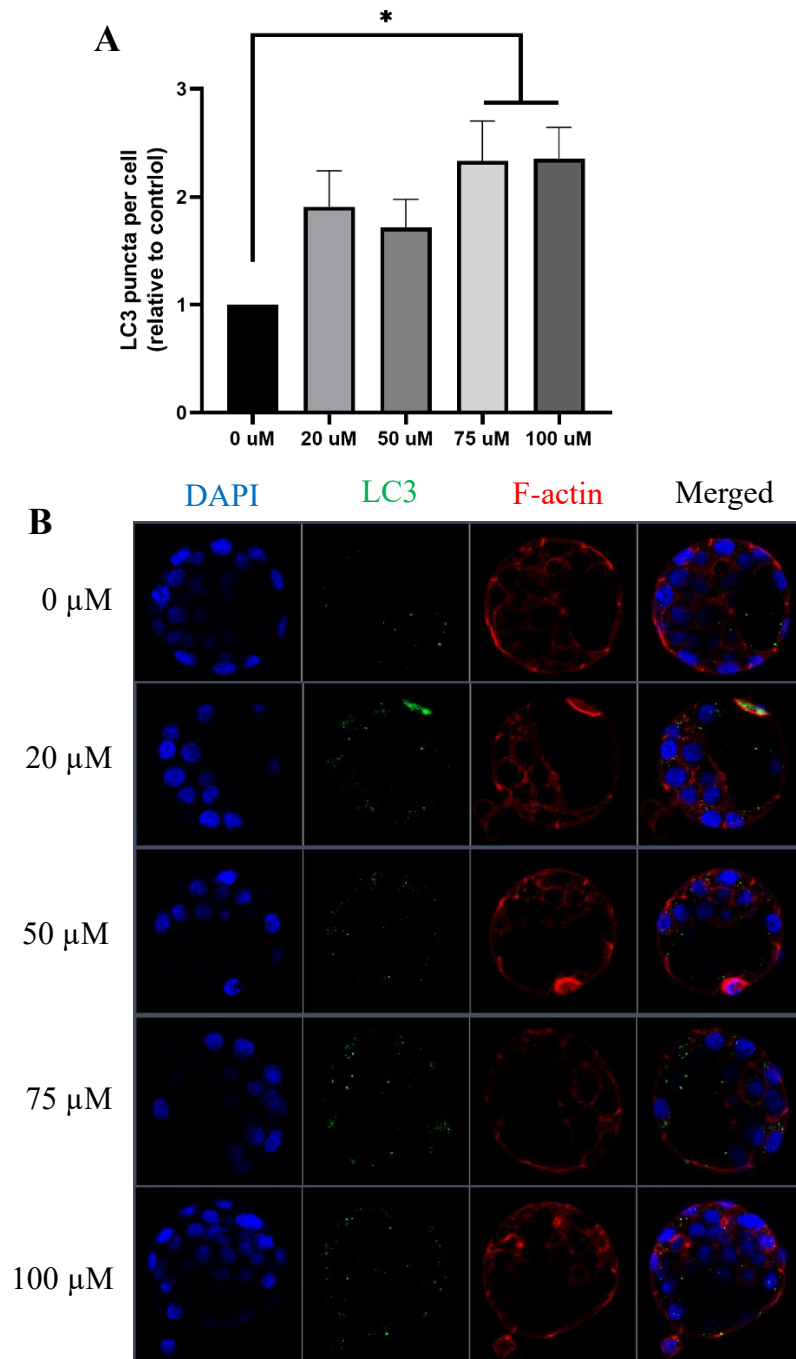
Thus, it was established that exposure of CQ at 75 μ M for two hours to mouse preimplantation embryos would allow for detectable differences in autophagic marker expression through western blot and immunofluorescence analysis.



Supplementary figure 2. Representative images of mouse preimplantation embryos treated with various concentrations of chloroquine at the last two hours of treatment period. Scale bar = 75 μm .



Supplementary figure 3. Protein expression of LC3-II of blastocyst embryos under various concentrations of chloroquine treatment for 2 hours, analyzed by Western Blot (+ SEM). Normalized to β -actin; 30 – 40 blastocysts per lane. N=3, one-way ANOVA with Tukey's HSD post-hoc test. Significant differences are indicated by * $p < 0.05$; ** $p < 0.005$. Representative images of western blot of LC3-I (16 kDa), LC3-II (14 kDa), and β -actin (45 kDa; loading control).



Supplementary figure 4. Number of LC3-II protein aggregates observed in blastocysts treated with various concentrations of chloroquine treatment for 2 hours, analyzed by immunofluorescence (+ SEM). N=3, one-way ANOVA with Tukey's HSD post-hoc test. Significant differences are indicated by * $p < 0.05$. Representative fluorescent images of mouse embryos after CQ exposure for 2 hours. Scale bar = 100 μ m.

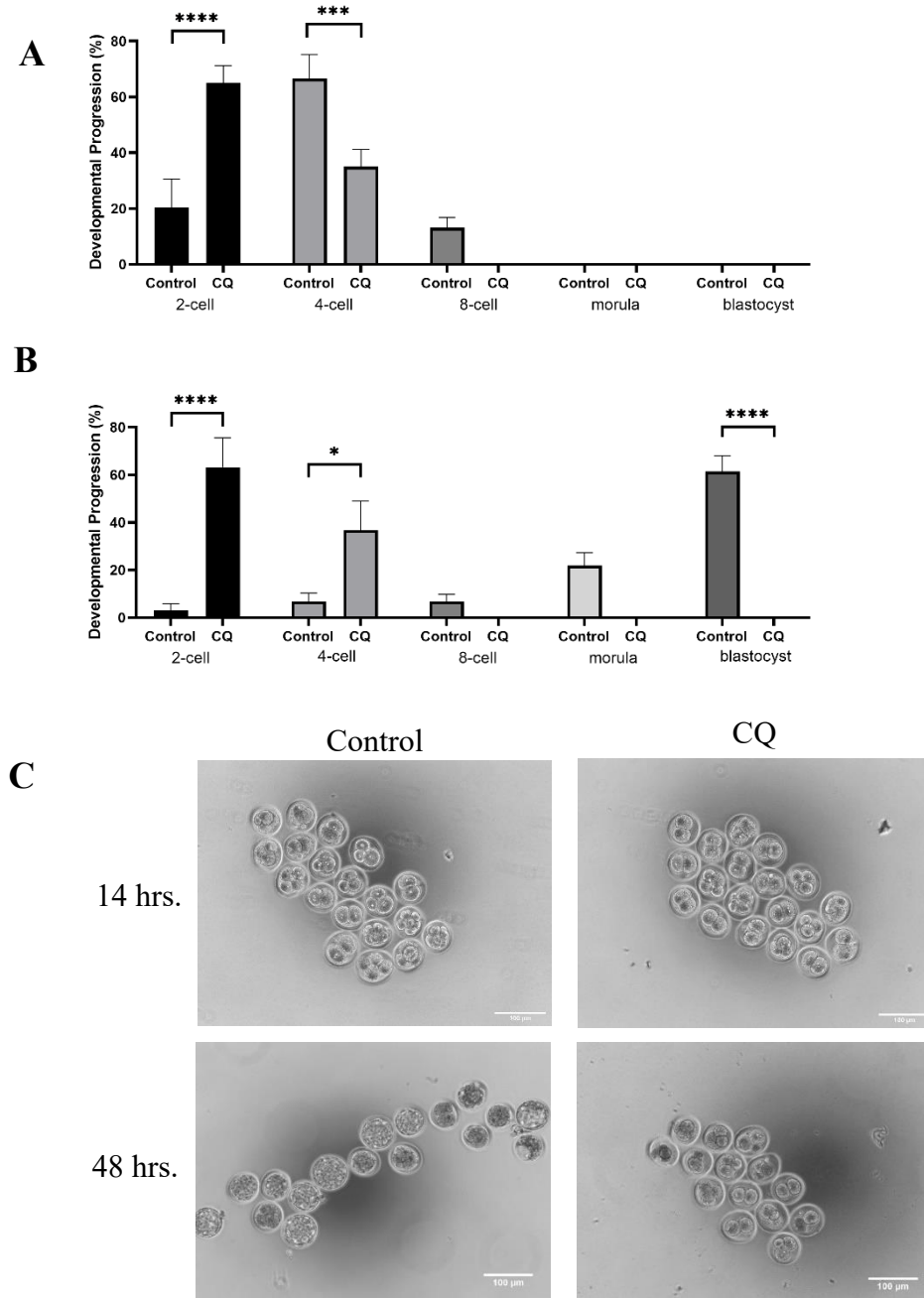
Appendix C: Chloroquine effects on preimplantation development

I investigated the effects of 75 μM of CQ on preimplantation embryo development. I exposed 2-cell mouse embryos to 75 μM of CQ for 14 and 48 hours. Developmental stage progression was assessed, and the embryos were analyzed for LC3-II puncta count.

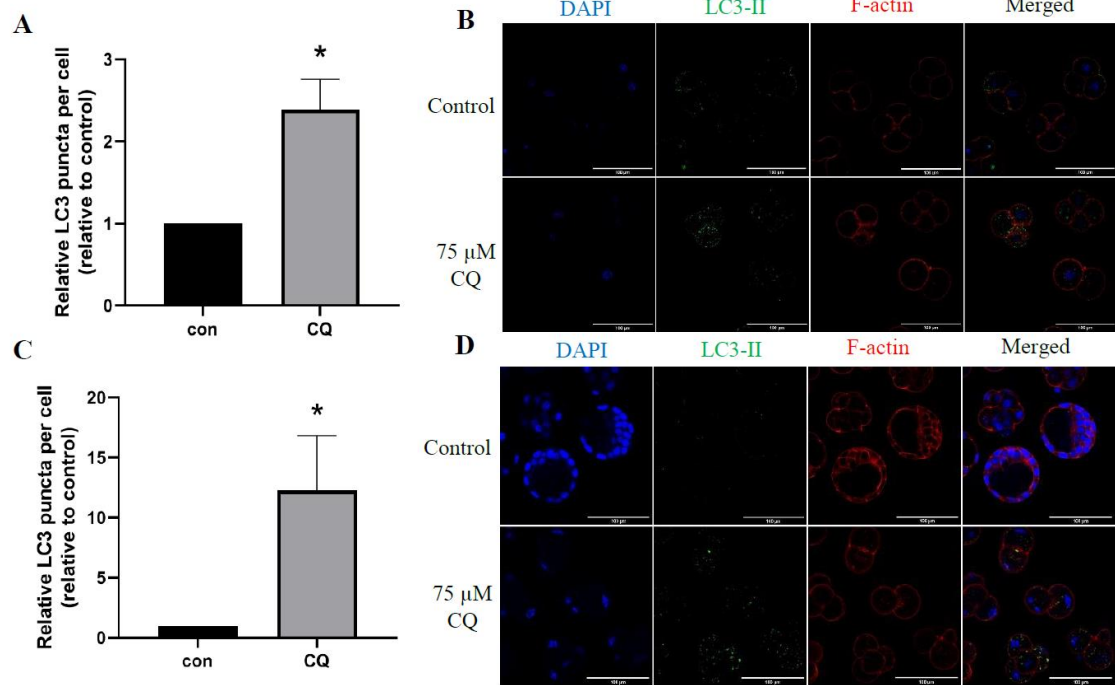
After 14 hours of CQ exposure, there was a significant reduction in progression to the 4-cell stage compared to control (**Supplementary figure 5A**, $P < 0.001$, Sidak's multiple comparisons test). Correspondingly, 14 hours of CQ exposure resulted in a significant increase in embryos at the 2-cell stage compared to control (**Supplementary figure 5A**, $P < 0.0001$, Sidak's multiple comparisons test). Representative images of 2-cell mouse embryos to placed into KSOMaa medium alone (control) or under treatment with 75 μM of CQ for 14 hours are shown in **supplementary figure 5C**.

After 48 hours of CQ exposure, there was no progression of 2-cell embryos to the 8-cell, morula, and blastocyst stages; though only blastocyst development compared to control was considered statistically significant (**Supplementary figure 5C**, $P < 0.0001$, Sidak's multiple comparisons test). Correspondingly, 48 hours of CQ exposure resulted in significantly more embryos arresting at the 2-cell stage and greater development of embryos to the 4-cell stage compared to control (**Supplementary figure 5A**, $P < 0.05$, Sidak's multiple comparisons test). Representative images of 2-cell mouse embryos placed into to KSOMaa medium alone (control) or with 75 μM of CQ treatment for 48 hours are shown in **supplementary figure 5C**.

Analysis of LC3-II puncta through immunofluorescence revealed significantly greater LC3-II puncta count per cell in CQ group compared to control group, at both 14 and 48 hours of exposure (**Supplementary figure 6A and 6C**, $P < 0.05$, two-tailed unpaired t-test). Representative images of exposing 2-cell mouse embryos to KSOMaa medium alone (control) or under 75 μM CQ treatment for 14 and 48 hours are shown in **supplementary figure 6B and 6D**, respectively.



Supplementary figure 5. Developmental progression (+ SEM) of 2-cell mouse embryos in 75 μ M of CQ or KSOMaa medium alone (control) for 14 (A) and 48 hours (B). Percent development to each embryo stage was analyzed. N=3, two-way ANOVA with Sidak's multiple comparisons test. Significant differences are indicated by * $p < 0.05$, *** $p < 0.001$, and **** $p < 0.0001$. Representative images of 2-cell mouse embryos in KSOMaa medium alone (control) or in 75 μ M of CQ for 14 and 48 hours (C).

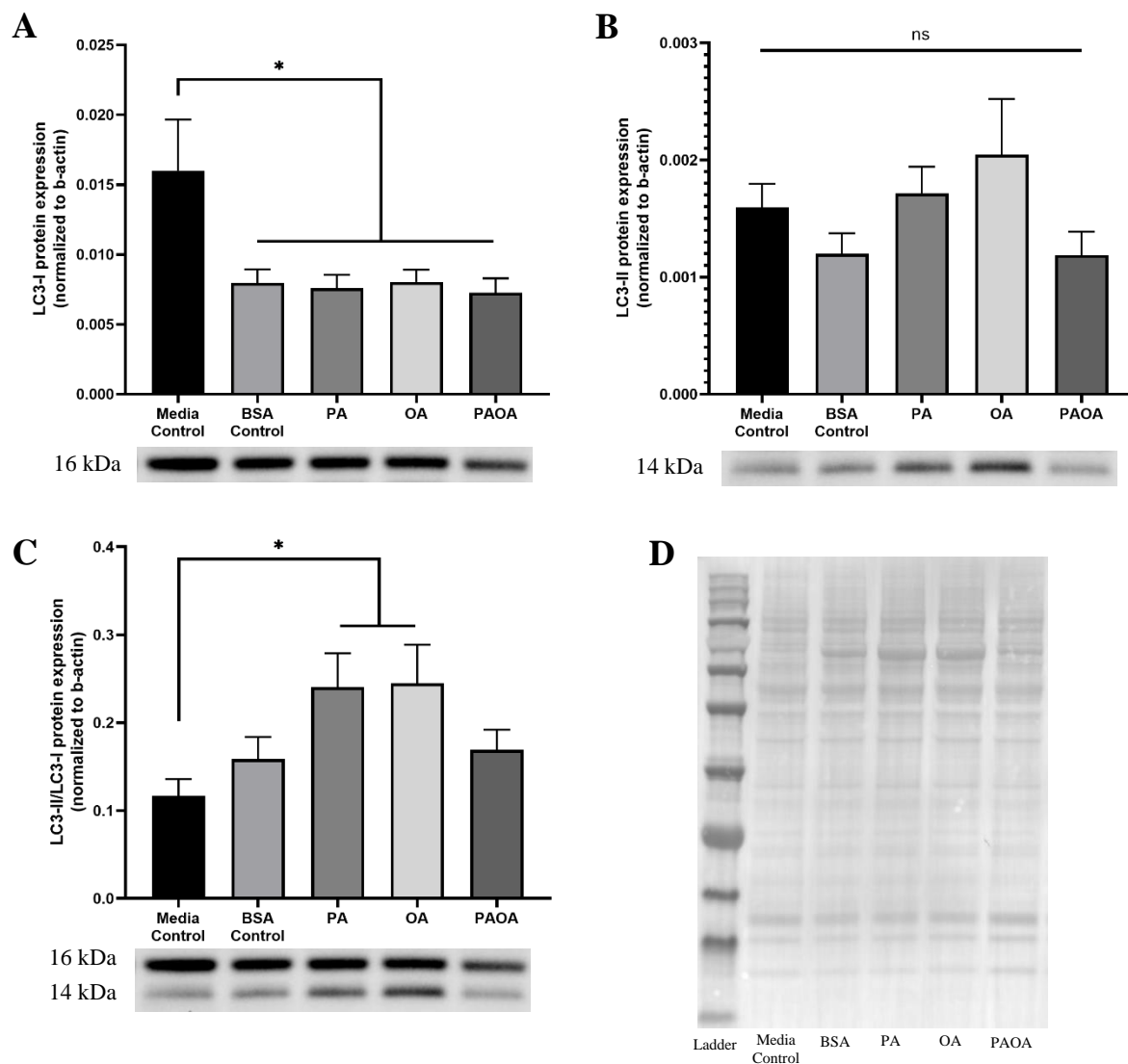


Supplementary figure 6. Relative LC3-II puncta aggregate per cell (+ SEM) of 2-cell mouse embryos in 75 μM of CQ or KSOMaa medium alone (control) for 14 (**A**) and 48 hours (**C**). $N=3$, two-tailed unpaired t-test. Significant differences are indicated by $*p < 0.05$. Representative images of 2-cell mouse embryos in KSOMaa medium alone (control) or 75 μM of CQ for 14 (**B**) and 48 hours (**D**).

Appendix D: Effects of PA and OA on mESC autophagy

Mouse embryonic stem cells (mESC) are derived from inner cell mass of a mouse blastocyst. mESCs represent an excellent alternate model for the investigation of NEFA treatment effects to early mammalian developmental autophagy, and preimplantation stages. R1 wild type mESCs were cultured in KSOMaa (BSA control), and KSOMaa plus 100 μ M PA and 250 μ M OA, individually and in combination, for 48 hours. Medium control consisting of only mESC growth media was also included in the experimental design.

Supplementary figure 7 summarizes the findings from this experiment. Densitometric analysis of western blot of LC3-I was not significantly different across treatment groups (**Supplementary figure 7A**, $P > 0.99$, Tukey's multiple comparisons test) except for the mESC medium control (**Supplementary figure 7A**, $P < 0.05$, Tukey's multiple comparisons test). No differences in LC3-II protein levels were detected between all treatment groups (**Supplementary figure 7B**, $P > 0.05$, Tukey's multiple comparisons test). The ratio of LC3-II to LC3-I protein levels, however, were significantly higher in the PA-alone and OA-alone groups compared to mESC medium control (**Supplementary figure 7C**, $P < 0.05$, Tukey's multiple comparisons test). PA-alone and OA-alone groups were not significantly different from each other. **Supplementary figure 7** includes representative images of western blot of LC3-I and LC3-II. The western blot also confirms the specificity of the LC3 antibody used in this thesis.



Supplementary figure 7. Protein expression of LC3-I (**A**), LC3-II (**B**), and the ratio of LC3-II:LC3-I (**C**) of mESCs in 100 μ M PA, 250 μ M OA, 100 μ M PA and 250 μ M OA, KSOMaa media (BSA control), or mESC growth medium (media control) for 48 hours (+ SEM). N=3, one-way ANOVA with Tukey's HSD post-hoc test. * $p < 0.05$. Representative images of western blot of LC3-I (14 kDa) and LC3-II (16 kDa) included in **A-C**. Ponceau S as loading control (**D**).

Appendix E: Ethics Approval



2018-075:13

AUP Number: 2018-075

AUP Title: Mechanisms Controlling Preimplantation Development

Yearly Renewal Date: 08/01/2022

The **annual renewal** to Animal Use Protocol (AUP) 2018-075 has been approved by the Animal Care Committee (ACC), and will be approved through to the above review date.

Please at this time review your AUP with your research team to ensure full understanding by everyone listed within this AUP.

As per your declaration within this approved AUP, you are obligated to ensure that:

1. This Animal Use Protocol is in compliance with:
 - o [Western's Senate MAPP 7.12 \[PDF\]](#); and
 - o [Applicable Animal Care Committee policies and procedures](#).
2. Prior to initiating any study-related activities—[as per institutional OH&S policies](#)—all individuals listed within this AUP who will be using or potentially exposed to hazardous materials will have:
 - o Completed the appropriate institutional OH&S training;
 - o Completed the appropriate facility-level training; and
 - o Reviewed related (M)SDS Sheets.

Submitted by: Cristancho, Martha on behalf of the Animal Care Committee



Dr. Timothy Regnault,
Animal Care Committee Chair

Animal Care Committee
The University of Western Ontario
London, Ontario Canada N6A 5C1



*** THIS IS AN EMAIL NOTIFICATION ONLY. PLEASE DO NOT REPLY ***

Curriculum Vitae

Name: Zuleika C. L. Leung

Post-secondary Education and Degrees:

Master of Science
 Physiology and Pharmacology
 Collaborative Program in Developmental Biology
 The University of Western Ontario
 London, Ontario, Canada
 2019-2021

Bachelor of Medical Sciences
 Honors Specialization in Interdisciplinary Medical Sciences
 The University of Western Ontario
 London, Ontario, Canada
 2015-2019

Honours and Awards:

Western Graduate Research Scholarship (WGRS)
 2019-2020

Children's Health Research Institute Trainee Award
 2020-2021

Developmental Origins of Health and Disease Canada Flash Talk Presentation award
 2021

Related Work Experience:

Graduate Research Assistant
 The University of Western Ontario
 2019

Teaching Experience:

Graduate Teaching Assistant
 Physiology and Pharmacology 3000E
 The University of Western Ontario
 2019-2021

Presentations:

June 2021 **Leung, Z. C. L.**, Calder, M. D., Betts, D. H., Rafea, B. A., Watson, A. J. Oleic acid rescues altered autophagy induced by palmitic acid during mouse preimplantation development. European Society of Human Reproduction and Embryology, Online (Poster Presentation).

- June 2021 **Leung, Z. C. L.**, Calder, M. D., Betts, D. H., Rafea, B. A., Watson, A. J. Oleic acid rescues autophagy changes induced by palmitic acid during mouse preimplantation development. Developmental Origins of Health and Disease Canada Annual Academic Meeting, Online (Flash Talk Presentation).
- May 2021 **Leung, Z. C. L.**, Calder, M. D., Betts, D. H., Rafea, B. A., Watson, A. J. Oleic acid rescues palmitic acid-induced autophagy during mouse preimplantation development. Child's Health Research Day, London, ON (Video and Poster Presentation).
- May 2021 **Leung, Z. C. L.**, Calder, M. D., Betts, D. H., Rafea, B. A., Watson, A. J. Oleic acid rescues palmitic acid-induced autophagy during mouse preimplantation development. London Health Research Day, London, ON (Poster Presentation).
- April 2021 **Leung, Z. C. L.**, Calder, M. D., Betts, D. H., Rafea, B. A., Watson, A. J. Oleic acid rescues palmitic acid-induced autophagy during mouse preimplantation development. Paul Harding Obstetrics and Gynaecology Research Day, London, ON (Oral Presentation).
- November 2020 **Leung, Z. C. L.**, Calder, M. D., Betts, D. H., and Watson, A. J. Early Mouse Embryo Autophagy under Fatty Acid Treatments. Physiology and Pharmacology Research Day, London, ON (Poster Presentation).
- November 2019 **Leung, Z. C. L.**, Calder, M. D., Betts, D. H., and Watson, A. J. Fatty Acid Treatments and Early Embryonic Autophagy. Physiology and Pharmacology Research Day, London, ON (Poster Presentation).